Crack Detection in Crane Shafts Using Acoustic Emission

by

Parry C. Berkowitz, B.A.Sc.,

Thesis

Presented to the Faculty of the Graduate School of

The University of Texas at Austin

in Partial Fulfillment

of the Requirements

for the Degree of

Master of Science in Engineering

The University of Texas at Austin

May 1998

Crack Detection in Crane Shafts Using Acoustic Emission

Approved by
Supervising Committee:

Timothy J. Fowler

Dr. Timothy J. Fowler

Dr. Michael D. Engelhardt

Dedication

To my parents, Joseph and Roza, for epitomizing all I strive to be.

Acknowledgements

I wish to express my sincere gratitude to my supervisor, Dr. Timothy J. Fowler, for his guidance, advise, expertise, mentorship, and good humor. He will always be an inspiration to me in my professional career.

Funding for this project was provided by the Naval Facilities Engineering Research Council through a contract given to Texas Research Institute/Austin, and generously allotted to this project by them. My thanks to Dr. Mike Dingus, and Russell Austin.

My thanks to all the faculty and staff at the Ferguson Structural Engineering Laboratory; truly a world class facility complete with world class people.

To some of the best friends I've ever had: Charles Bowen, Matthew Thiel, Dave McIlrath and especially Jon Richter. Your friendship means a great deal to me. Thanks you for showing me how much more there is to life outside of school, and for being there to depend on during stressful times, and to celebrate with during joyous times. May the future show us fewer of the former, and an abundance of the latter – always together.

My acknowledgements would not be complete without an expression of my thanks to my family and friends. To my parents, Joseph and Roza Berkowitz, and my sister, Michaela Berkowitz, your love, support and encouragement has made all the difference in the world. Thank you.

May, 1998

Abstract

Crack Detection in Crane Shafts Using Acoustic Emission

Parry C. Berkowitz, M.S.E.

The University of Texas at Austin, 1998

Supervisor: Timothy J. Fowler

Acoustic emission testing of naval portal crane shafts was carried out at the Ferguson Structural Engineering Lab at the University of Texas at Austin. The crane shafts were provided by the United States Navy in order to examine the feasibility of using acoustic emission to find fatigue cracks in existing shafts. The results of the test program were used to develop a field test procedure based on acoustic emission technology.

The laboratory testing comprised fatigue cycling of the shaft at various load levels while monitoring with digital acoustic emission instrumentation. A specially designed stand was used to apply the torsional load to the shaft via its keyway, the same way as loads are transferred while in the crane. A field test at Pearl Harbor Naval Shipyard verified the viability and effectiveness of the proposed method in a real setting, and was effective in calibrating data obtained in the laboratory.

The data was analyzed using standard acoustic emission parameters. The data confirms that acoustic emission can detect the presence and growth of fatigue cracks under torsional loads. Emission from the crack is significant and readily detectable at thresholds commonly used in field testing environments.

Table of Contents

List of Tables

List of Figures

CHAPTER 1

INTRODUCTION

In recent years the United States Navy has experienced several failures of spool and rotate pinion (sluing) drive shafts. These failures have resulted in uncontrolled dropping of the sometimes sensitive payloads being lifted. The following is an excerpt from a report detailing one such failure: [1]

> On February 28, 1995 a catastrophic failure occurred in the rotate pinion (i.e., sluing) shaft of Naval Crane P-71 at Pearl Harbor Naval Shipyard (PHNS). The 25 ton portal crane was manufactured by R. W. Kaltenbach Corporation in 1945. The failed shaft, from the sluing assembly of a crane rated to 56,000 lbs, failed at the inside (or top) face of the pinion gear while lifting a 16,000 pound load. Fracture occurred at the transition in diameter where the shaft is reduced to accommodate the pinion gear. The failed crane is a single rotate system; if the single rotate pinion shaft fails, no backup system prevents the machinery house from rotating.
>
> Plastic deformation, i.e., necking, was not evident at the failure surface, indicating failure by slow growth of cracks. Fracture surface appearance of the failed shaft indicate that the fatigue cracks initiated at the shaft's surface and propagated towards the shaft center. The smooth, shiny appearance of the fatigue crack faces near the surface reveal that the faces rubbed together, indicating that the cracks propagated during high repetition cycling under nominal loads. Final failure occurred by rapid crack propagation in a small region of the shafts center, also characteristic of damage progression under nominal loads. The above indications lead to the conclusion that failure was caused by reverse torsional fatigue.

Figure 1.1 shows a typical Navy portal crane. These cranes are primarily located in naval shipyards where they are used to transfer payload to and from aircraft carriers, battleships, and submarines. Figure 1.2 shows a spool drive shaft and drum. The fracture, detailed in the failure report excerpt, occurred near the interlocking gears seen in the center of the photograph.

Figure 1.1: Typical Naval Portal Crane

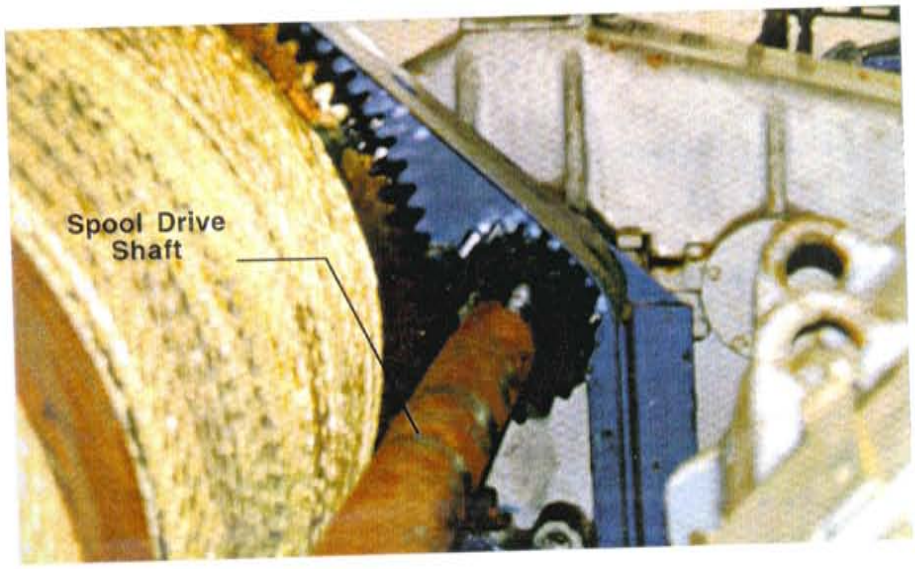

Figure 1.2: Spool Drive Shaft and Drum In-Situ

To locate the defects responsible for the observed failures using conventional nondestructive testing techniques, such as ultrasonic inspection and magnetic particle inspection, would require substantial disassembly of the crane in order to gain access to the areas of interest. The process of disassembling and reassembling the crane is many orders of magnitude more costly than the nondestructive test itself. It is estimated that there are some nine thousand of these cranes in the Navy's inventory, and thus a clear need is evident for a global nondestructive testing technique that may be applied in-situ which can detect fatigue cracks in the crane shafts. The global technique, in conjunction with complimentary nondestructive evaluation techniques for follow-up localized inspection if necessary, will allow the Navy to diagnose the health of their cranes

without having to withstand the economic burden of disassembling each one before it can be inspected.

Following the failure of the first crane shaft, the Navy ordered all other crane shafts from the same manufacturer and vintage to be nondestructively examined for cracks. The Navy's in-house NDT personnel used both ultrasonic, and wet fluorescent magnetic particle testing to try and detect the cracks. The results were less than satisfactory.

The geometry of the shaft, especially in-situ, makes obtaining good results with traditional NDT methods very difficult. The problems experienced by the Navy were that one of the methods would give a positive indication of a defect, and then the other method would not. In one case, both methods gave no indications and then the shaft failed catastrophically only a few days after the inspection took place. The failure analysis reveled the presence of a major structural crack in the location where it was suspected when the nondestructive examination was ordered. It is impossible to say with any degree of certainty why the defect was missed. As with most traditional applications of the aforementioned NDT techniques, operator skill and acuity plays a key role in the sensitivity of the method. This is yet another reason why a global nondestructive testing technique which has a clearly identified evaluation criteria is needed in order to assure the continued safe operation of the cranes.

CHAPTER 2

BACKGROUND THEORY

2.1 ACOUSTIC EMISSION

Acoustic emission is an important tool for assessing the structural integrity of equipment in the chemical and petroleum industries. Over the past twenty years it has developed into a reliable, cost effective indicator of structural problems, and is now viewed as a mature technology. The method is used extensively for in-service examination of "cherry picker" manlifts, pressure vessels, tanks, and tank cars. There are many standard test procedures which use acoustic emission as the sole means to evaluate the health of equipment. Examples include: Section V of the American Society of Mechanical Engineers Code[8], the American Association of Railroads Procedure[15], and others. As a global test, it is complementary to other nondestructive examination methods which are used for follow-up inspection.

Acoustic Emission (AE) is an extremely useful tool for materials research. It is a highly sensitive technique for detecting active microscopic processes, as well as crack propagation. As such events give rise to elastic waves which propagate through the material, AE monitoring may be used to detect and locate the source of the waves and can inspect damage by using remote sensors, rather than requiring complete volumetric scanning. [2]

The usefulness of AE testing has been considerably enhanced in recent years by the incorporation of the microcomputer into AE instrumentation. Not only has the computer revolutionized the acquisition, recording and analysis of the large amount of data arising from an AE study but, above all, the combination of relevant hardware and software, together with careful mechanical procedures has succeeded in minimizing the problem of background noise. Thus AE has become a viable tool even in the noisy environment of the fatigue test.

Fatigue crack formation and initiation are generally preceded by progressive material deterioration, induced by dislocation motion and saturation, and a loss of resistance in terms of life. Monitoring this deterioration in real time allows the measured quantities to be used as indicators of the extent of fatigue damage.

Although the technology has been used extensively in the petroleum and chemical industries, it has had only limited application to bridges, cranes, and other civil engineering structures, even through its unique characteristic as a noninvasive global test makes it particularly valuable. AE can be used in conjunction with other conventional complementary nondestructive test and evaluation techniques, such as ultrasonic inspection or radiography, which can be used for follow-up local inspection in areas where the AE data suggests that a problem may lie.

All acoustic emission testing procedures are based upon a signal detection technique which ensures coverage of the entire item of equipment under test and thus specifications for equipment and sensor calibration, along with attenuation measurements, are included in all test procedures.

2.2 WAVE PROPAGATION THEORY

Wave propagation theory involves the study of fluctuations in the value of various mechanical quantities characterizing the state of matter – fluctuations of the pressure or other components of stress, or fluctuations of density, temperature, and the position of individual particles of a given material. Generally speaking, the science can be divided into two domains; primary measurement and secondary measurement. The former endeavors to determine the magnitude and waveform of the oscillations of one of these quantities at any given position in the body, whereas the goal of the latter is to characterize the propagation of these oscillations through the body by determining the speed of propagation, the intensity, or rate, of propagation of the energy, and the absorption rate of the energy. Acoustic Emission relies upon both primary and secondary parameters in the interpretation of experimental data.

Most of the early measurements used mechanical devices that would determine only the magnitude of the oscillation of displacement or velocity. The advent of electronic amplifiers led to the development of electro-mechanical transducers which convert the oscillating mechanical quantities into an electromotive force (EMF). This development is of particular significance in discussing the present subject as many AE instruments rely on amplified signals from piezoelectric pressure sensors mounted on the surface of the material being tested in order to collect valid data.

The piezoelectric sensors contain piezoelectric elements that develop an EMF in response to mechanical stress. In the pioneering days of the technology Rochelle salt crystals were used as the element, because of their high sensitivity. Present-day piezoelectric sensors generally use polarized ceramic piezoelectric elements of barium titanate, lead zirconate, or others which have high sensitivity, good durability, and are available in many the common shapes required for various sensor designs. A cross section of a typical AE sensor is shown in Figure 2.1.

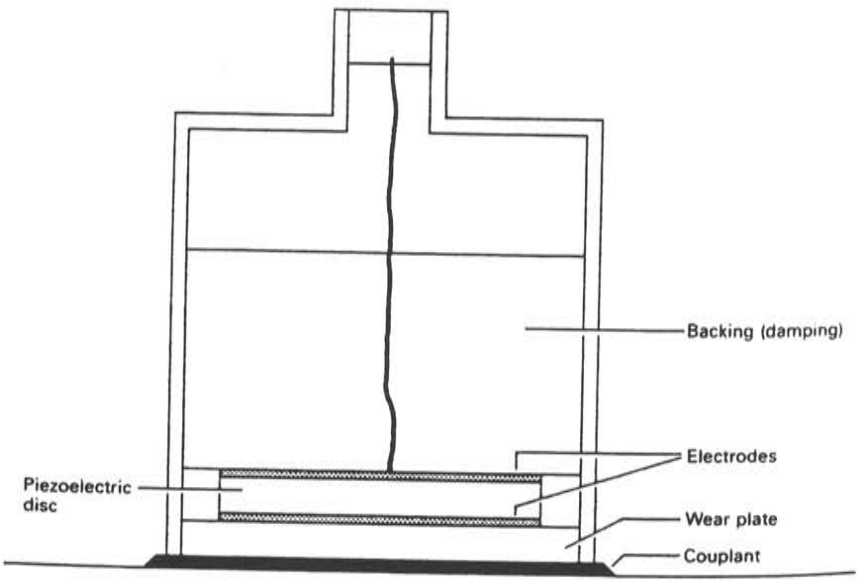

Figure 2.1: Cross Section of a Typical AE Sensor Coupled to an Object

The ratio of the generated EMF to the oscillating pressure generating the EMF is called the sensitivity of the sensor. The sensitivity is determined by a calibration procedure. Acoustic emission sensors are often calibrated so that one microbar of pressure on the sensor face causes one microvolt of output from the resonating crystal. Sensors which conform to these standards have proved to be effective and accurate in recording the acoustic energy generated from structural sources in a large variety of common engineering materials. Common resonance frequencies for AE sensors are on the order of 150 kHz through 300 kHz. Lower frequency measurements can be made, going as low as 5 kHz, using active transducers known as accelerometers. Among the most recent contributions to the field of AE is the wide band sensor, which, in essence, has no base resonating frequency - rather it is able to pick up and report the true frequency of the events taking place. Wide band sensors have an effective operating range between 50 kHz and 1.2 MHz. All certified AE sensors, though, are shipped with calibration curves which show their specific response to a given frequency pulse, as shown in Figure 2.2.

Measurements of the distribution of acoustic intensity around a sound source have become increasingly common place since the advent of digital spectrum analyzers. The intensity is a vector quantity whose component in a specified direction is the acoustic power passing through a unit cross section perpendicular to the specified direction, this being equal to the time average of the product of the instantaneous sound pressure and the instantaneous particle velocity component in that direction. With a digital spectrum analyzer, the intensity is usually measured by evaluating the cross-spectral density of the

sound pressure at the sensor face; the spectral density of the intensity at any frequency can be shown to be proportional to the imaginary part of the cross-spectral density of the pressure at that frequency. This cross spectral technique is suitable for both narrow and wide bands. [4]

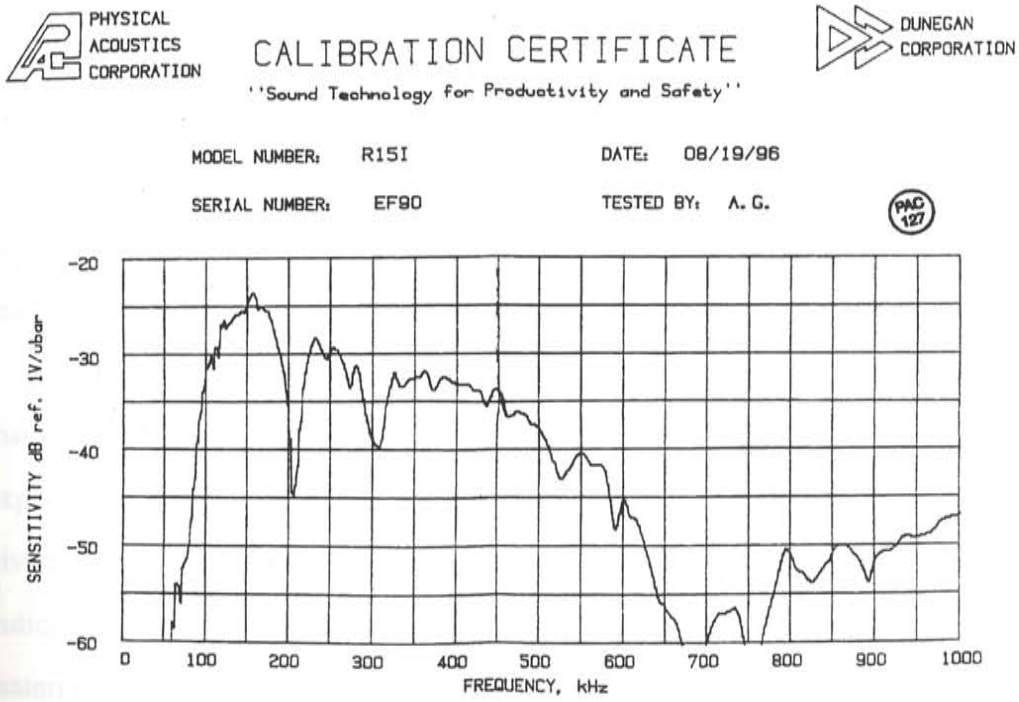

Figure 2.2: Typical AE Sensor Calibration Curve [3]

It is of much practical interest to understand some of the physical phenomena associated with acoustic wave propagation. Sound waves travel in solid materials by elastic deformation of the material, which as touched upon earlier, is called an elastic wave. In solid material, the shape of the wave

changes, as it travels. This is due to the different frequency components traveling at different velocities.

The wave propagates undisturbed until it reaches some obstacle. The obstacle, which can be a heterogeneity in the material, or a physical object, distorts the sound wave is several ways. Pressure waves, as with light, are effected by reflection, refraction, diffraction, interfaces and scattering. Each is described briefly.

When a wave hits a rigid obstacle, or an air void, part of it bounces off the obstacle, a characteristic known as reflection. The reflection of the sound back toward the source is called an echo. The echo sound wave generally undergoes a phase transformation in the reflection process.

Refraction is the change of direction of a wave when in travels from one material into another where it has a different velocity. The following example explains refraction: Imagine a sound wave that is constant over a plane in a given material and a line drawn perpendicular to this plane (i.e., the normal) indicates the travel direction of the wave. When the wave travels to a different material, the normal bends, thus changing the direction of the sound wave. This normal line is called a ray. This process is shown schematically in Figure 2.3.

When a pressure wave hits an interface, part of the wave reflects and part goes through the interface. The part that goes through the interface is the transmitted wave. Reflection and transmission are related phenomena, which may be used to understand the nature of acoustic emission sources.

Diffraction is associated with the bending of sound waves around or over barriers. A sound wave can often be heard on the other side of a barrier even if

the listener cannot see the source of the sound. However, the barrier projects a shadow, called the shadow zone, within which the sound cannot be heard. This phenomenon is similar to that of a light that is blocked by a barrier.

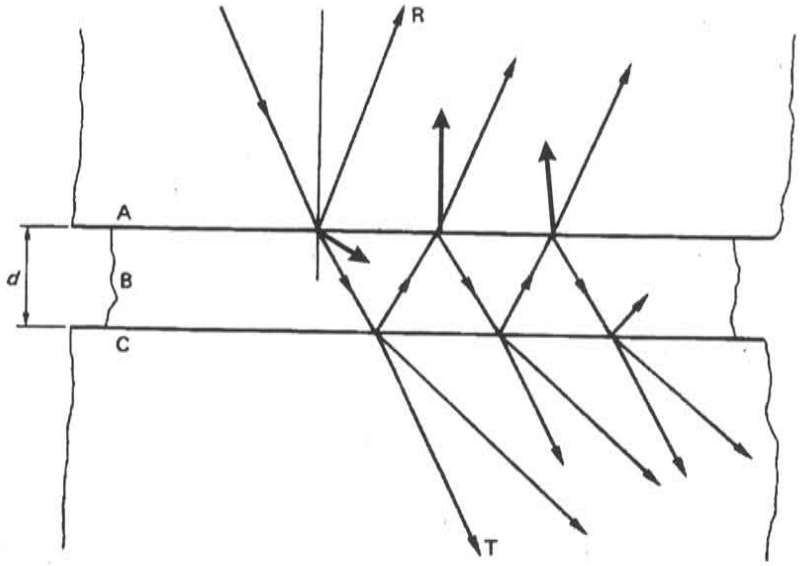

Wave refraction on an interface between two materials, A & C, with a coupling layer, B. T denotes the transmitted portion of the wave, and R the reflected portion.

Figure 2.3: Sound Wave Refraction

Interference is the phenomenon that occurs when two pressure waves converge. In linear wave theory the pressure waves can be superimposed. When this occurs, the resultant pressure wave is the sum of the two waves, taking into account the magnitude and the phase of each wave. Traditionally, however,

logarithmic scales are used in measuring magnitudes, and thus the result of superimposing the crest of two waves would only be an increase of 6 dB.

Wave scattering is a related property to reflection and transmission. It is the phenomenon that occurs when a pressure wave goes around an obstacle and breaks up, producing a different pressure pattern around that obstacle. Although metals such as steel are, in a physical sense, homogeneous, obstacles such as air voids, weld inclusions, and hard grains are commonly encountered. The pressure travels off in all directions around the obstacle. The part of the wave that travels back toward the source is called the backscattered wave, and the wave that travels away from the source is known as the forward-scattered field.

A good working knowledge of these physical phenomena is important to be able to correctly interpret acoustic emission data. Although none of the parameters measured in AE testing specifically measures any of the described phenomena, all of the stress waves the sensors pick up are, in one way or another, related to these properties.

2.3 THE ACOUSTIC EMISSION SIGNAL

Through various mechanisms acoustic emission generated by a material defect propagates from the source within the solid body to the sensor, usually located on the surface, in a manner similar to earthquake waves traveling through the interior of the earth to the surface. As the signal travels, it is attenuated by the heretofore described physical phenomena. Generally speaking, high frequency components are attenuated more than low frequency

components, and sensors located far away from the source receive only the low frequency components of the wave. The range of frequencies typically encountered in AE are on the order of 50 kHz to 500 kHz. Depending on the type of sensor used, and the type of information required, various filtering schemes have been developed for various purposes that can modify the signal received.

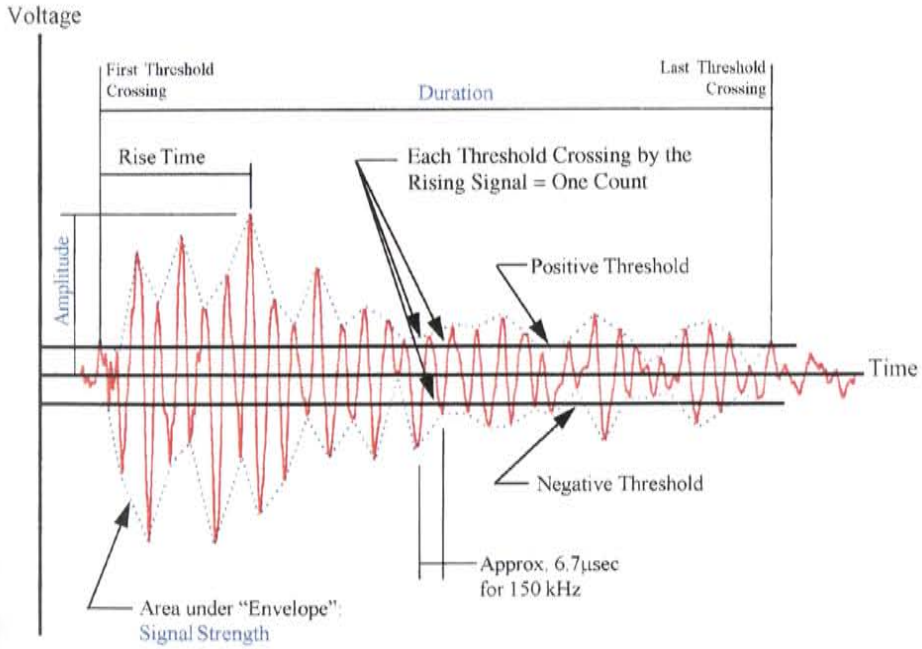

Figure 2.4: Typical AE signal - Voltage VS Time - Showing definitions of Amplitude, Duration, Threshold, counts, and Rise Time.

Figure 2.4 shows typical output from an AE sensor. When a stress wave strikes the face of the sensor, it causes the output signal to rise above a preset

threshold. This signal is commonly referred to as a "hit". The threshold value will vary depending on the type of data required, and the circumstances of the test. It is used to selectively reject signals with amplitudes below the threshold which will not provide meaningful data, as they may be caused by spurious sources such as ambient, electronic, or electromagnetic noise.

Acoustic emission has been observed to occur in bursts, which manifests itself as a number of separate sensor hits within a short period of time. The cascade of hits is, in itself, very telling, as different cascade patterns are characteristic of different types of defects. It has been noted that emission bursts are similar to records of some earthquakes, but over a much shorter time period. The early hits are small in magnitude and foretell the main energy release. Hits occurring at the end of the bursts can be aftershocks, caused by smaller events due to the same phenomena which caused the original emission, and would generally be of much lower energy.

Although the waveform of the type presented in Figure 2.4 is a depiction of what the actual piezoelectric sensor would output, most modern acoustic emission instrumentation, uses the rectified signal, as depicted in Figure 2.5 to perform the required analysis. The area under this rectified signal envelope, or MARSE (Measured Area under the Rectified Signal Envelope), is a measure of the relative energy in the signal. In acoustic emission practice, this is sometimes used as the Signal Strength, even though it is approximating half the true signal strength. With fully digital instrumentation, such as that used in this research, the full waveform is recorded, and the user may calculate the energy without having to rectify the signal, if so desired.

Signal strength is an important parameter in assessing the validity of acoustic emission data, as the loss of high frequency components and a decrease in amplitude of the stress wave during travel causes an apparent longer low frequency signal for which the area under the envelope would have the same approximate area as the case before the wave had traveled.

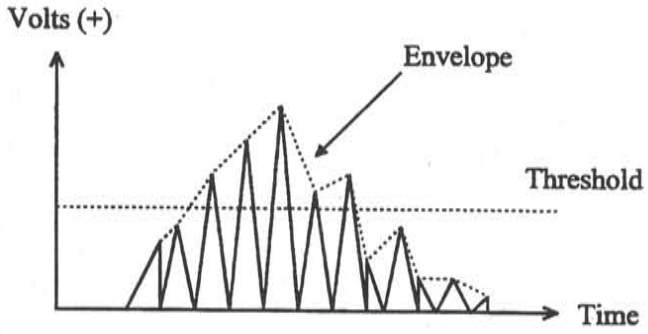

Figure 2.5: Depiction of a MARSE signal

The piezoelectric sensors require a preamplifier to overcome voltage losses between the sensor and the recording instrument. Some sensors have this preamplifier built into the sensor unit itself, whereas others require the use of an external device. The sensors which incorporate the preamplifier in themselves are preferred as there is less opportunity for spurious electronic or electromagnetic interference to contaminate the data. Generally, the preamplifier adds 40 dB to the amplitude of the signal. This 40 dB is usually

subtracted out of the signal by the recording instrument before recording or displaying the data.

In order to assure an adequate acoustic bond between the solid body being tested and the sensor, some type of acoustic coupling compound must be used. For the present research hot melt glue was used to attach the sensor to the component being tested. The hot melt glue not only provided a good, strong, method of adhesion, but also proved to be an excellent acoustic coupling. As an alternative, a silicone based grease can be applied to the sensor face, and the sensor affixed to the component being tested by means of tape or spring loaded magnetic holddowns.

After attaching the sensors to the component to be tested, it is necessary to verify their correct operation. This is done by breaking a 0.3 mm 2H pencil lead in close proximity to each sensor on the surface of the solid body while monitoring with the AE equipment. The American Society for Testing of Materials (ASTM) outlines a procedure for doing this, which was adhered to at all times in order to assure scientifically admissible data (ASTM E1316 [18])

2.4 AE PARAMETERS

Well known AE parameters are used to understand the processes occurring within the crane shafts. Signal strength and amplitude are typically used together to provide a measure of the magnitude of typical events, such as material yielding in advance of the crack tip, or crack advancement, where a high parametric value is representative of significant damage within the material.

The arrival time of the signal is used for source location applications. If signals are captured by the required number of sensors located on the surface, the source of the emission can generally be localized. This is done in much the same way as an earthquake epicenter is located in seismology. Once the source has been identified, a detailed local inspection can be ordered to more clearly define the type and geometry of the defect.

The Kaiser effect is a powerful and important tool in the evaluation of acoustic emission data. The effect is defined as follows: if a material is stressed and monitored with AE, the stresses removed, and then reapplied, no acoustic emission occurs until the load reaches the level corresponding to the maximum load in the previous stage. This effect is seen in most metal and composite materials.

The Felicity effect is the breakdown of the Kaiser effect. It forms an important part of the evaluation criteria for new and in-service pressurized and atmospheric containment vessels. The Felicity ratio is defined as the ratio between the load at the onset of acoustic emission during a reload test and the maximum load applied to the element during the previous loading interval.[3] It has been shown that the Felicity ratio is related to the degree of deterioration or damage of the element. A value very close to unity is characteristic of a material in good health, while smaller values (less than 1) are representative of the fact that damage has occurred.

The similarities between these two parameters arise from the fact that the Kaiser effect may well be represented as a special case of the Felicity ratio equal to unity. Figure 2.6 presents the Kaiser and Felicity effect, as obtained from a

typical test. In this figure, the Kaiser effect may be noted in the second loading stage. The emission begins again just as the load reaches the maximum value attained at the end of the first loading.

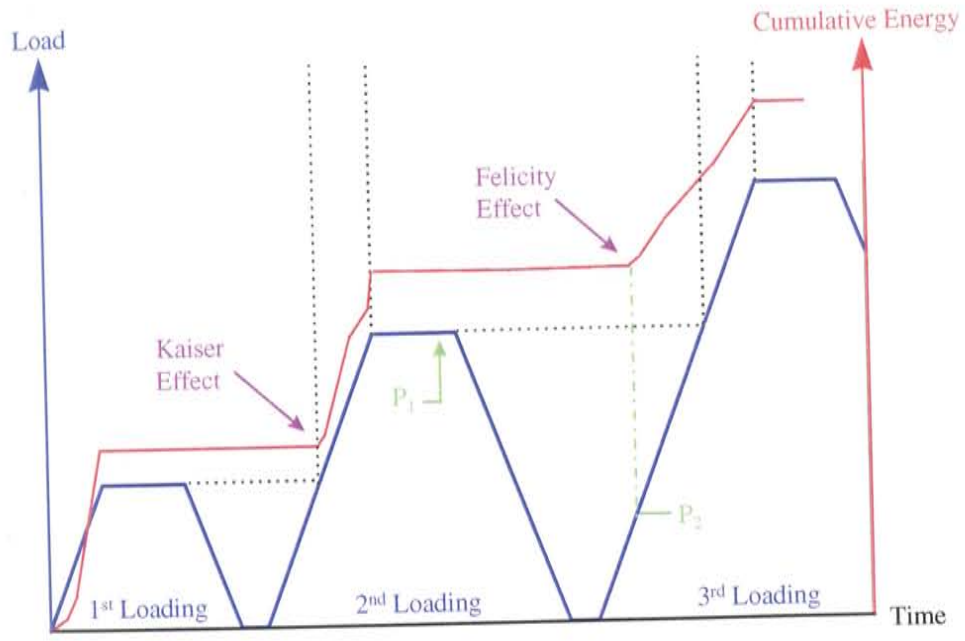

Figure 2.6: The Kaiser and Felicity Effects

The Felicity effect can be seen in the third loading, since the emission starts before the load reached the maximum value of the previous loading. For this case, the Felicity ration is P_2/P_1.

Another important technique in the evaluation of AE data is the Intensity analysis, which provides a measure of the structural significance of a defect. The two basic parameters used for this analysis are the Severity Index and the

Historic Index. These indices are defined in section 12.6 of the proposed standardized testing procedure included as an appendix. Basically the indices are obtained from the cumulative signal strength of a series of events in a test, and give a good indication of the absolute magnitude as well as the change in the magnitude of the emission. The change in magnitude of the emission can, in turn, be related to the significance of the damage in a given structure.

2.5 AE AND FATIGUE CRACK GROWTH IN THE LITERATURE

The mechanisms that cause genuine AE in metals are discussed by Fang and Berkovitz[5], Heiple et al [6,7], and Williams [8]. While these authors all differ to some degree on precise definitions [such as nomenclature, description of the exact microscopic behavior, number of different mechanisms, and differentiation between mechanisms], all tend to agree on the following general classification schemes:

Gross Yielding. This is the most common mechanism of AE generation in metals. Heiple and Carpenter[7] provide a comprehensive summary of work done by many researchers in the 1970's and 1980's into the precise metallurgical processes [involving crystal lattice types of different metals, effects of grain boundaries, lattice twinning, microscopic inclusions, etc.]. The authors put forth that AE during yielding is due primarily to the movement of dislocations, which are imperfections in the crystal lattice. Since the energy from the motion of one dislocation is too small to be detected, there must be a progressive "unpinning" of many dislocations at once to cause detectable AE. That is, dislocations pile

up at a microscopic obstruction, until the increasing stress causes one dislocation to begin to move, triggering an avalanche of dislocation movements.

Elastic Crack Growth. The energy released during the actual separation of the crack faces [by "either transgranular cleavage or intergranular fracture along the grain boundaries", according to Fang and Berkovitz[5]] causes high energy AE. This emission is fairly easy to distinguish, with very high amplitude and high signal strength hits. Most AE testing procedures [for example, the ASME Boiler and Pressure Vessel Code[8]] recognize this by treating any AE with an amplitude higher than 70 dB as evidence of the existence of cracks. Elastic crack growth is encountered more often in brittle materials, such as cast iron, or steels with a high carbon content.

Plastic, or Fatigue Crack Growth. The consensus of all the literature is that fatigue crack cracking does cause AE. Together, Heiple et al[6,7] and Fang and Berkovitz[5] describe four specific mechanisms of AE generation during fatigue crack growth, as shown in Figure 2.7. In roughly sequential order of formation, they are:

1. Dislocation movement [plastic flow] in the plastic zone, very similar to the yielding mechanisms described above [called Stage I by Fang and Berkovitz[5]];
2. Fracture/decohesion of inclusions in the plastic zone as the crack advances, also called crack nucleation or initiation [Stage II];
3. Crack advancement, similar to the elastic crack growth described previously [Stage III]; and
4. Crack face rubbing, also known as crack closure.

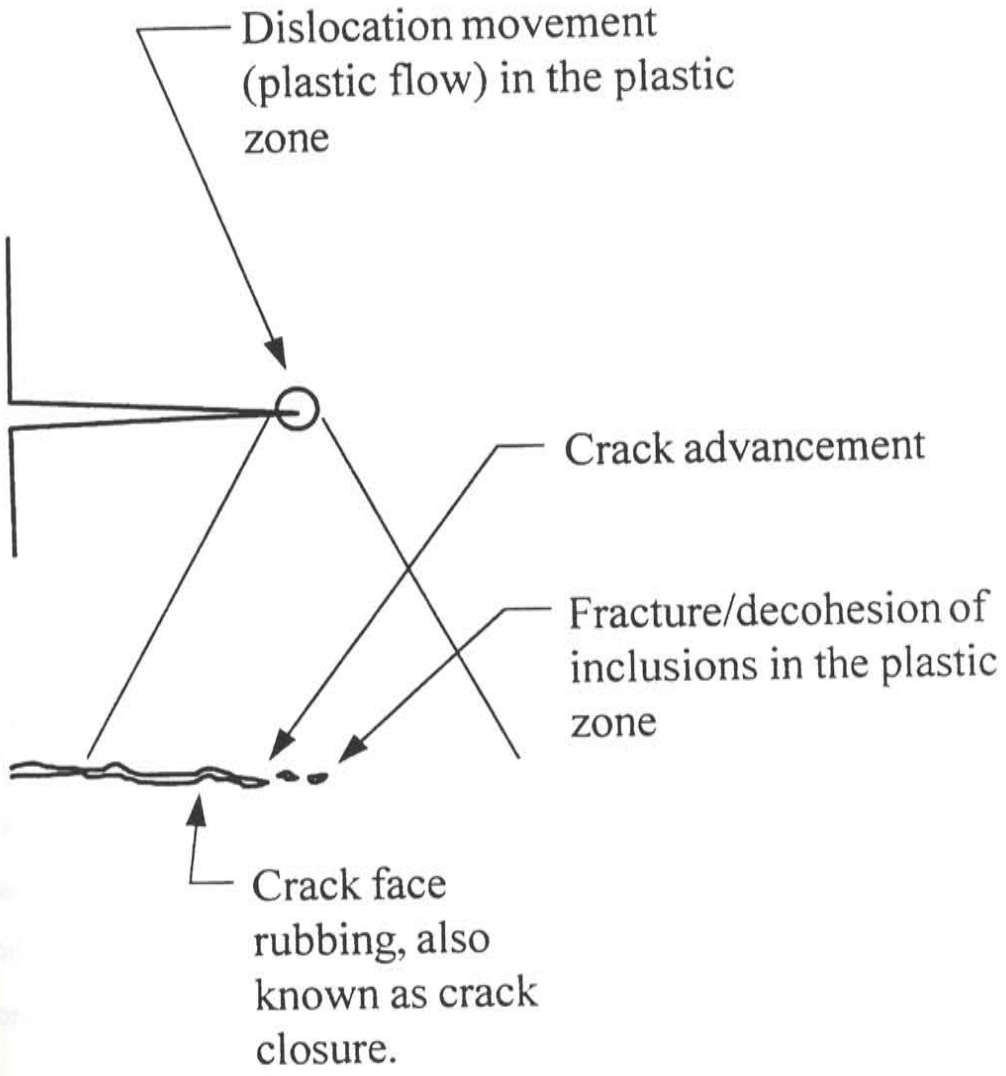

Figure 2.7: Causes of AE in Fatigue Cracks

These four mechanisms will all occur during fatigue crack growth. Each mechanism will create AE with different characteristics. At this time, there is no consistent, satisfactory way to determine which mechanism corresponds to each hit.

Fang and Berkovitz[5] performed tests on several unnotched tensile dogbone coupons machines from nickel alloys. Different specimens were tested with several different levels of maximum stress (σ_{max}), and different stress range types: tension-compression cycles $R = (\sigma_{min} \div \sigma_{max} = -1)$, tension-zero [approximately] cycles (R=0.01) and tension-tension cycles (R=0.2). In all cases of the low range of maximum stress investigated, the AE behavior (after the first few cycles) was dependent only on the stress range $\Delta\sigma$. Figure 2.8 shows the behavior of cumulative AE counts, η (a common measure of cumulative AE in the 1970's and 1980's) versus time. Note the change in AE behavior during each of the three stages described in the forgoing discussion. The lower graph indicates that the slopes are a function of $\Delta\sigma$, but the general trend is the same for all the tests.

Williams[9] describes tests on mild steel pipes with an axial partial thickness slit. It can be seen that the experimentally observed behavior of the cumulative AE:

$$\frac{d\eta}{dN} = C_1 \Delta K^{m_1}$$

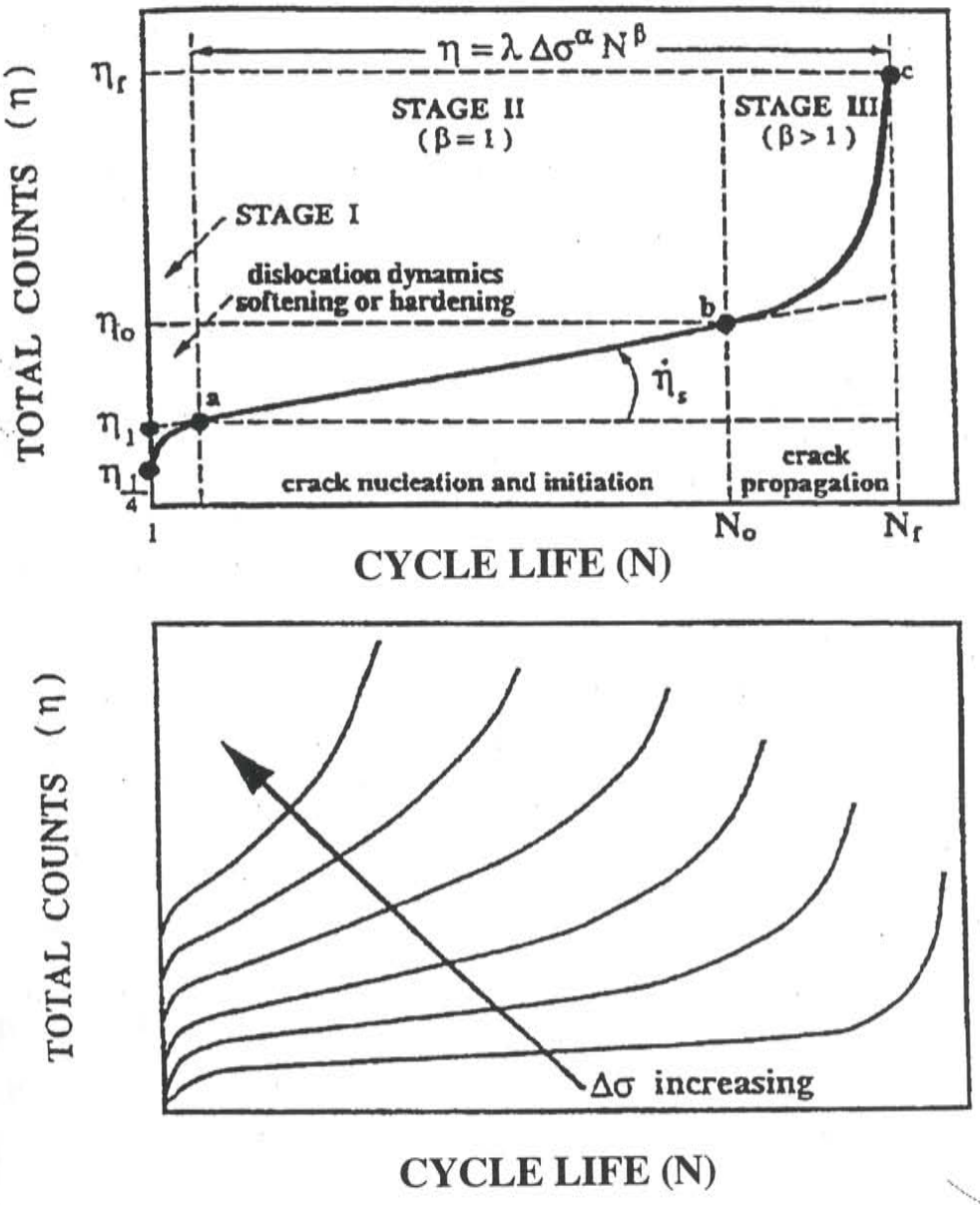

Figure 2.8: **AE Behavior During a Fatigue Test**

has a very similar form to the Paris law:

$$\frac{da}{dN} = C_2 \Delta K^{m_2}$$

where:

η is the cumulative AE counts,
a is the crack length,
N is the number of cycles,
ΔK is the range of K, and
C_1, C_2, m_1, m_2 are material constants.

Williams shows that for many cases, $m_1 = m_2$, leading to:

$$\frac{d\eta}{dN} \alpha \frac{da}{dN}$$

This means that AE during any period of time is proportional to the fatigue crack extension during that time. Although it was not done by Williams, this implies that might indeed be possible to calibrate AE to remaining fatigue life.

Whittaker[10] does exactly that. He describes tests performed on aluminum wedge-opening-loading specimens, which are fatgue-precracked. Whittaker analyzed the Felicity ratio from several different fatigue tests. The Felicity ratio (FR) for each cycle is defined by:

$$FR = \frac{\text{Load at Onset of AE During Current Cycle}}{\text{Maximum Load During Previous Cycle}}$$

A Felicity ratio of 1.0 is an indication of an undamaged specimen. Felicity ratios lower than 1.0 indicate damaged specimens. As a specimen undergoes fatigue damage, it would be expected that the Felicity ratio would progressively drop. Whittaker's data shows a very good correlation between the Felicity ratio and the remaining fatigue life, as shown in Figure 2.9.

In light of experience gained during laboratory experimentation, the author feels that counts might not necessarily be a good measure for estimating fatigue life, but rather energy, or perhaps signal strength. By looking at counts, the relative magnitude (or intensity) of the hits are ignored. For this reason, as seen in Chapter 4, the analysis portion of this research uses the change in energy with respect to number of cycles as a primary evaluation tool.

Siedlaczek et al[11] take quite a different approach. Their work surrounded low cycle (i.e., high $\Delta\sigma$) fatigue tests of unnotched structural steel tensile dogbone coupons. During the first few cycles, significant AE was generated, likely due to localized plastic flow caused by high stresses at small imperfections. As the test proceeds, the AE quiets down. Siedlaczek attributes this to dislocation density saturation (when so many dislocations are present that there is no way for all the dislocations to move, much like a traffic jam). When crack growth is initiated, AE begins to increase again. It is theorized that as new

crack surfaces are created, this allows dislocations to "escape" to the new free surface of the crack, permitting further crack growth.

The most common problem in AE monitoring of fatigue cracking is that AE from fatigue cracking is often masked by background noise. Researchers dealt with this problem in different ways Many of the researchers referenced used guard sensors. These are sensors placed near potential sources of

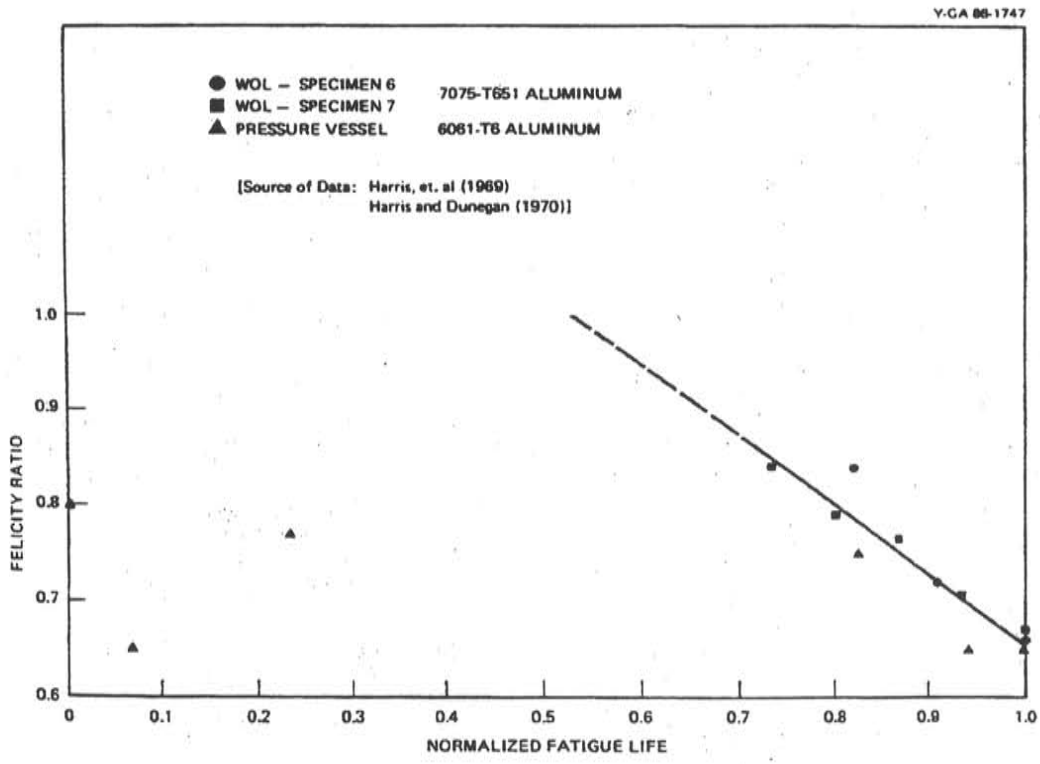

Figure 2.9: Correlation of Felicity Ratio to Fatigue Life

background noise. When they are hit with AE before the other sensors, they lock out the instrumentation so no AE is collected for a short period of time. The use of guard sensors in field testing has been generally discredited since the late 1980's for all common AE test procedures, since it often removes genuine AE occurring about the same time as the background noise. It is, however, still used for materials research applications in the laboratory environment.

Almeida and Hill[12] report on tests of aluminum tensile coupons with rivets (a source of rubbing noise) and notched in the center to initiate fatigue cracks. They trained neural networks to differentiate between rubbing noise and fatigue cracks. Using source location software to check their results, they report that events which occurred at the crack tip were correctly classified as fatigue cracks 95% of the time.

Scala et al[13] describe tests on an aluminum bulkhead of an aircraft. They also reported that AE from fatigue cracking was drowned out by the background noise. They used fracture mechanics principles to determine the most likely location of fatigue crack initiation. They then placed AE sensors nearby, and used localized source location techniques to filter out any noise that did not originate from these regions. This approach also appeared to significantly improve the results.

2.3 STRESS AND FRACTURE MECHANICS ANALYSES

The failures observed by the Navy all initiated at the load transfer point in the shafts, at the key and keyway interface. A traditional stress analysis is very difficult owing to the complex geometry of system as well as the fact that the load is being transferred to the shaft by subjecting the key in both bearing and torsion, which in turn subjects the transfer point to a combination of stresses including a significant amount of shear. In order to gain a complete understanding of the stress and strain fields, a finite element analysis was performed on a model of the specific geometry.

The fracture mechanics analysis is equally, if not more difficult. Traditional stress concentration factors K_I (tension), K_{II} (shear), and K_{III} (torsion) needed for the fatigue life calculations cannot be calculated manually given the geometry of the load interface and the manner in which it is being loaded. The complex stress field and its interaction with each of the stress concentration factors is not at all resolvable using single parameter fracture mechanics tools. This is nowhere more evident than in the shafts themselves. The surface breaking cracks observed in the shafts started from the corner of the keyway, and the crack proceeded into the volume of the material toward the shoulder in a curved fashion. The curved nature of the crack shows that no single K factor can be used to estimate the effects of the phenomena observed to be taking place. Approaches using multiple K factors in an "interaction" equation have been proposed by Broek[14] but only work using highly idealized boundary condition

CHAPTER 3

EXPERIMENTAL PROGRAM

3.1 GENERAL APPROACH

Two phases of laboratory testing were carried out at the Ferguson Structural Engineering Laboratory at the University of Texas at Austin. The laboratory testing afforded the opportunity to monitor the shafts under a variety of loading conditions in a controlled environment, and helped prepare for the field test that took place at the Pearl Harbor Naval Shipyard in Honolulu, Hawaii on a real Naval portal crane.

The purpose of the first phase of laboratory testing was to investigate the feasibility of using acoustic emission to find existing fatigue cracks in the crane shafts under static loading. The shafts were loaded in pure torsion, in a manner analogous to the way they would be loaded within the crane, and the acoustic emission generated was characterized. During this phase, background noise, test threshold, and acoustic attenuation were some of the parameters investigated to judge if the technology was suited to the application.

The second phase of testing incorporated and refined the results of the static loading phase with the goal of benchmarking AE from different size cracks and to learn if AE intensity increased as the crack grew and became more structurally significant. A secondary goal was to develop a better understanding

of the behavior and failure mechanism of the shafts under fatigue loading. The ultimate goal of the dynamic testing phase was to gain enough data and experience to write a standardized test procedure that could be used by the Navy's NDT personnel and contractors to examine and evaluate the crane shafts in-situ.

The knowledge and experience gained during both phases of testing was put to use during a field test at the Pearl Harbor Naval Shipyard in Honolulu, Hawaii in February 1997. The purpose of the field test was to demonstrate that the technology could be successfully used in a non-laboratory setting, as well as to validate and calibrate laboratory data for future field work. The field work provided an opportunity to evaluate the proposed standardized test procedure, and gave a good indication of the types of difficulties that would be encountered during future field testing, remedies for which were proposed in the final draft of the test procedure.

3.2 Static Loading Phase of Laboratory Testing

3.2.1 Test Frame

The static testing phase of the present research was not carried out by the author. However, it will be discussed presently as an understanding of the first phase is critically important to an understanding of the subsequent work. A complete report detailing the first phase of testing, written by the original researchers, can be found in the reference [12].

The setup for the acoustic emission tests was intended to put the shaft specimen in pure torsion. The exact dimensions of the test frame were designed for the particular geometry of the specimen from crane P-68 at Pearl Harbor Naval Shipyard, a four foot long full axle. The frame was also designed to be easily expandable, so that future experiments on partial axles, different length specimens, and different loading combinations could be conducted. This first test, however, did not incorporate any effects other than pure torsion.

The loading system was designed to mimic the actual end support conditions of the axle found in the field. Thus, torsion was introduced by locking into a mechanical keyway, rather than welding a plate to the end of the axle. This also allowed for other nondestructive examination tests during and after the acoustic emission tests, with no change in the original axle.

The test setup is shown in Figures 3.1 and 3.2. The axle is placed horizontally in the frame. It is supported and loaded by two end blocks keyed into the front and back, which were specially machined to the dimensions of the axle. At the back end, the end block was sized so that it would lock between the flanges of a W12×40 steel column, and thus be restrained from rotating. The only other reaction at this end is a bearing-only connection onto a steel tube section below, with an elastomeric bearing pad. Therefore, this back end can resist torsion and the dead load of the specimen, but does not restrain the shaft with a bending moment.

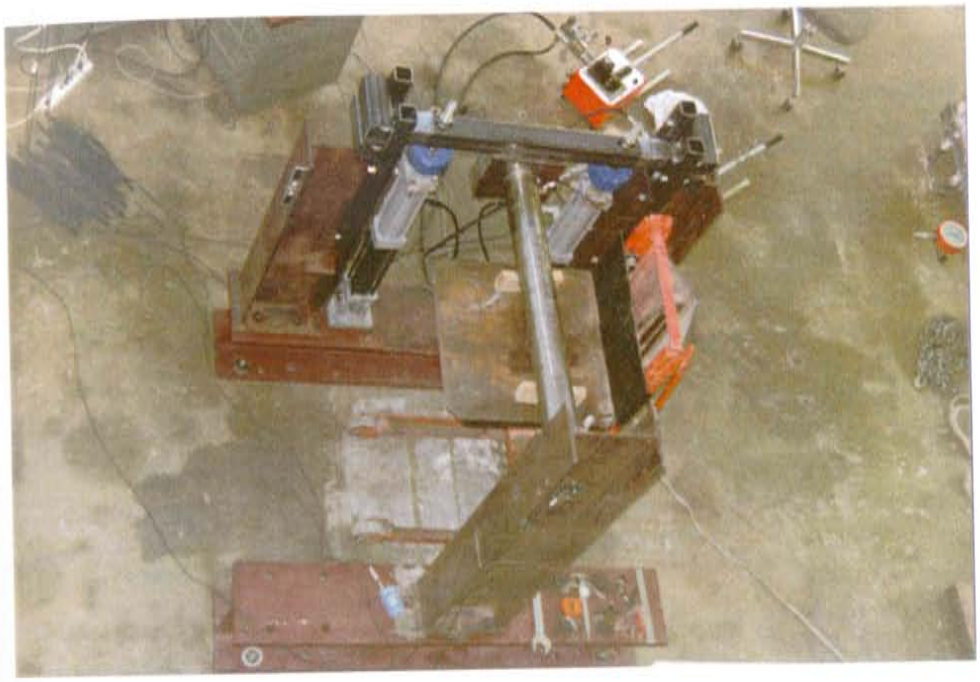

Figure 3.1: Test Setup During Static Loading Phase. View from Above.

The front end is also locked into an end block, but this end block is welded to a tubular steel arm that is supported on two reversible hydraulic rams. The rams are Model 10023 Double-Acting Hydraulic rams made by Shore Western Manufacturing. They have a maximum capacity of 50 kips. The rams are pressurized by two PowerTeam Series P460 two-speed hydraulic hand pumps, operated in unison by a single operator. The load in each ram was measured with load cells.

Figure 3.2: Loading End of Test Frame. View from Front End.

The steel tube at the front is "braced" with steel guides at each end to prevent out of plane rotation when the specimen is under high torsional loads. The braces are mounted to W12×40 columns, one on each side of the rams. All W12×40 columns and rams are bolted to frond and back W12×150 base beams, which in turn are bolted to a concrete reaction floor.

The test frame and rams were designed to apply a load of 200 in-kips of torsion to the specimen. This is twice the design load of 100 in-kips, which provides additional capacity to increase the loads past the design loads if desired, or to test different specimens in the future.

3.2.2 Loading

Examination of the free body diagram in Figure 3.3 clarifies how torsion is introduced into the specimen. Essentially, the torsion is introduced by putting one ram in tension and the other in an equal amount of compression. As one ram piston is slowly raised and the other is slowly lowered, statics requires the two forces to be equal and opposite. This force couple is resisted by the end blocks at the other end with the torsional load being transmitted through the specimen.

The test was setup so that the shaft could be subjected to both clockwise and counterclockwise torsion. Figure 3.3 shows the details of the loading scheme used. It may be observed that the torsional loads were applied in the clockwise and counterclockwise directions in turn, with a maximum load of 50 in-kips, one half of the design load.

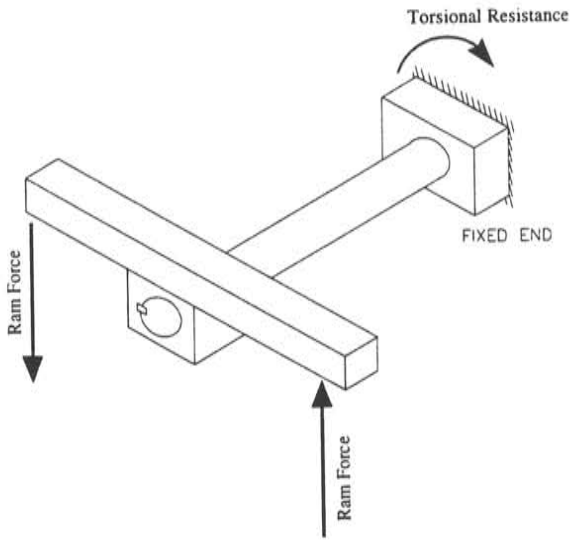

Figure 3.3: Loading Scheme Used During Static Loading Phase

The load was applied in a series of steps with intermediate load holds. Clockwise and counterclockwise (when viewed from the front of the stand) loads were alternated. This loading scheme was chosen to allow analysis of loading data, load hold data, and the Felicity effect. Loading was performed over a number of days rather than the 5,000 seconds shown in Figures 3.4 and 3.5. For purposes of analysis and display, however, the periods between tests are not important and have been omitted. The first series of tests consisted of clockwise loading to 10 in-kips, followed by a counterclockwise loading to 30 in-kips, and a clockwise loading to 30 in-kips. Following these tests, the data was analyzed to determine if modifications to the test rig or test procedure were required.

Analysis showed the data to be genuine and further tests were conducted to the 50 in-kip load level.

The data obtained during clockwise loading was considered as a single set of data for analysis purposes. Similarly, the counterclockwise data was also considered as a single data set. The loading for each direction was considered in conjunction with these data and is shown in Figures 3.4 and 3.5. For each load direction, the periods when load was applied in the opposite direction, when analysis was being conducted, and when no testing was being performed are shown as a nominal time at zero load.

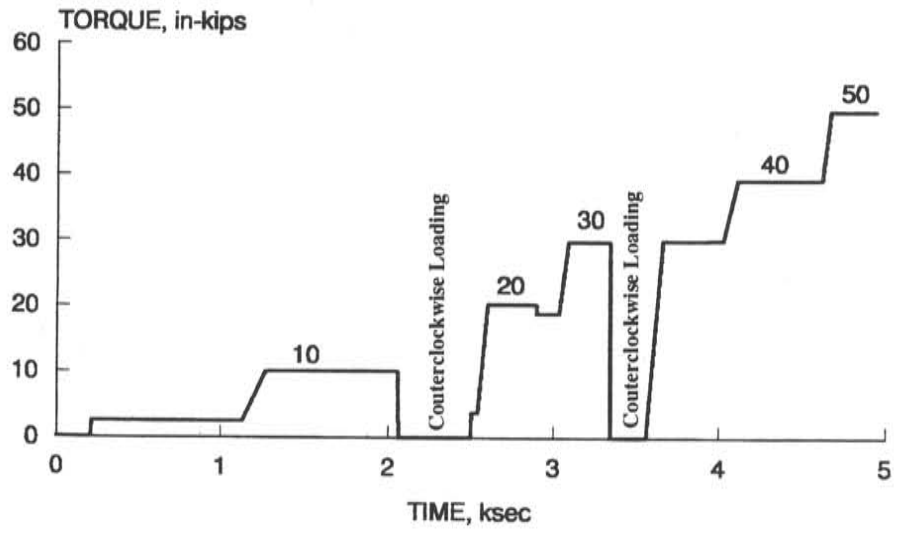

Note: For display purposes, time periods for counterclockwise loadings have been shortened and are shown as periods of zero load.

Figure 3.4: Static Clockwise Loading

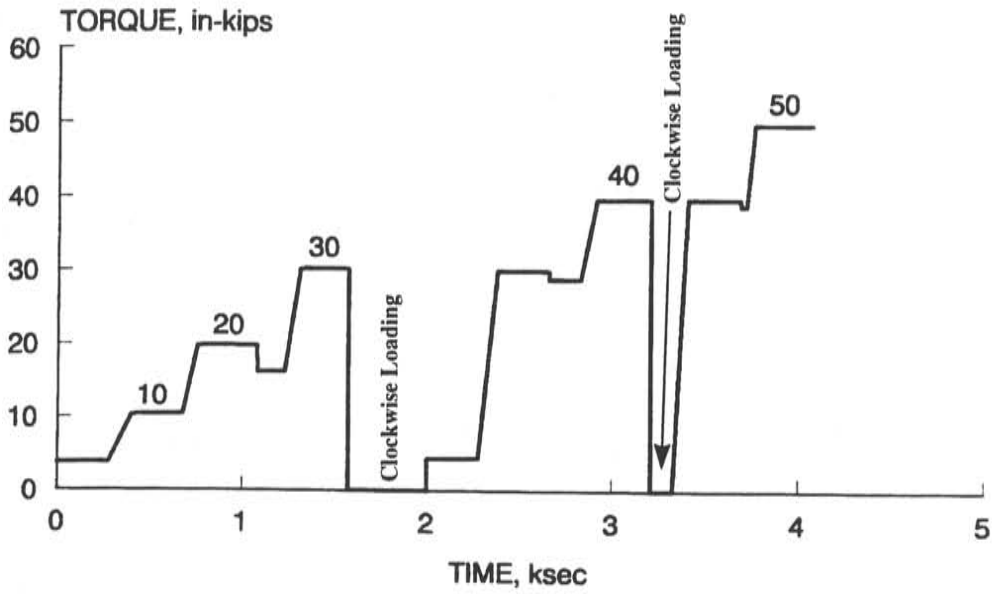

Note: For display purposes, time periods for clockwise loading... etc. have been shortened and are shown as periods of zero load.

Figure 3.5: Static Counterclockwise Loading

3.2.3 Instrumentation

Two acoustic emission instruments were used to acquire data. The first, shown in Figure 3.6, is a two-channel LOCAN AT instrument, manufactured by Physical Acoustics Corporation (PAC). It is an analog instrument, with an Intel 8 MHz 8086 CPU. Sensors were R15I resonant sensors (resonant at 150 kHz), also manufactured by PAC. The sensors, thresholds, gains, and other settings for this instrument were set to match those common in the acoustic emission field testing industry. These settings are detailed in Table 3.1.

Figure 3.6: LOCAN AT Analog Acoustic Emission Instrument

The other instrument was a four-channel MISTRAS-2001, shown in Figure 3.7, also manufactured by PAC. This is a digital instrument, based on an 166 MHz Intel Pentium CPU system, and capable of recording and saving the digitized waveform of each signal it reads. In this test, acoustic emission data was sampled every 500 nanoseconds. This system was connected to several different types of sensors, to investigate the effect different sensors had on the signal received. Again, thresholds, gains, and other settings for this instrument were set to match those common in the acoustic emission field testing industry, and where possible the same as used on the LOCAN AT. These settings as well, are detailed in Table 3.1.

Figure 3.7: MISTRAS-2001 Digital Acoustic Emission Instrument

At the front, an S9208 broadband sensor was used. At the rear, a very low frequency RA2 accelerometer with a resonant frequency of 20 kHz was used. In addition, R30I resonant sensors (300 kHz) were used front and back. These high frequency sensors were used to take advantage of the greater attenuation of high frequency signals to reduce the number of reflections in this relatively small specimen. The R15I and R30I sensors had integral preamplifiers with 40 dB gain. Separate preamplifiers, set for 40 dB gain, were used for the RA2 accelerometer and S9208 sensor. The sensor layout used is shown in Figure 3.8.

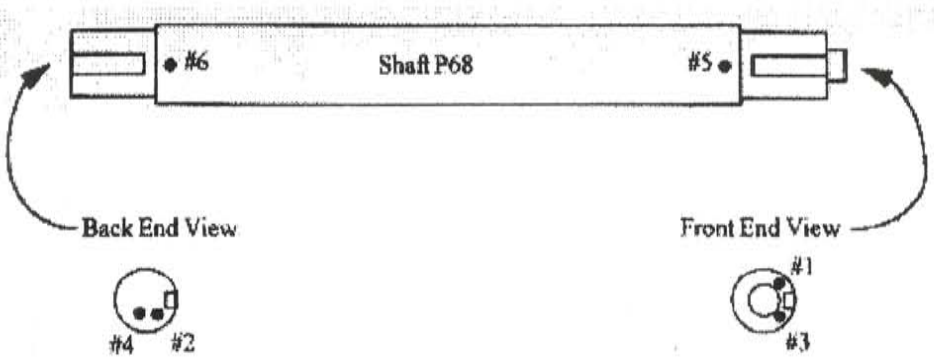

Channel	Instrument	Sensor Designation	Sensor Type
1	MISTRAS	S9208	Broad Band
2	MISTRAS	RA2	Low Freq. Resonant
3	MISTRAS	R30I	High Freq. Resonant
4	MISTRAS	R30I	High Freq. Resonant
5	LOCAN	R15I	Standard Resonant
6	LOCAN	R15I	Standard Resonant

Figure 3.8: Sensor Placement on Shaft

Table 3.1: Instrument Settings Used During Testing

Setting	*20 & 150 kHz Sensors*	*300 kHz & S9208 Sensors*
Threshold	45 dB	45 dB
Sample Rate*	4 MHz	8 MHz
Pre-Trigger*	20 µsec	20 µsec
Hit Length*	1000 µsec	1000 µsec
***Peak Definition Time** (RTTO)*	200 µsec	200 µsec
Hit Definition Time	400 µsec	400 µsec
Hit Length Time*	1000 µsec	1000 µsec

* Only used with Digital Instrument

The sensors were attached to the shaft using hot melt glue. Before testing commenced, pencil lead breaks were performed next to each sensor, as set out by ASTM E1316, to ensure the acoustic coupling was adequate, and that the sensor was functioning properly.

3.2.4 Summary of Results

The exact details of the data and analysis methods used can be found in the reference[12]. The following is a summary of the results and conclusions reached in Phase I, as they pertain to the second phase of testing:

1. Acoustic emission can be used to detect fatigue cracks in crane shafts. Defects were detected in the crane shaft from Naval Portal Crane P-68.
2. A major structural defect, probably a fatigue crack, was detected at the back end of the shaft.
3. A less significant structural defect was detected at the front end of the shaft. It is probable that this defect is also a crack.
4. Both indications were detectable at a small percentage of the design load.
5. The indications were active under clockwise loading. Significant activity was also observed under counterclockwise loading. It is probable that this activity is due to reverse compression yielding at the tip of the crack.

6. 150 kHz sensors are sensitive to the emission and can be used for testing crane shafts. Emission was readily detectable at thresholds commonly employed in field testing.
7. In the event of background noise, 300 kHz sensors will provide adequate coverage of the crane shafts.
8. The Jolly-Stuart zonal source location technique makes it possible to distinguish which end of the shaft is the source of the emission.
9. The test frame can be used to test a range of crane shafts. Background noise from the loading frame and movement of the shaft and keyway was insignificant.
10. There is a high probability of success that a practical field test procedure can be developed.

3.3 Dynamic Loading Phase of Laboratory Testing

3.3.1 Test Frame

For the dynamic testing phase, the test frame had to be extensively modified. While it was originally thought that the frame could be used in the exact form it was in during the static testing phase, initial trials showed that modifications had to be made.

An automated control system consisting of an MTS 407 Programmable Electronic Controller and a MTS 293 Hydraulic Manifold was used in place of the hand pumps previously connected to the rams. These are shown in Figure

3.9. The controller and hydraulic system allowed for the load to be cycled at any given rate. The system was under load control, with feedback from load cells in the rams governing the amount of load applied. The electronic controller passed the load level through an output which was in turn used as a parametric input for the acoustic emission instrumentation.

Figure 3.9: MTS Automated Controls Systems, as implemented

During initial trials it was found that there was too much play between the shaft and frame, and the frame itself was not stiff enough under the rapidly applied cyclic loads. One of the main problems was the way the back end of the shaft was restrained. From the foregoing description of the static loading phase

setup it was established that the end blocks at the back end of the shaft transferred the torsional load to the floor by doubly bearing on the flanges of wide flanged rolled section, and transferred its dead load by using a slender column member. While this setup was perfectly adequate for the case of the shaft being loaded and unloaded slowly, when attempted with any speed, much movement and associated noise was observed. To remedy the problem, a frame at the back end of the shaft was setup to resist the torsional load. In essence, the end blocks were welded to a cross beam which was in turn welded to two stub columns. The setup was similar to that at the front end of the frame, except the stub columns replaced the loading rams to resist the load rather than apply it. The new restraint system was much stiffer, and also served to carry both the torsional load and the gravity load to the reaction floor below. The modified frame is shown in Figure 3.10.

Figure 3.10: Test Frame Modified for Dynamic Loading

Background noise during the dynamic loading was much more of a problem than during the static loading. Rapid movement of the loading rams, shaking of the frame, and movement within the key and keyway system all contributed to the problem. As much of the noise as possible was removed, however, in many cases this was impossible, and a scheme to acoustically isolate the shaft from the remainder of the test frame was adopted. Teflon pads were placed at all metal to metal contact points, as shown in Figure 3.11. Additionally, the existing key was replaced with a new, tight fitting one to minimize movement during load reversal.

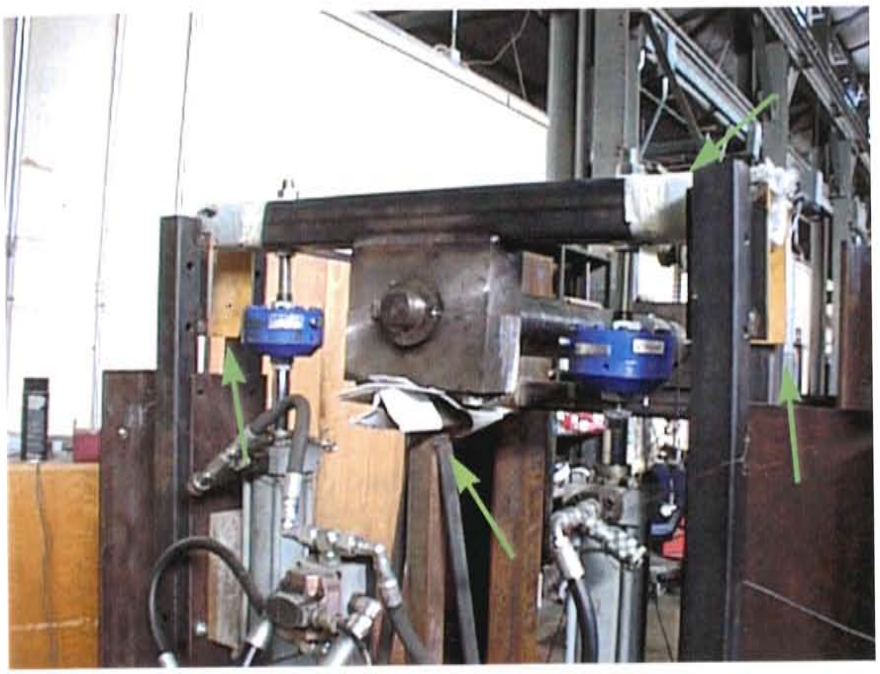

Figure 3.11: Teflon pads were applied to acoustically insulate the shaft from the frame.

3.3.2 Loading

Loading of the shaft consisted of 4,500 cycles at each load level starting at 40 in-kips working up to 100 in-kips in increments of 5 in-kips. A 10% overload was applied every 1,500 cycles. Additionally, a single overload cycle of 150 in-kips was applied at the end of the testing regime. The loading envelope is shown in Figure 3.12.

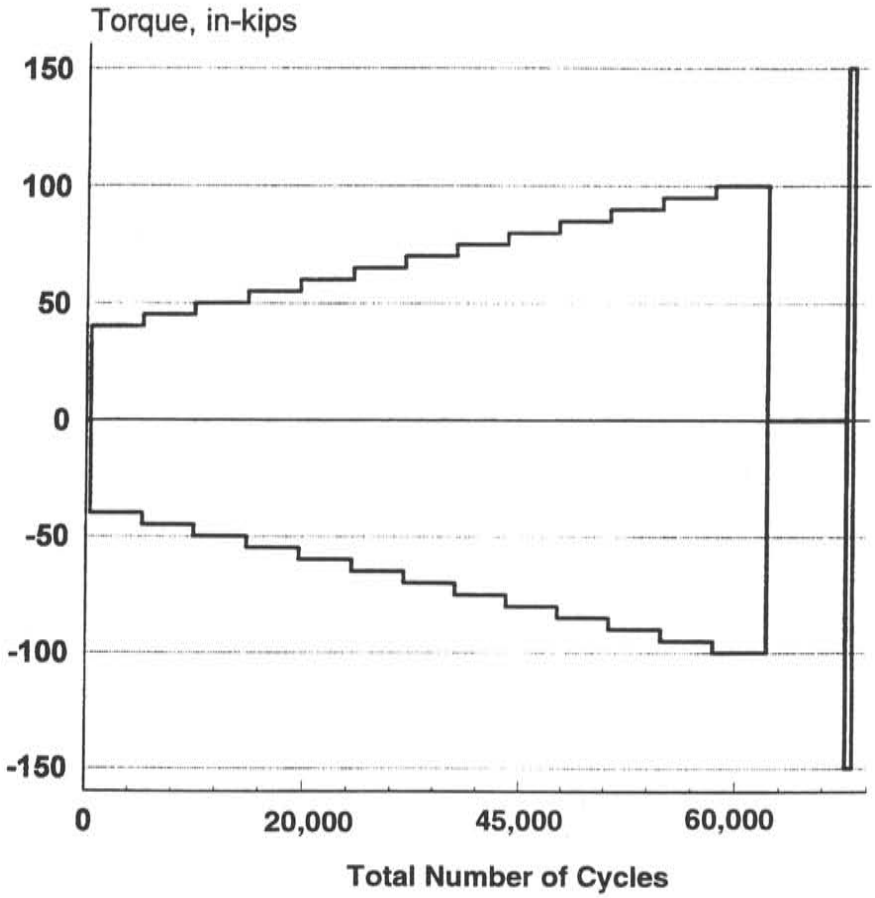

Figure 3.12: Loading Envelope used During Dynamic Testing Phase

Cycling took place at a rate of 0.17 Hz, or six cycles per minute with continuous AE monitoring. The MTS control system was programmed for a square waveform, thus incorporating a load hold at the peak positive and peak negative load during each cycle. A typical load history is shown in Figure 3.13.

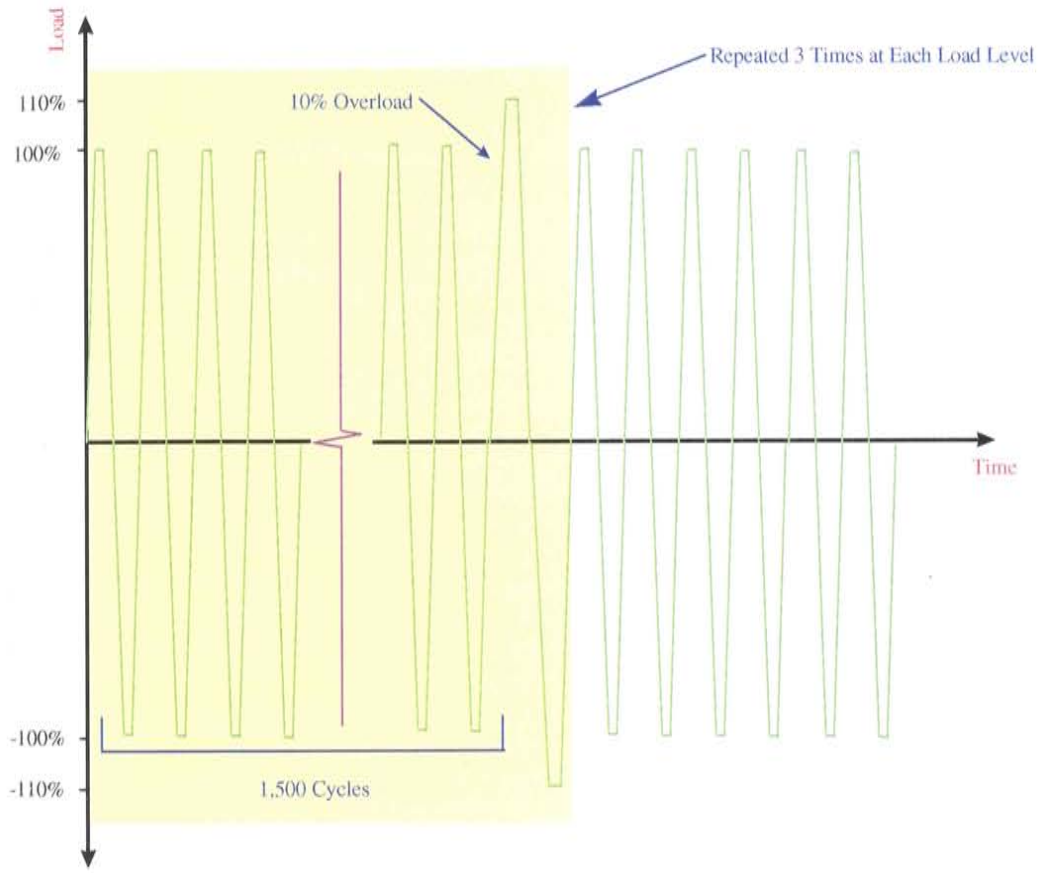

Figure 3.13: Typical Loading Scheme During Fatigue Cycling

Overloads of 10% of the fatigue load were manually applied every 1,500 cycles. The purpose of the overload was to obtain AE data from an overload of a growing crack. This provided data for the standardized test procedure and calibration of the acceptance criteria and intensity plots. The overload was applied by manually adjusting the set point of the rams using the control knob on the MTS 407 Digital Controller. As can be observed in Figure 3.12, the load is

applied extremely rapidly when the automated square waveform is used. For the overload cycles it was felt that a slow application of the load was better suited to the purpose, as the Felicity effect and other load based parameters could be more accurately ascertained. Additionally, applying the load slowly further minimized the amount of frame borne background noise originating from the rapid movement of hydraulic fluid into and out of the rams, and the subsequent vibration in the stand. The slow loading rate is how the load is applied in the field tests, as well. Because of the higher load being used and the relatively small number of times the shaft was subjected to an overload at each fatigue load level a load hold of 90 seconds was used. An idealized Load vs. Time graph for the overload cycles is shown in Figure 3.14. AE monitoring was done throughout the entire cycle.

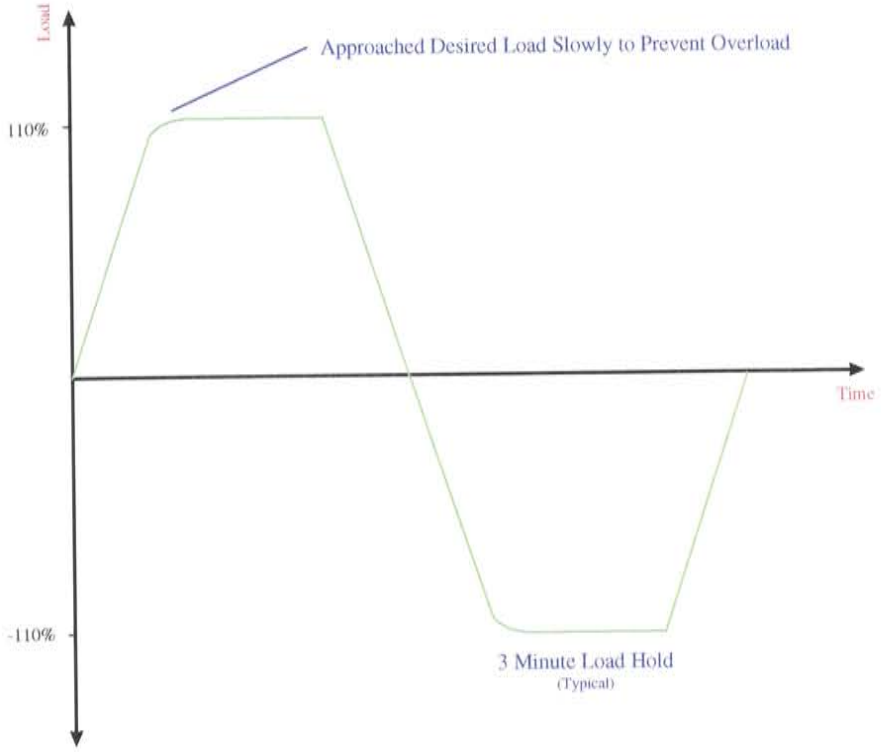

Figure 3.14: Load vs. Time for an Overload Cycle

3.3.3 Instrumentation

In the dynamic testing phase a six channel MISTRAS-2001 digital acoustic emission instrument was used to acquire data. The initial promise shown when using the four channel digital instrument during the first phase of testing played a large role in the decision to go exclusively digital. Another reason supporting the use of the digital instrument is that it could emulate the traditional analog instrument (i.e., not capture waveforms) but the converse cannot be said. The instrument settings described in Table 3.1 were used again

during the second phase of testing, however the sensor types and thresholds used were optimized based on the initial trials which showed problems with noise due to the inherently more noisy environment of dynamic fatigue testing, and other problems experienced with the RA2 accelerometer and S9208 broadband sensor during the static loading phase of experimentation.

The first phase of testing showed that the 150 kHz and 300 kHz integral resonant sensors captured all the data of interest. Based on this fact, and previous negative experiences with broadband sensors and accelerometers in terms of sensitivity and background noise, the choice was made to use exclusively the R15I and R30I sensors. Another factor in this decision was that the data being collected in the lab during the dynamic testing phase was to be used in preparing for an actual field test, and the writing of a field test procedure. A majority of field testing procedures use the 150 kHz and 300 kHz resonant sensors, exclusively.

A placement scheme was developed based on pencil lead breaks as shown in Figure 3.15 and Figure 3.16. Sensors are placed at each end of the shaft at the shoulder region near the end of the keyway. Placing the sensors only at the end of the shaft is consistent with all of the observed failures in the field, which started at the end of the keyway. The edge spacing of the sensors from the shoulder was incorporated to prevent loss of data due to the shadow zone created by the geometry of the shoulder. In order to assure full acoustic coverage of the region of interest, the sensors around the circumference were mounted 120° from each other, as shown in Figure 3.16. Another factor in choosing the mounting scheme was the ability to implement it in the field. The

shaft ends are rarely accessible when the shaft is mounted in the crane, and thus the additional flexibility afforded by having the sensors some distance back from the shoulder help to make the technique more widely applicable in the field.

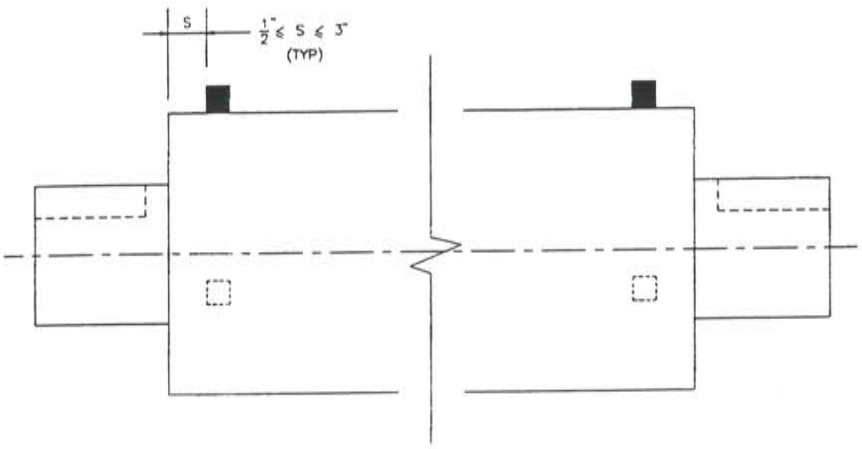

Figure 3.15: Sensor Placement Along the Length of the Shaft

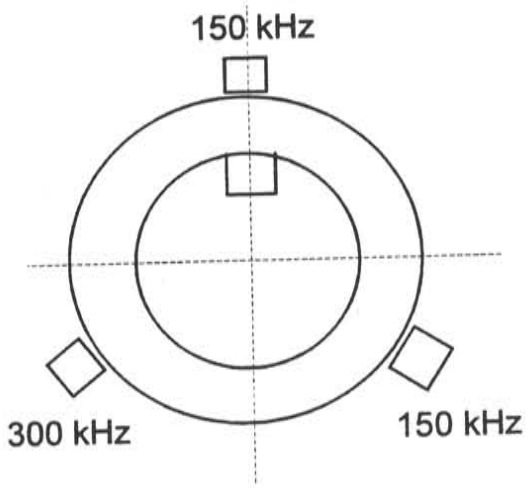

Figure 3.16: Circumferential Sensor Mounting Schematic

The sensors were attached to the shaft using a thin layer of hot melt glue, as was the case during the static loading phase. Before the sensors were attached, the area where the sensor would be mounted was thoroughly cleaned of all rust and debris, especially greasy residues. This was accomplished by means of sanding the surface of the shaft lightly with fine grained sandpaper, and then wiping the area with a paper towel wetted with an environmentally acceptable degreasing solvent, then allowed to air dry. Figures 3.17 and 3.18 show the sensors mounted on the shaft in the laboratory.

Figure 3.17: Mounted Sensors at Front of Shaft

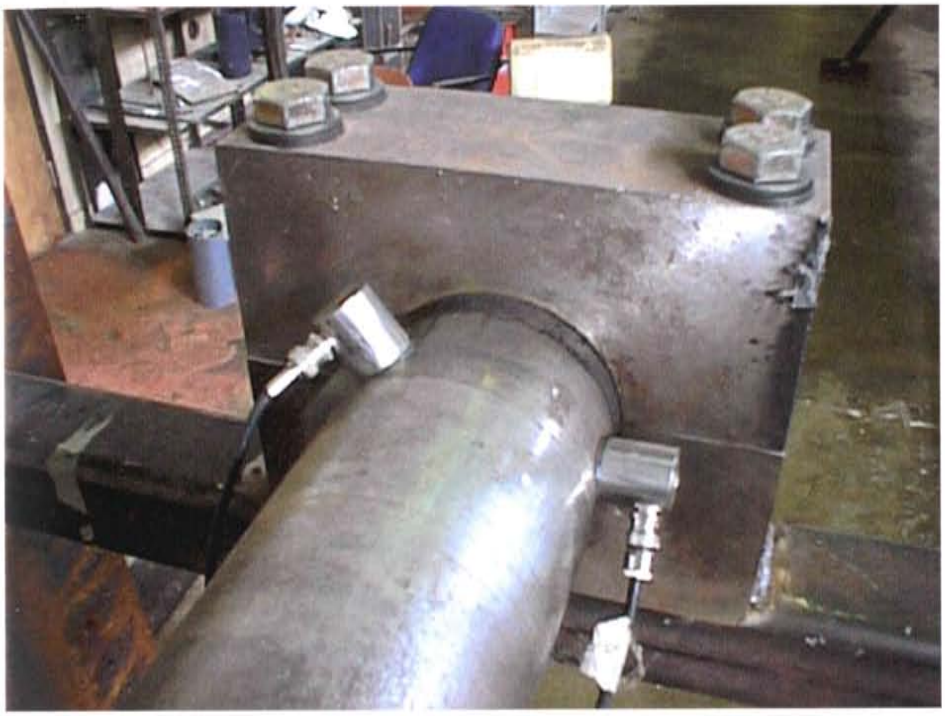

Figure 3.18: Mounted Sensors at Rear of Shaft

Following standard ASTM procedure, pencil lead breaks were performed adjacent to each sensors to ensure that each sensor was adequately coupled, attached and functioning properly. This procedure ensured that the hot melt glue was not too thick, and that the full sensor face was in contact with the shaft. As a matter of interest, pencil lead breaks were performed down the length of the shaft in increments of approximately 6 inches in order to attempt to characterize the acoustic properties of the shaft. Lead breaks performed anywhere on the length of the shaft were picked up by all sensors, with varying amplitude,

confirming that attenuation was not a problem and emission anywhere in the shaft would be picked by at least one of the sensors.

3.3.4 Testing

Tests were conducted on a different rotate pinion shaft than was used during the static loading phase of testing. The rotate pinion drive shaft used for the dynamic testing phase was taken from crane P-66 at the Pearl Harbor Naval Shipyard. It was taken out of service during maintenance when the same shaft in its sister crane, P-65, was found to be cracked. Navy NDT personnel were unable to ascertain precisely if the shaft in crane P-66 was at all damaged using conventional nondestructive examination techniques.

Testing took place over the period of January through October, 1997. Much of the first few months were devoted to modifying the test frame and preparing for the field test at the Pearl Harbor Naval Shipyard.

Both fatigue loading and overloading were monitored; in total over 60,000 cycles. The immense amount of data generated was stored on the computers hard disk drive, and routinely burned onto compact disc for subsequent analysis, and long term storage.

3.4 THE FIELD TEST

3.4.1 Background

An acoustic emission test was conducted on crane number P-64, a Meyerstein 50 ton portal crane. The crane had recently been pulled from service due to a vibration problem detected by the operator during main hoist drum motion under load. A sister crane, P-63, was also pulled from duty at the same time. In-situ ultrasonic testing indicated the presence of cracks in the crane shafts, but this result was not confirmed my magnetic particle inspection. Shafts were removed from P-63 and sectioned, but cracks were not found.

Pearl Harbor Naval Shipyard has many cranes, of which only a small handful are currently in service – the remaining cranes are in need of maintenance or repair. The Navy was interested in returning crane P-64 to duty, but first needed to determine if the crane was safe to operate.

In previous tests conducted by the Navy, vibration sensors were mounted on the main hoist shaft face and drive gearbox. Vibrations were detected, and the vibration frequency matched the meshing frequency of the drive gear. The vibrations were observed during movement of the shafts while lifting a load. During the load tests performed as part of the present research, no such vibrations were observed.

3.4.2 Scope of the Test

During the tests performed, AE data was collected on the following shafts:

- Main hoist drive shaft (length ~5 feet)
- Main hoist drum shaft (length ~13 feet)
- Boom hoist drive shaft (length ~5 feet)
- Boom hoist drive shaft (length ~13 feet)

Data was collected during two loading schedules. Each schedule followed the following sequence:

1. The crane was loaded to a nominal load value (~10% of rated capacity).
2. The load was increased and held for 5 minutes.
3. The load was decreased to the nominal value.
4. Steps 2 - 3 were repeated until the maximum test load was reached.

Figure 3.19 shows the loading schedule graphically.

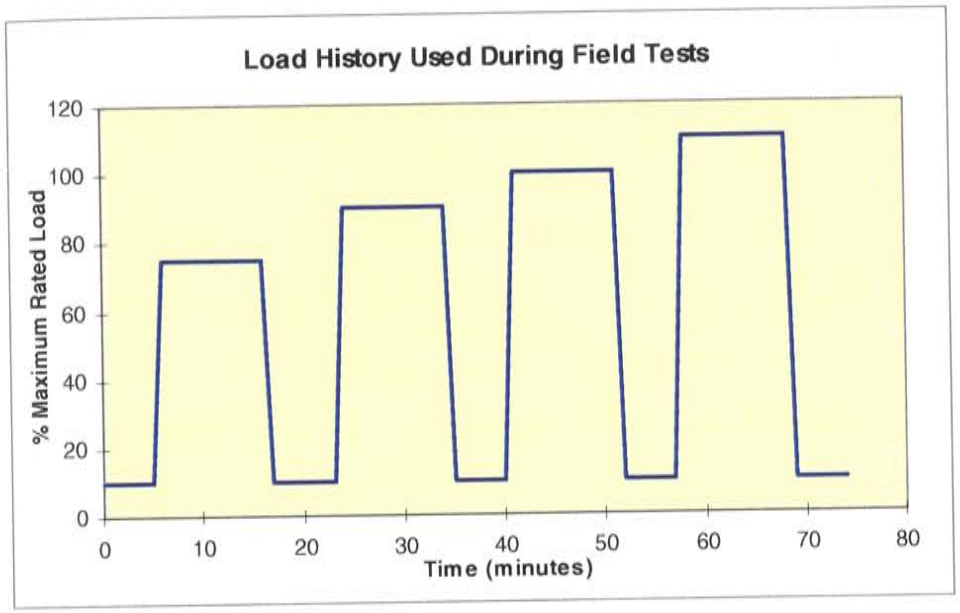

Figure 3.19: Load History used for Field Tests

3.4.3 Loading Strategy

To avoid the complication of shaft (and AE sensors) movement during testing, the main hoist was connected to a 126,000 lb. assembly of certified weights. It was originally intended that this load would exceed the amount of load to be applied during testing, and thus would never be physically lifted. This was the case during the testing of the main hoist shafts. The load load was applied by "booming up", or attaching the main hoist to the weights and raising the boom to apply load. Thus, the main hoist shafts did not move significantly during the main hoist shaft tests.

During the boom hoist shaft tests, the load cell failed during the execution of the load schedule. This failure was probably due to a short in the cable that ran from the load cell to the crane cab - the cable broke at one end after the test was complete.

Failure of the load cell left the crane operator "blind" with respect to the amount of load being applied. The entire load of certified weights was thus lifted completely off the ground, causing the crane to experience higher loads than had been planned. This unforeseen event did have some advantages:

1. The crane probably have never lifted a load this large - this load exceeded the maximum annual certification load of 100% = 55 long tons = 123,200 pounds. AE testing is most effective if the test article has not experienced the load in recent history.
2. Because certified loads were lifted completely off the ground, the final maximum load was well established even though the load cell failed.

3.4.4 Main Hoist Shaft AE Test

During the first test, the main hoist drive shaft and the main hoist drum shaft were instrumented with AE sensors, and AE data was collected continuously throughout the execution of the load schedule. During this test, the boom was held at minimum radius. According to engineers at the shipyard, this reduced the load experienced by the boom hoist to 50% of the value that would occur if the boom were held at maximum radius. This was carried out because

acoustic emission is in a sense a "one time" occurrence, and the best data is collected when the structure under study is experiencing a load larger than any loads lifted during its recent load history. Thus, the boom could be set to maximum radius during the evaluation the boom shafts, and the boom drive and drum shafts would see a higher maximum load than they did during the main hoist test.

3.4.5 Boom Hoist Shaft AE Test

During this test, the boom was extended to maximum radius, and the boom drive shaft and drum shaft were instrumented with AE sensors, These sensors were monitored continuously throughout the load schedule.

Loads were applied to the boom by applying force to the main hoist cable, which was attached to the 126,000 pound load. In this manner, a load could be applied to the boom without moving the boom drum or drive shafts.

3.4.6 Advantages and Disadvantages of the Loading Schemes

The primary advantages of the loading schemes used in the two tests were:

1. The shafts under test did not rotate, thus avoiding problems with sensor cables running to the sensors attached to the shaft.
2. It was possible to bring the main hoist to maximum load while experiencing only a 50% maximum load on the boom hoist.

Disadvantages included:

1. It required a long time to complete the tests, since the load schedule had to be repeated twice.
2. The drum shafts were not rotated. They experienced a unidirectional bending moment where the ends of the drum meet the shaft, as the cable tends to "lift" the drum free of its mounts (bearings at each end of the shaft).

This situation raised concern that the drum shafts were not completely tested. Since the bending moment was applied in only one direction, it was feared that a crack might be in compression, thus not providing a detectable AE signal. This was a valid concern, and required careful consideration, and a refined method of loading the shaft, as can be found in the proposed standardized testing procedure included in the appendix. The following is a summary of some of the important information:

1. As the main hoist and drum shafts rotate during the raising and lowering of loads, the bending moment load is applied over the full 360° of shaft rotation. This should encourage radially symmetric crack initiation sites that are equally dispersed in all radial directions. This type of crack growth has been seen to be responsible for sudden catastrophic failures, and is well documented in Navy reports.[1]

2. Note that the boom shafts are different from the main hoist shafts, which rotates during the raising and lowering of loads. Boom shafts only move when the boom is raised or lowered. The boom may experience more frequent loading at the particular drum and drive shaft orientations associated with maximum and minimum boom angle, or some other angle preferred by a particular crane operator.

3. Acoustic emission is most commonly associated with cracks under tension. However, AE can be generated during compression by compression yielding, crack closure, or crack face rubbing.

3.4.7 Instrumentation

During the first test, AE sensors were placed on the main hoist drum shaft and the main hoist drive shaft. In the second test, the sensors were mounted in the same manner on the boom hoist drum and drive shafts. The layout of the sensors is shown schematically in Figures 3.20 and 3.21.

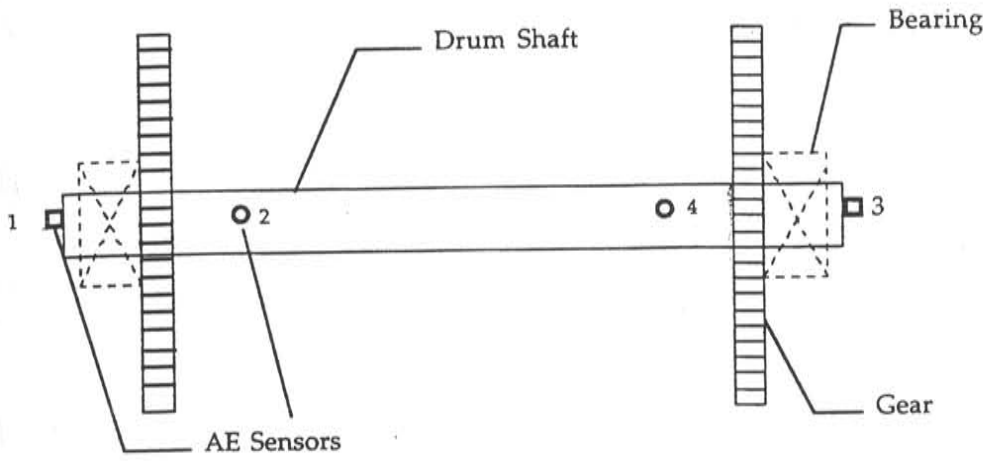

Figure 3.20: Schematic Layout of AE Sensors on the Drum Shaft

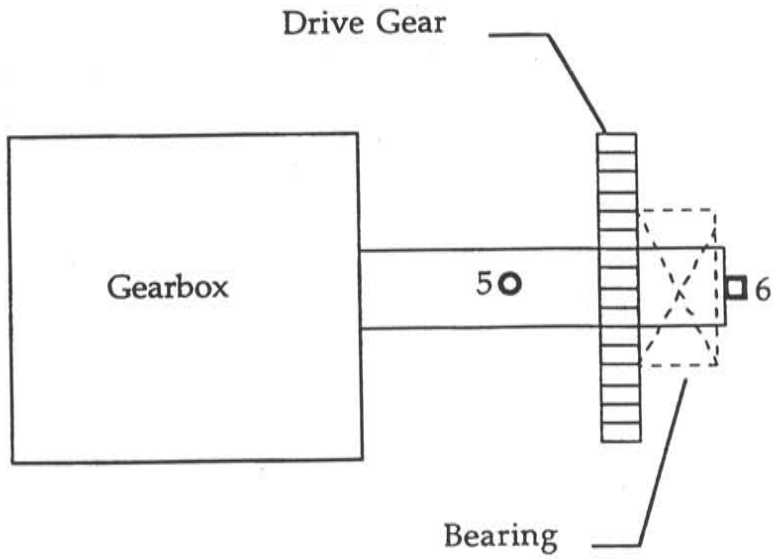

Figure 3.21: Schematic Layout of AE Sensors on the Drive Shaft

The sensor type and placement in Figures 3.20 and 3.21 was as follows:

Type:

Numbers 1, 3 and 5: Broad Band Sensors

Numbers 2, 4 and 6: 150 kHz Resonant Sensors

Location:

Numbers 1, 3 and 6: Located on shaft ends

Number 2: Located 18" from nearby drum shaft end (main host test)

Number 4: Located 15" from nearby drum shaft end (main hoist test)

Number 5: Located 21" from end of drive shaft (main hoist test)

Number 2: Located 16" from nearby drum shaft end (boom hoist test)

Number 4: Located 19" from nearby drum shaft end (boom hoist test)

Number 5: Located 16" from end of drive shaft (boom hoist test)

All six sensors were monitored using the PAC MISTRAS digital AE monitoring equipment.

3.4.8 Sensor Mounting

Once the location for an AE sensor was determined, files and sandpaper were used to remove the paint and reveal the bare metal of the crane shaft. The

exposed metal was then cleaned with environmentally acceptable grease solvents to achieve the cleanest possible surface.

Hot melt glue was used to attach the sensors to the crane shafts. It has the advantage of quick set, and can be removed easily using bare hands. However, there is some evidence to suggest that care must be taken when using this type of glue. After initial sensor placement and preliminary lead break tests, two sensors on the main spool shaft were found to be improperly coupled, and were thus remounted. These sensors had been mounted the night before and seem to have lost some coupling overnight. After remounting these two sensors, another preliminary pencil lead breaks series was conducted and it was discovered that, in the process of reattaching these sensors, a brush against one of the sensors caused by the limited maneuvering room in the crane machinery room caused another sensor to come unattached. This sensor was also remounted and the pencil lead breaks were performed again. Afterwards, all sensors met the required parameters, so the final pencil lead breaks, PAC pulser, and Dunegan cracker procedures (see section 3.4.12) could be performed. Figures 3.22 through 3.25 show some typical mounting techniques used while in the field. Note, in some of the photographs shown in Figures 3.22 through 3.25 two sensors are shown where only one is indicated on the schematics in Figures 3.20 and 3.21. This is because multiple sensors types were tested, although only one sensor was used at a time during data collection.

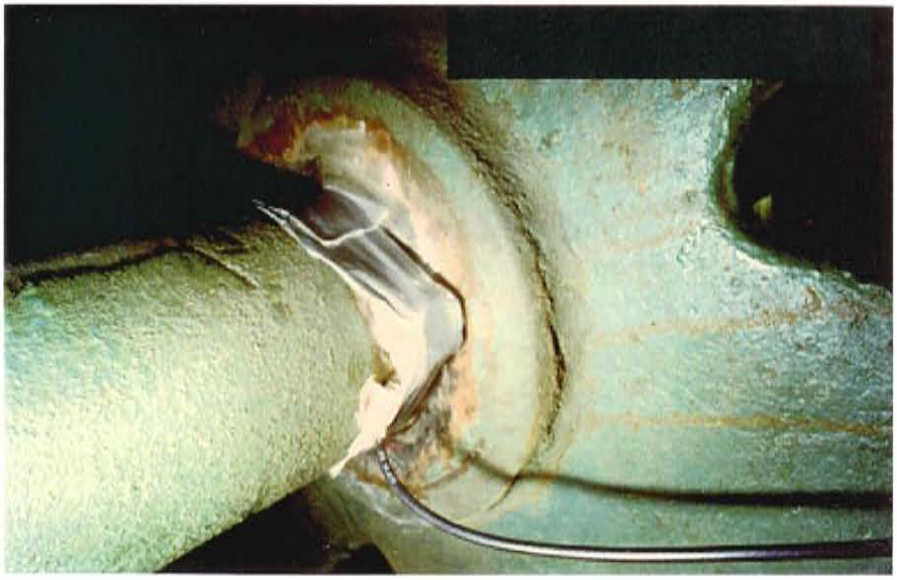

Figure 3.22: **Sensor Attached to Main Hoist Drive Shaft and Secured with Duct Tape In Case of Inadvertent Shaft Rotation**

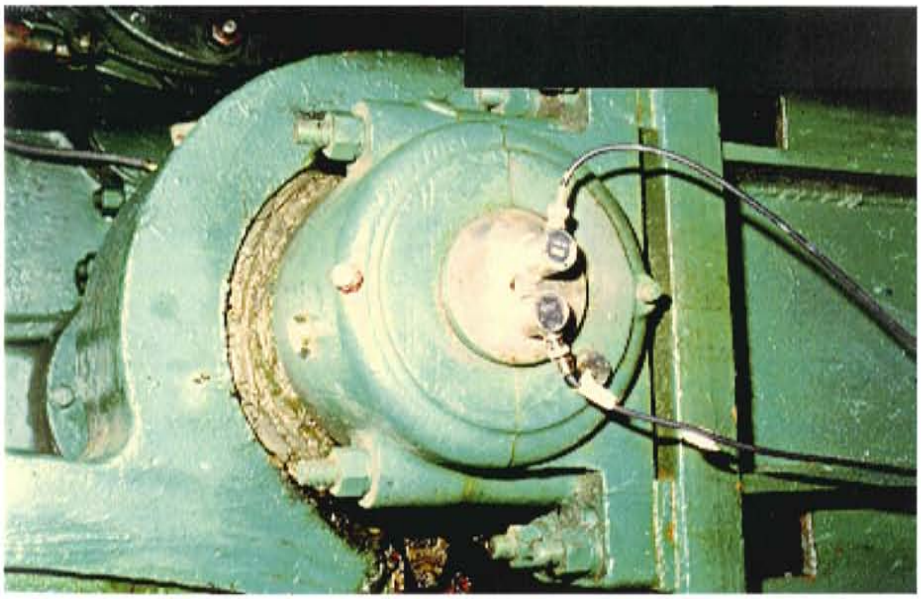

Figure 3.23: **Sensors Attached to Exposed End of Boom Hoist Drum Shaft**

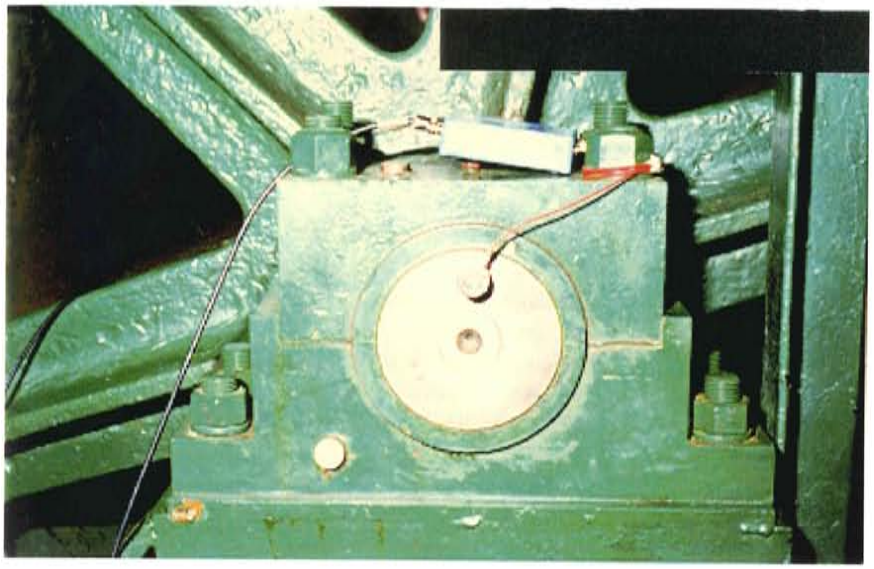

Figure 3.24: **Broadband Sensor Attached to Main Hoist Drum Shaft with External Pre-Amplifier**

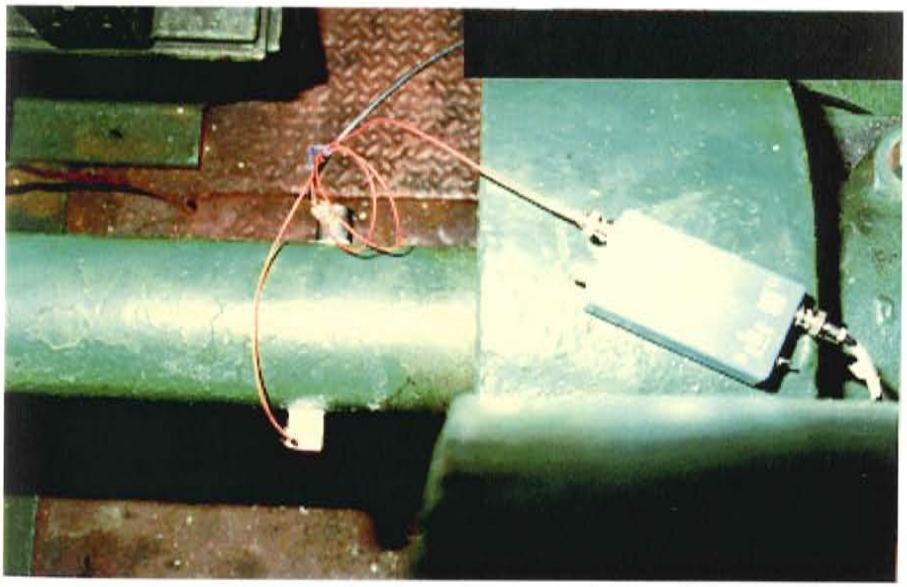

Figure 3.25: **Broadband Sensor Attached to Boom Hoist Drive Shaft with External Pre-Amplifier**

3.4.9 Verification of Sensor Sensitivity and Coupling

Verifying that AE sensors are properly coupled to the test piece and are functioning correctly with sufficient sensitivity is crucial to acquiring meaningful AE data. Such verification is performed twice: immediately before load testing begins, and immediately after completion of all AE tests. The most common verification technique is pencil lead breaks, in which a 0.3 mm 2H Pentel pencil lead is broken against the test piece. The pressure at which the pencil lead fractures causes a specific displacement on the surface of the metallic object. When the lead fractures, the material rebounds elastically the result of which is a pressure wave which is quite similar to that which occurs during an actual emission causing event. In addition to pencil lead breaks, two other methods were used to introduce signals into the crane shafts. Dunegan crackers were used to induce metallic cracking into a test piece attached to the crane shafts. A piezoelectric resonant transducer attached to a specially designed square wave generator (or pulser) was also used to generate simulated AE signals in the test piece. Each verification method will be described in more detail presently.

3.4.10 Pencil Lead Breaks

After placement of all AE sensors, a 0.3 mm Pentel 2H lead was broken 1" from each sensor. The lead was extended approximately 2.5 mm for each break, and breaks were done with the lead at 30 degrees with respect to the

surface of the shaft. Five breaks were recorded at each sensor, and it was confirmed that the amplitudes of the five breaks were within 4 dB of each other. It was also confirmed that the average amplitude recorded by each sensor was within 4 dB of the average amplitude recorded by all the other sensors of similar type. Typical average amplitudes for the 150 kHz resonant sensors were around 80 dB, while that number decreased to around 75 dB for the broad band sensors. It was much more difficult to obtain consistent results with the broad band sensors than it was with the resonant sensors.

The procedure used is in compliance with the American Association on Railroads Procedure of AE Evaluation of Tank Cars and Intermodal Tanks[15] for determining that sensors are working properly.

3.4.11 PAC Pulser

A Physical Acoustics Corporation (PAC) model C-101-HV electronic pulser was used to send a square wave pulse to a 150 kHz resonant transducer. The transducer introduced a very repeatable 150 kHz signal into the shaft. To evaluate sensor sensitivity using the pulser, the transducer was placed on the shaft 1" from each sensor, and was acoustically coupled to the shaft with high temperature silicone vacuum grease. As in the case of the pencil lead breaks, this AE simulation was repeated five times at each sensor, with the average amplitudes being compared to the average amplitude of other sensors of the same frequency. The pulser signal was found to more consistent in amplitude

than the pencil lead breaks, and again indicated that the sensors were well coupled to the shaft and operating with appropriate sensitivity.

It should be noted that additional pencil lead breaks and pulses were applied at various intervals from each shaft face. This data was used to study the signal attenuation characteristics of in-situ crane shafts, as well as those types which were not studied in the laboratory.

3.4.12 Dunegan Cracker

A Dunegan cracker is a device that couples true AE signals from a cracking metallic material into the desired test piece. The cracker holds a torqued, hydrogen-embrittled bolt. AE released from this bolt is transferred, via a waveguide, from the bolt into the test piece. The objective of using a Dunegan cracker is to verify that a specific AE set-up will detect real AE signals, and to observe how these real AE signals, generated only at one location on the test piece, are received at each of the sensors.

3.4.13 Verification After Load Testing

Pencil lead breaks were repeated on each shaft after completion of AE load testing. In all but one case (sensor number 5 on the boom drive shaft), the lead breaks after testing were very similar to the lead breaks before testing, leading to the conclusion that the AE sensors did not fail or lose coupling during the test.

Sensor number 5, which was a broadband sensor on the boom drive shaft, showed amplitudes slightly lower that it did prior to load testing. However, these amplitudes were still in the 70 to 80 dB range indicating that sufficient coupling existed to identify AE signals. The sensor was also remounted with hot melt glue and pencil lead breaks repeated to verify the sensor had not failed. After remounting, the sensor recorded amplitudes were very similar to pre-testing levels. It was thus concluded that small amount of decoupling of sensor number 5 occurred during AE data acquisition, but this decoupling was not large enough to seriously effect the test results.

CHAPTER 4

ANALYSIS AND RESULTS

4.1 FINITE ELEMENT MODELING

A three dimensional finite element model of the critical area of the shaft was developed using the ABAQUS 5.6-2 software package being run on a Cray T90 Parallel Vector Supercomputer. The goal of this analysis was to better understand the state of stresses that existed in the shaft under torsional loading, and to compare the crack propagation rates in the model to that in the real shaft under fatigue loading.

The full geometry of the specimen was modeled, taking advantage of the symmetry between the front and the rear of the shaft. As in the experimental setup, load was introduced into the model via the key and keyway system. Material properties such as elastic modulus, toughness, ultimate strength, and hardness were taken from Naval test reports provided, other required values such as Poison's ratio, and the yield stress were either back calculated from the other data provided by the Navy, or found in tables for the type of steel being used.

An initial crack was input into the model. The location and size of this crack was taken directly from Naval reports on other failed crane shafts, which had been sectioned. The location of the crack introduced into the model started at the inside corner of the keyway and was 1/8" long proceeding into the volume of the material. The choice of the initial size of the imperfection was somewhat

arbitrary, the main thrust being that it was in the direction of the proposed failure plane of the model, which was taken directly from observed failures in the field.

The loading of the model was identical to that used in the laboratory. The crack grew along its failure plane as shown in Figures 4.2 through 4.4. As a check, it was verified that the failure plane used in the model was indeed the path of greatest energy release as indicated by the contour integral calculation in the analysis. This lends great credence to the fact that the proposed failure plane (required for the finite element analysis to proceed) is indeed a plausible one. The geometry of the model is complex. Figure 4.1 shows the part of the model which is displayed in the remaining figures for the results from the finite element analysis.

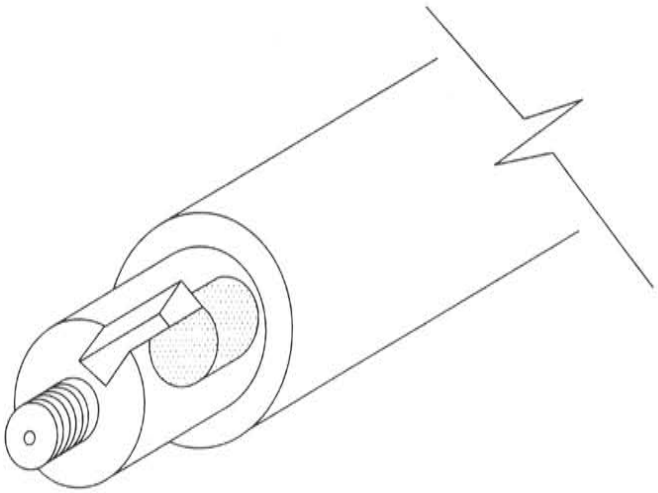

Figure 4.1: Section of Shaft shown in Finite Element Analysis Results

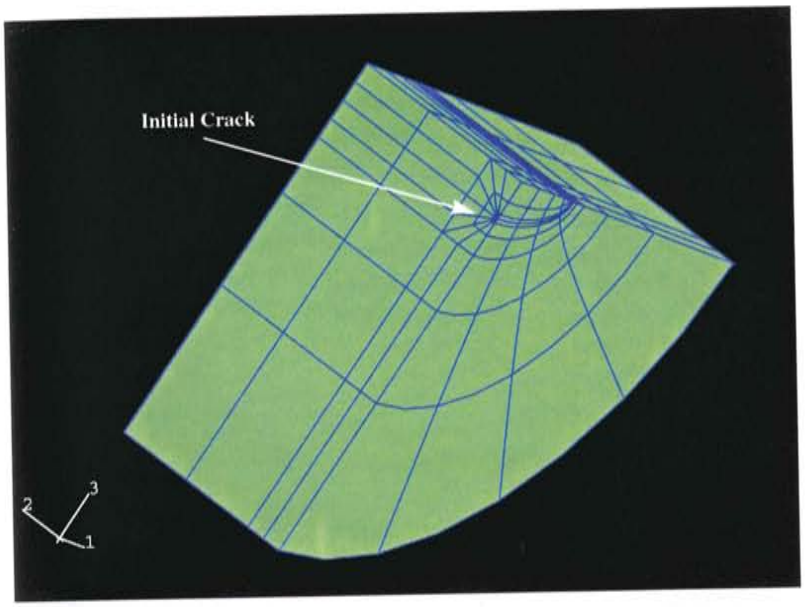

Figure 4.2: **Initial Crack Introduced into Model**

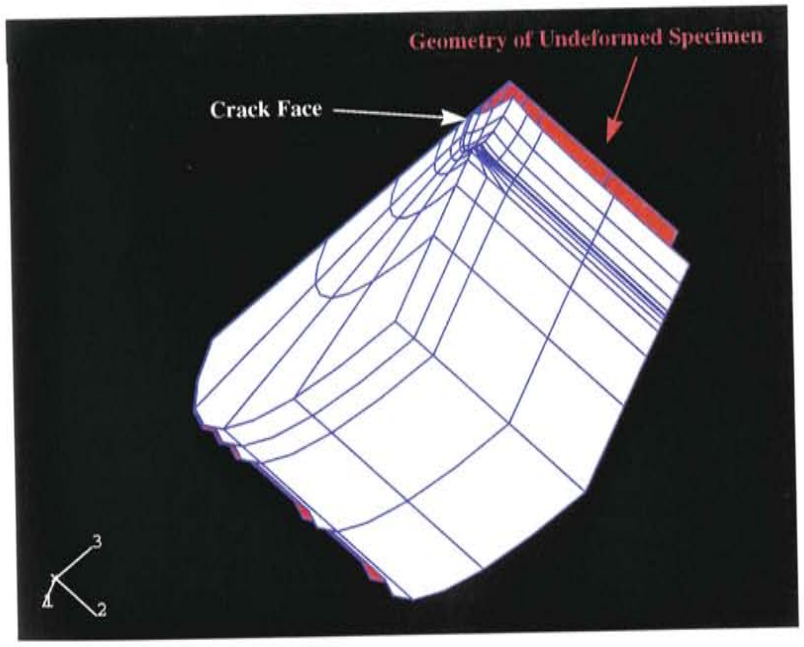

Figure 4.3: **Crack at the end of 55 in-kip Fatigue Load Level**

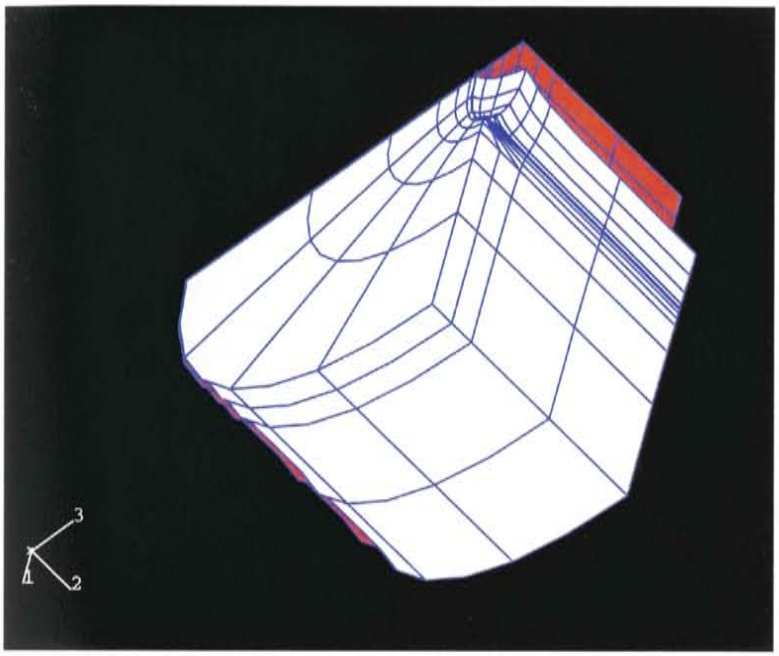

Figure 4.4: Crack at the end of 95 in-kip Fatigue Load Level

It may be seen from the foregoing figures that the crack propagates through the volume of the material as the fatigue cycling progresses, and the crack tip opening displacement (seen in the upper left corner of the model) gets progressively larger. The results obtained verify what was thought to be occurring in the shaft, intuitively. Additionally, the stress contour plots, seen in Figures 4.5 and 4.6 allowed for a better understanding of the stress field in the body as a whole, especially at the crack tip.

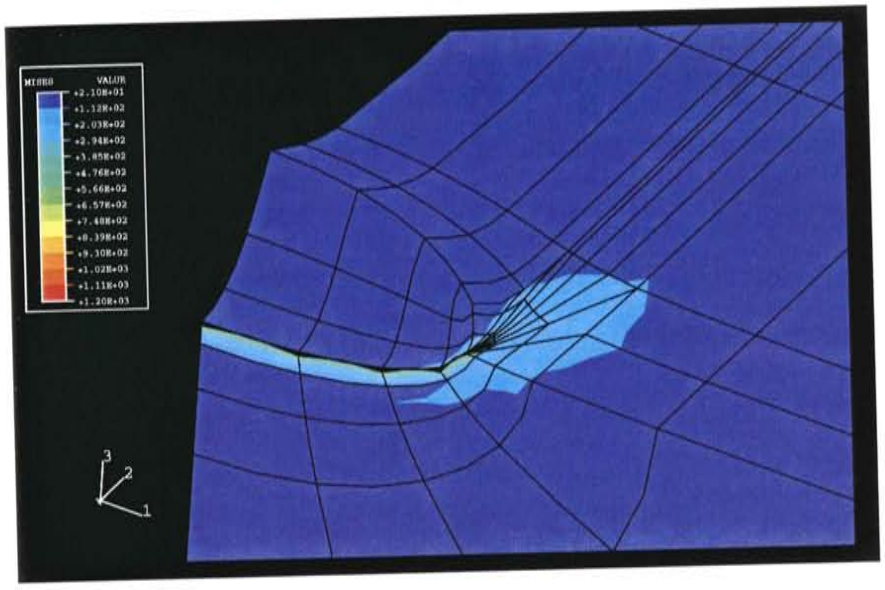

Figure 4.5: **Stress Contour of Entire Body under 55 in-kip Clockwise Loading**

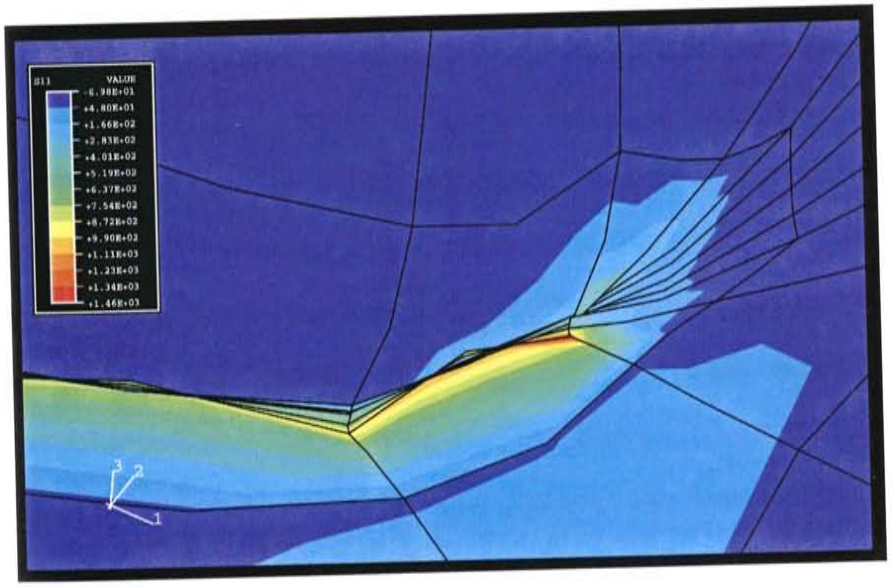

Figure 4.6: **Stress Contour of Area Near Crack Tip**

Using the stress analysis from the model, the shear stresses introduced into the shaft by the torsion were decomposed into stresses normal to the plane of the crack face. By so doing, the direction of twist that caused crack opening and the direction that caused crack closing was determined. In the present case, clockwise loading was seen to open the crack, while counterclockwise loading was seen to close the crack. This corresponds well to the data obtained from the AE testing, which will be discussed to follow.

4.2 ANALYSIS METHODS FOR THE AE DATA

4.2.1 Genuine and False Emission

Not all emission is genuine and the ability to distinguish genuine from false emission is a key issue in an acoustic emission test procedure. False emission can arise from a number of sources including mechanical rubbing, wind-induced movement of the cables and sensors, rain, sleet, thermal expansion due to the sun, and corrosion. False emission due to sliding friction was a particular problem with the setup used in the lab.

In the past few years, new techniques have been developed for identifying false emission and applying post-test filtering. Filters, such as the Swansong series of filters[15], eliminate spurious emission from the data record. Post test filtering of data files is almost always required, and many inspectors make it a standard practice to run all data through one of the Swansong filters.

For the present research, the Swansong II filter was used. The Swansong filters are based on the observation that certain telltale hit parameters, such as low amplitude and long duration, characterize sliding and mechanical rubbing. In the Swansong II filter, data are removed for a period of 1 second. The Swansong II filter is defined by the following:

$$\begin{aligned} &\text{If } (A_i - A_{th}) < 5 \text{ and } D_i > 2 \\ &\text{or } (A_i - A_{th}) < 10 \text{ and } D_i > 3.5 \\ &\text{or } (A_i - A_{th}) < 15 \text{ and } D_i > 4.5 \end{aligned} \qquad \text{(Equation 4.1)}$$

then eliminate all hits during the period (seconds):

$$(T_i - 0.5) \text{ to } (T_i + 0.5) \qquad \text{(Equation 4.2)}$$

where for a given hit, i

A_i is the amplitude (dB)
A_{th} is the data acquisition threshold (dB)
D_i is the hit duration (ms)
T_i is the arrival time (sec)

Equation 4.1 is used to define the telltale hits and must be applied on a channel-by-channel basis using the specific threshold for each channel. Tests have shown that some of the sensor hits caused by mechanical movement have large amplitude, high energy characteristics, and propagate throughout the system under test. Accordingly, emissions occurring immediately before and

immediately after a telltale hit are removed from all channels. For this reason, Equation 4.2 is applied to all channels on the item under test. The Swansong zone, per se, on a correlation plot is shown in Figure 4.7.

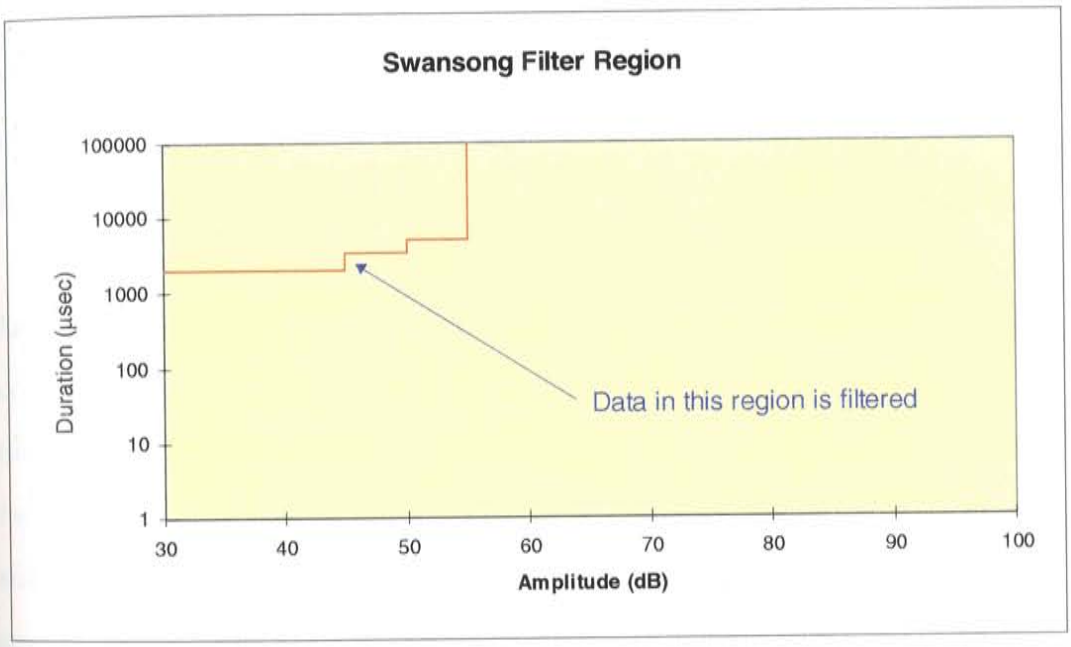

Figure 4.7: Swansong Zone on a Correlation Plot

4.2.2 Intensity Analysis

Intensity analysis is a measure of the structural significance of an acoustic emission source. The technique has been discussed in the literature[116] and the method has been used extensively for analysis of defects in metal equipment. The technique is based on test data from destructive vessel tests, controlled tests with detailed follow-up nondestructive evaluation, and over

1000 tank and pressure vessel tests. The empirical factors described to follow and the intensity grading have been developed by comparing the acoustic emission data with fracture mechanics and finite element based studies of detected defects.

Intensity analysis is a valuable tool for assessing the structural significance of a flaw. The results of the analysis provide guidance on continued operation of the equipment, and the need for follow-up visual inspection, more frequent testing, or possible shut down.

Intensity analysis is carried out on a per channel basis, and uses two factors based on signal strength. The first factor is known as historic index, and compares the signal strength of the most recent hits to the signal strength of all hits. Historic index is essentially independent of specimen size. The second factor, referred to as severity, is the average of the largest signal strength hits striking the sensor. The use of signal strength to define historic index and severity reduces the effect of distance from the sensor, and allows the intensity analysis to be used on the full range of field geometries. Historic index is defined by:

$$H(t) = \frac{N}{N-K}\left(\frac{\sum_{i=K+1}^{N} S_{0_i}}{\sum_{i=1}^{N} S_{0_i}}\right)$$

Where:

$H(t)$ is the historic index at time t.
N is the number of hits up to and including time t.
S_{0_i} is the signal strength of the ith hit.
K is an empirically derived factor that varies with the number of hits and is different for different materials.

Severity, S_r is defined as the average signal strength for the J hits having the largest numerical value of signal strength:

$$S_r = \frac{H_f}{J} \sum_{m=1}^{m=J} \psi(h)_m \; S_{0_m}$$

where:

S_{0_m} is the signal strength of the mth hit (m being ordered on the magnitude of the signal strength).
J is an empirically derived constant that depends on the material of construction. Typically, $J = 10$ for most metals.
H_f is known as the Maize factor and depends on the loading. For tests which use an overload procedure, $H_f = 1$.
$\psi(h)_m$ is a function of the threshold h.

In many common test AE test procedures, such as the MONPAC[16] procedure, the results of the intensity analysis for each sensor are plotted on a chart divided into zones as shown in Figure 4.8 which shows intensity analysis results for a pressure vessel. The meaning of the six zones lettered "No Significant Emission" through E is shown in Table 4.1. As will be described in Chapter 5 a modification and simplification of this approach was developed for the crane shafts.

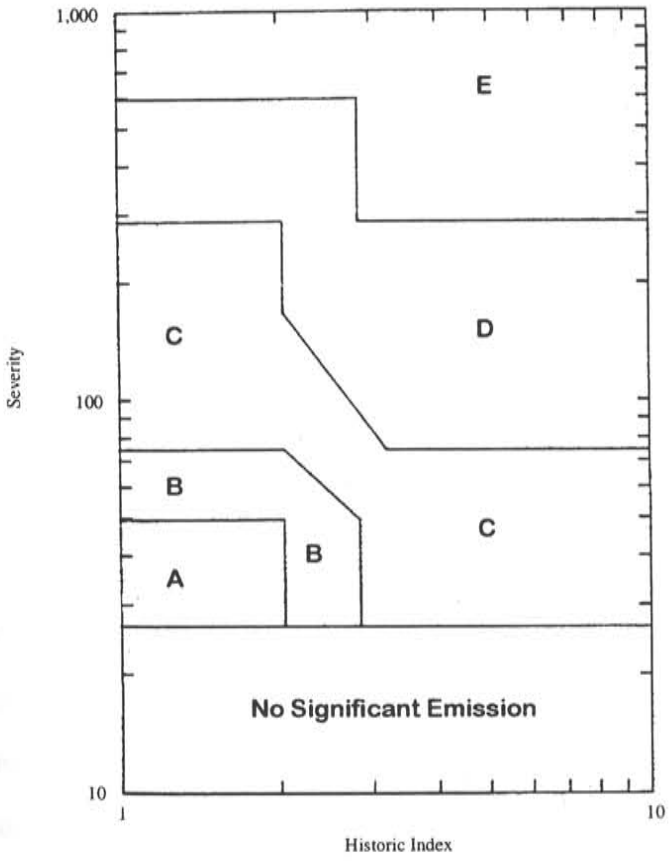

Figure 4.8: Intensity Plot for a Metal Pressure Vessel used in the MONPAC Test Procedure

Table 4.1: **Significance of Intensity Zones for Metallic Pressure Vessels**

Zone Intensity	*Recommended Action*
No Significant Emission	Insignificant Acoustic Emission. No follow-up recommended.
A	Minor defect, note for reference in future tests.
B	Note for reference in future tests and check for minor surface defects such as corrosion, pitting, gouges, or cracked attachment welds.
C	Defect requiring follow-up evaluation. Evaluation may be based on further data analysis, or complementary nondestructive examination.
D	Significant defect requiring follow-up inspection.
E	Major defect requiring immediate shut-down and follow-up inspection.

4.2.3 Source Location

For the present work, the Jolly-Stuart method of source location was used. This zonal location technique is robust and defines a small area which contains the defect. The Jolly-Stuart technique uses all sensor hits to refine the zone of interest. This is in contrast to conventional time-of-arrival source location which requires a minimum number of hits from an AE event to locate an emission source. Time-of-arrival source location utilizes hit arrival times and assumed wave velocity to calculate the position of the source. For a number of reasons, this technique has given incorrect answers and most codes and standards utilize zone source location [17].

The Jolly-Stuart method divides sensor hits into two categories, first hit and ancillary hit. As a stress wave propagates through a structure it will strike a number of sensors. The first sensor struck will record the "first hit". Subsequent hits to other sensors are referred to as "ancillary hits". Reflections, which can strike the first hit sensor and other sensors are also considered ancillary hits. Ancillary hits are ordered as second, third, fourth, etc. hits. The Jolly-Stuart uses the following algorithm for determining first and ancillary hits:

- Order all hits by time. For hits with the same time, order by amplitude. For hits with the same amplitude, order by signal strength.
- Consider hits in the time range, T to T+ΔT, as being caused by the same stress wave. T is the time of the first hit arrival. ΔT is the time for the stress wave to travel to other sensors. Hits that occur beyond this time range are considered to be from a different stress wave.
- If a hit has an amplitude of 5 dB or greater than the first hit, consider the new hit as a first hit and restart the process.

For the four foot long crane shafts studied in the laboratory, the travel time, ΔT, was one millisecond. This travel time represents the time for the wave to travel the complete length of the shaft and back plus 15 percent. Accordingly, reflections at the sensor nearest the emission source were considered ancillary hits.

4.3 DATA ANALYSIS

A large amount of data was collected during the course of experimentation, as both the overload data and the fatigue load data for over 60,000 cycles were recorded. The data was analyzed in separate groups consisting of positive overloading, negative overloading, load holds for both positive and negative overloading, and positive and negative loading and load holds during the fatigue loading. All the data was subject to the Swansong II filter before analysis. The data sets were spot checked at regular intervals by looking at the waveforms and power spectra for individual hits to verify their validity and admissibility.

4.3.1 Positive Overloading

A total of 39 positive overloads were conducted during the course of the experiment. In order to isolate the data of interest, a post test filtering process was adopted. The computer program ATPOST by PAC, supplied as part of the MISTRAS-2001 software package, was used in this effort. Ideally, because of the Kaiser and Felicity effects, during an overload cycle the sample should generate no acoustic emission until it reaches a load greater than the fatigue load level being used, unless it is damaged. Some of the problems with background noise described in Chapter 3 came to bear during extremely low loads in the fatigue and overload cycles. It is suspected that the reasons for this stemmed from the hydraulic fluid moving between the rams near the zero load and the key shifting bearing positions as the load was transferred from one direction to the

other. The latter cause came to dominate toward the end of the testing regime as the key was worn down, and the amount of potential movement during a bearing shift increased.

The filter used the load parametric input to determine what data to accept into the filtered data set. Data would start to be accepted at about 30% of the ultimate load level reached, and stopped immediately prior to the load level, to prevent any of the load hold data being captured. This is shown schematically in Figure 4.9. Typical data as collected during the entire overload cycle is shown in Figure 4.10

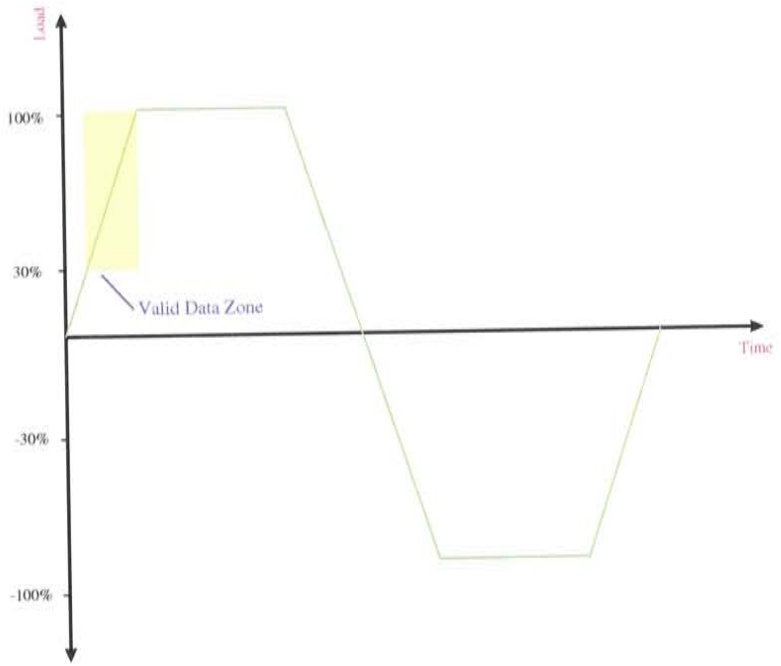

Figure 4.9: Values of Load for which Data was Accepted during Positive Overload Data Filtering

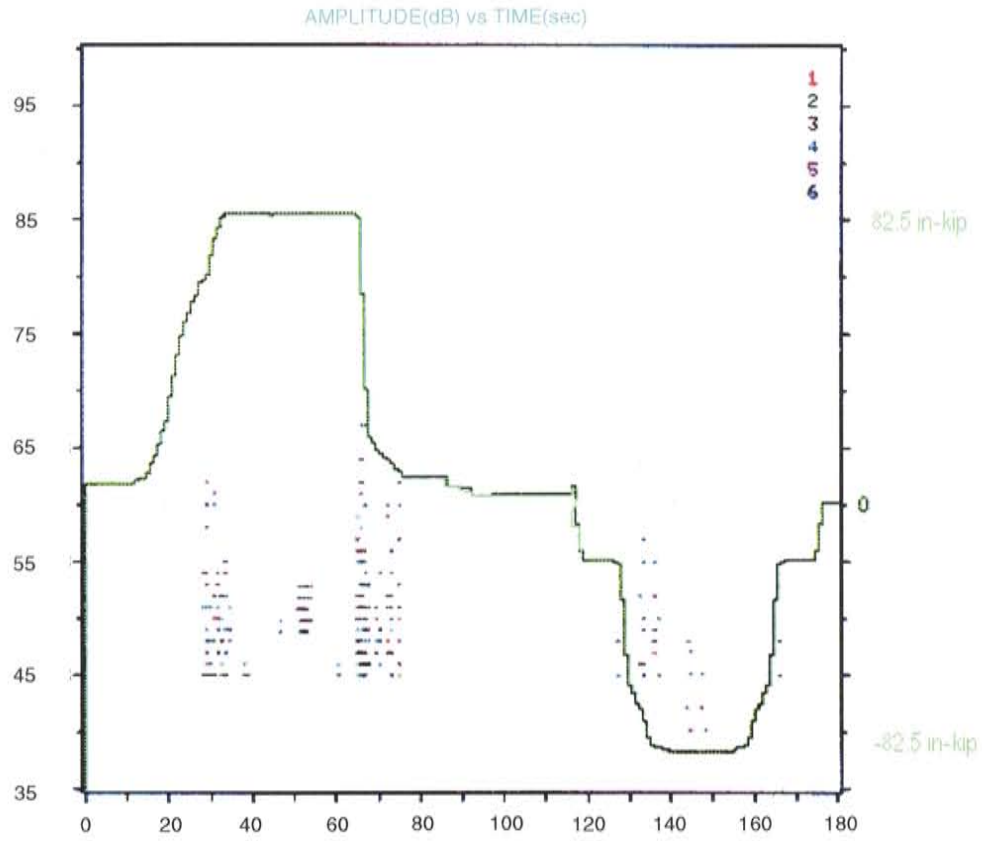

Figure 4.10: Typical Data Set Collected During Overload Cycle. Load Parametric is Superimposed on Amplitude vs. Time Plot

The data for each of the two overloads and load holds for a specific fatigue load level was analyzed separately. The cumulative signal strength for the hits on all channels in the zone of interest was calculated, and is shown in Figure 4.11.

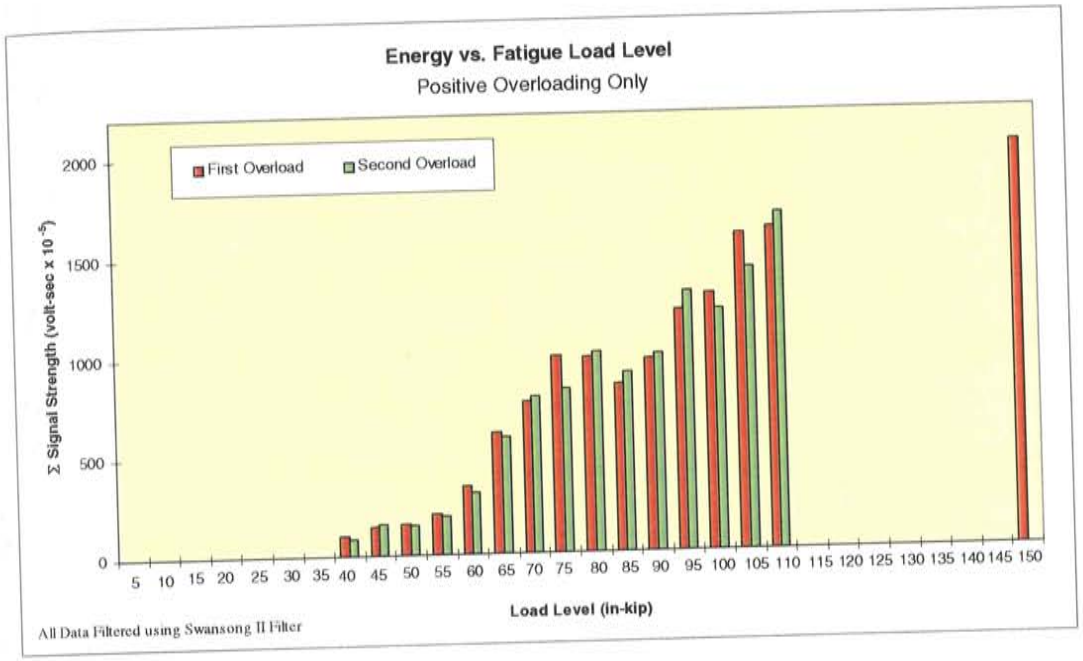

Figure 4.11: Energy vs. Fatigue Load Level During Positive Overloading

The data obtained was remarkably good. It is important to note that the data presented in Figure 4.11 is not cumulative. The data at each fatigue load level is separate and unique from the data before it. Emission appears at fatigue load level of 40 in-kips, the starting load level, which in the present case is greater than the load the shaft ever experienced when being used in the field. Emission over the next few overload levels remains reasonably constant, indicating that under the fatigue load cycling, the rate of damage accumulation is constant, and seemingly load independent. The damage occurring at these low load levels is likely quite minor. A visible "knee" appears in the data trend at a fatigue load of 60 in-kips, and from that point on damage begins to accumulate

at a much faster rate. It is interesting to note that the trend is almost linear as load level increases, indicating that greater loads cause damage to occur more rapidly. This result is consistent with the fracture mechanics finite element analysis data and known material failure mechanics theories, although it is inconsistent with Williams[91] approach detailed in the literature review. Williams suggests that the range $\Delta\sigma$ affects the rate of crack growth; the experimental evidence points toward the absolute value of σ as a predictor.

The Felicity ratio for each overload was also calculated. The calculation was done manually for all overloads. A load versus time plot was superimposed on a hit amplitude versus time plot with equivalent scale x-axes. The load level at which emission was first detected was divided by the fatigue load level in order to determine the Felicity ratio. The data used in these calculations was previously filtered, and only included data in the zone of interest. Figure 4.12 shows the results of the calculations.

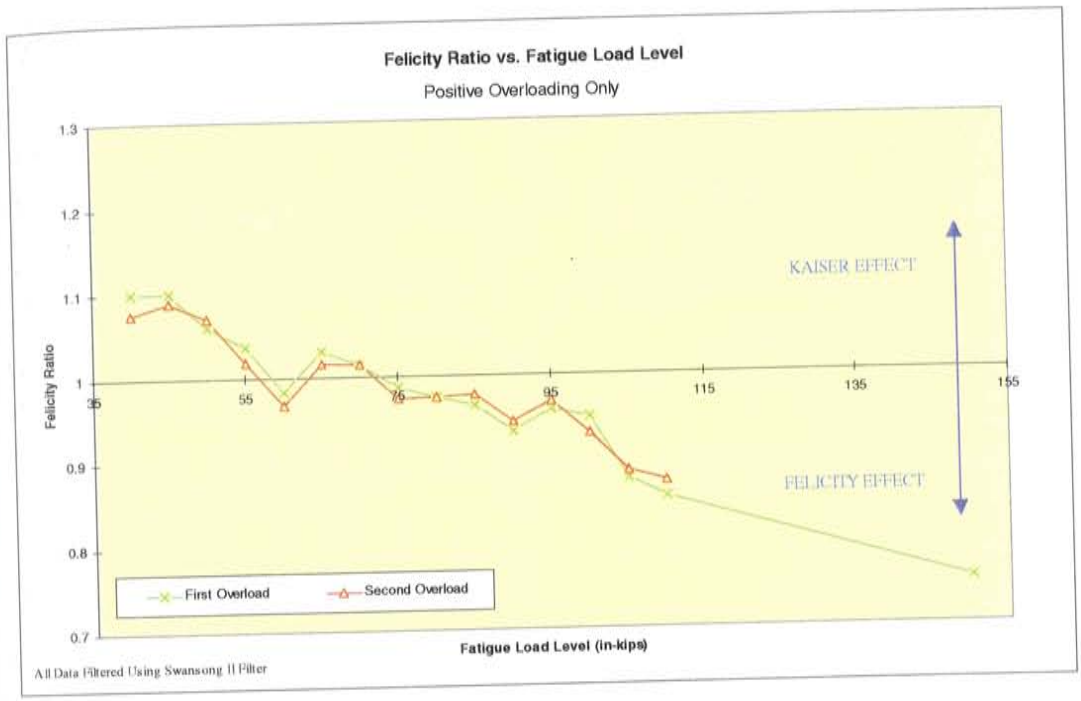

Figure 4.12: Felicity Ratio vs. Fatigue Load Level for Positive Overloading

The lower load levels show Felicity ratios greater than unity, indicating that the crane shaft is performing well. The Felicity ratio starts to decrease to a value less than one at around the same point as the "knee" in the cumulative signal strength versus load plot occurs. An interesting result. The data trend is decreasing in a reasonably linear fashion. The points at which the Felicity ratio increases slightly compared to its previous can perhaps be explained by the fact that the blunted cracks didn't grow as much during the preceding load cycles, however the increase does not always occur with both data points at a particular

load level and the change in values are sufficiently small as to safely assume that they are insignificant, and do not reflect on the general trend observed.

In acoustic emission testing a Felicity ratio as low as 0.95 is cause for concern, and usually requires that follow-up action be taken. The data at the upper load levels shown in Figure 4.12, decreasing toward 0.8 is indeed cause for alarm. The extremely low Felicity ratio, in combination with the high cumulative signal strengths observed at the upper load levels indicates that there is significant cracking in the shaft which is active under clockwise loading.

4.3.2 Negative Overloading

Analysis of the negative overloading regime was carried out in an identical fashion to the positive overloading regime. Again, a 30% to nearly 100% of load "zone of interest" filter was applied, as was the Swansong II filter. Figure 4.13 graphically illustrates the zone for negative overloads.

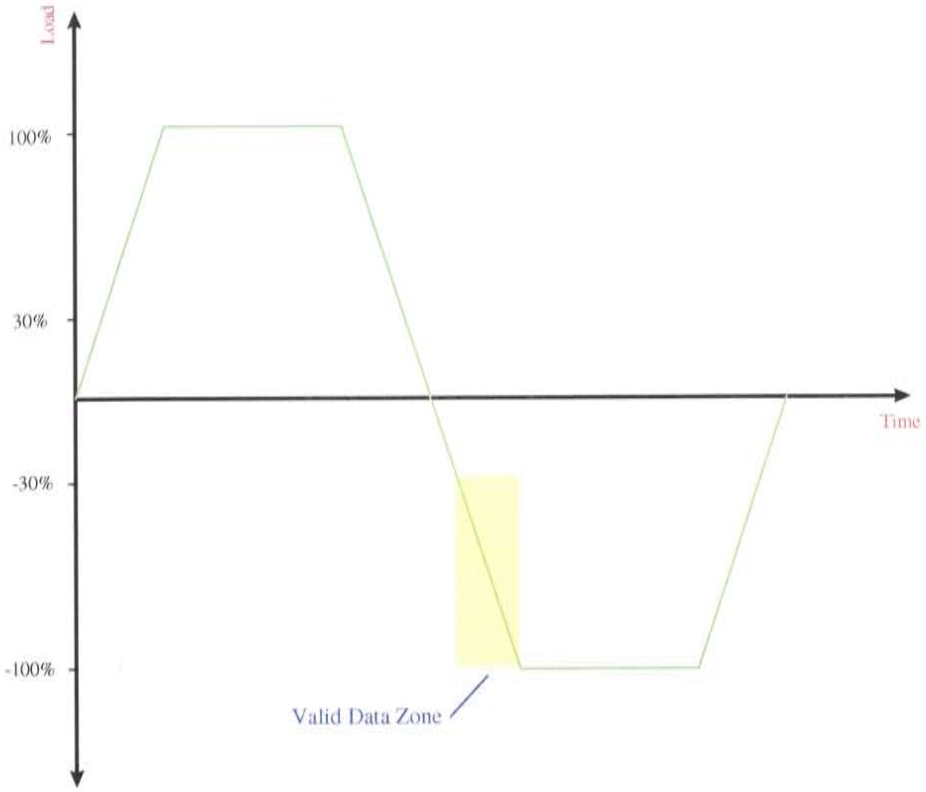

Figure 4.13: Values of Load for which Data was Accepted during Negative Overload Data Filtering

The unloading data going from 30% of the maximum positive load down to zero load was of little interest. As seen in Figure 4.10, generally speaking this load range had few hits and most of the hits recorded were subsequently filtered out when the Swansong II filter was applied, leading to the conclusions that mostly non-genuine emission was being generated during the unloading phase. Figures 4.14 and 4.15 are plots of Energy versus Fatigue Load Level and Felicity

Ratio versus Fatigue Load Level, respectively. They were calculated in the identical manner as the positive overload data, described previously.

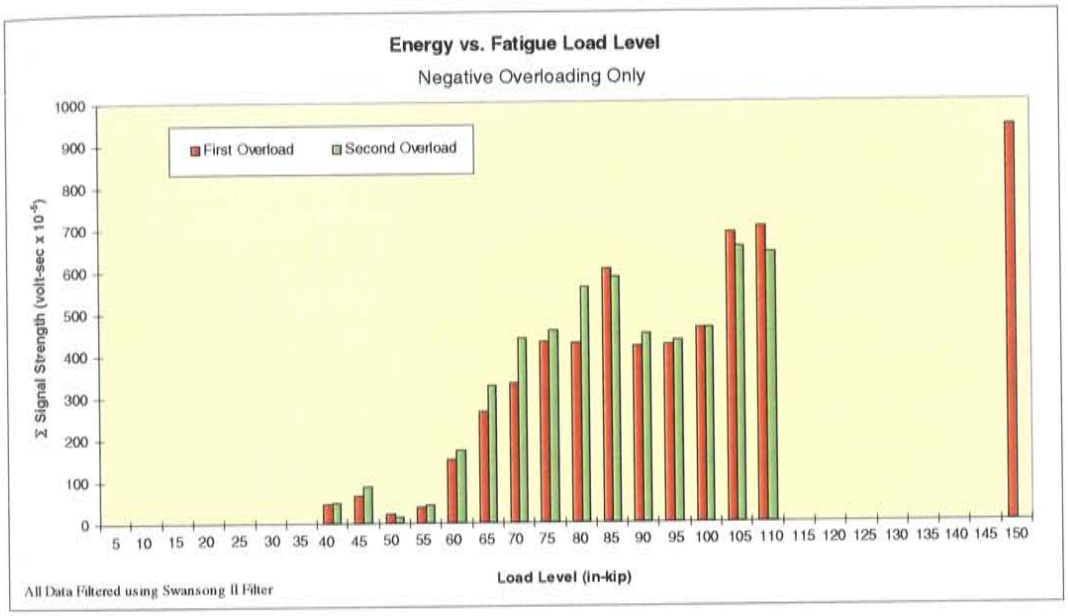

Figure 4.14: Energy vs. Fatigue Load Level During Negative Overloading

By way of comparison, the data from the positive overload cycle and the negative overload cycle show the same general trend. The cumulative energy increases in a fairly linear fashion, although there are more dips and flat plateaus in the negative overload data than in the positive overload counterpart. This may be an indication that if the crack is opened by positive load, the negative load (crack closed) with shear dominating may be more sensitive to changes in

crack growth. They represent a relatively small deviation from the linearity of the data trend, and are thus thought to be insignificant.

An important feature to notice in the negative overload data is that the magnitude of the cumulative energy released at each fatigue load level is lower than that released during the positive loading. This indicates that the crack is more active in one direction than in the other, meaning that more damage is occurring under clockwise loading than is under counterclockwise loading. This is consistent with the finite element analysis results which showed the crack to be opening when the shaft was subject to clockwise load. In relative terms, the cumulative signal strength levels during negative loading are approximately one half of what they are during positive loading. The combined state of stress under the counterclockwise load is likely promoting crack closure, and some compression yielding, a phenomenon well documented in the literature, but obviously to a much lesser extent than the clockwise loading is causing damage by crack opening.

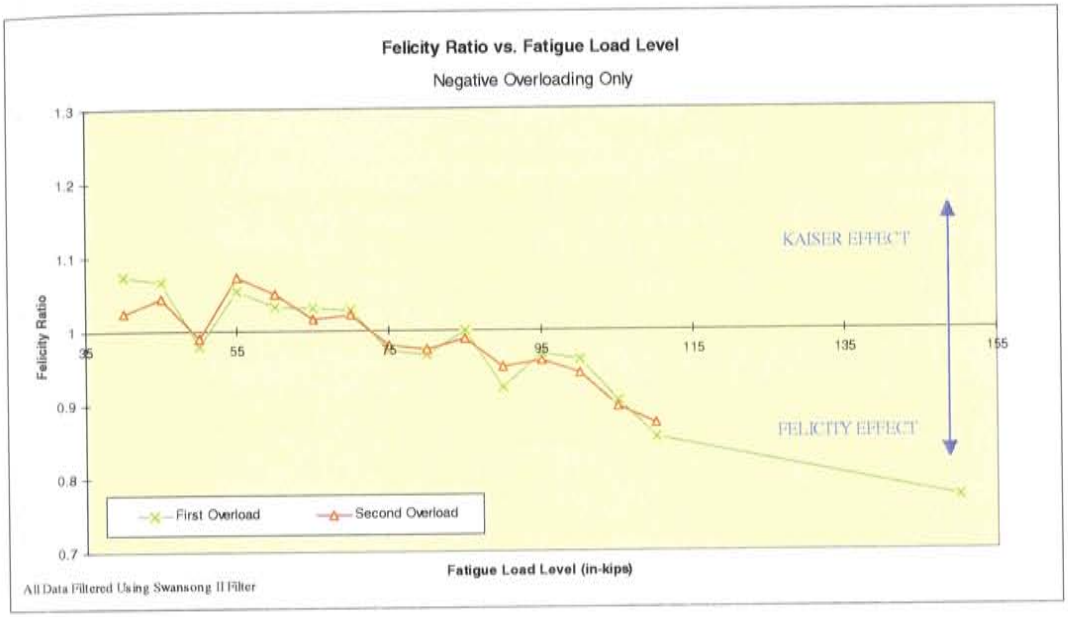

Figure 4.15: Felicity Ratio vs. Fatigue Load Level for Negative Overloading

The results from the Felicity Ratio calculations for the negative overloading are consistent with the results obtained from the positive overloading. The trend of a decreasing Felicity Ratio with increasing load is again observed, as are the minor fluctuations in the data. The fluctuations are not of great magnitude, and are once again thought to be negligible compared with the overall trend observed. It is interesting to note that the Felicity Ratio for both the positive and negative overloads fall below unity and remain there at a fatigue load level of 75 in-kips. This may be a positive indication that for this

specific shaft, the damage occurring as a result of loading in one direction begins to affect the behavior of the shaft in the other direction at this particular load.

4.3.3 Positive and Negative Overload Load Holds

The data for the positive and negative load holds for each overload cycle was contained within the same data set as the positive and negative overload data. The ATPOST program was used to filter all but the load hold data by using the load parametric with very narrow bands around the maximum load reached. This is shown schematically in Figure 4.16.

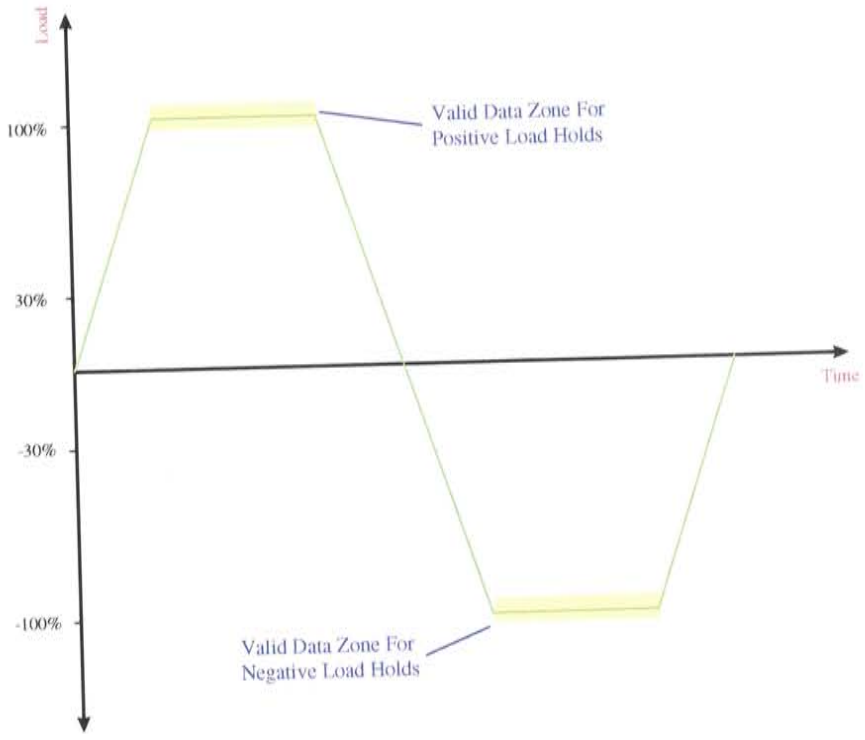

Figure 4.16: Values of Load for which Data was Accepted for Load Hold Data Analysis

As with the overload data, the cumulative signal strength for each load hold was calculated, and is shown in Figures 4.17 and 4.18. Unlike the overload data, however, the Felicity Ratio was not calculated, as it has no meaning in the case of load holds.

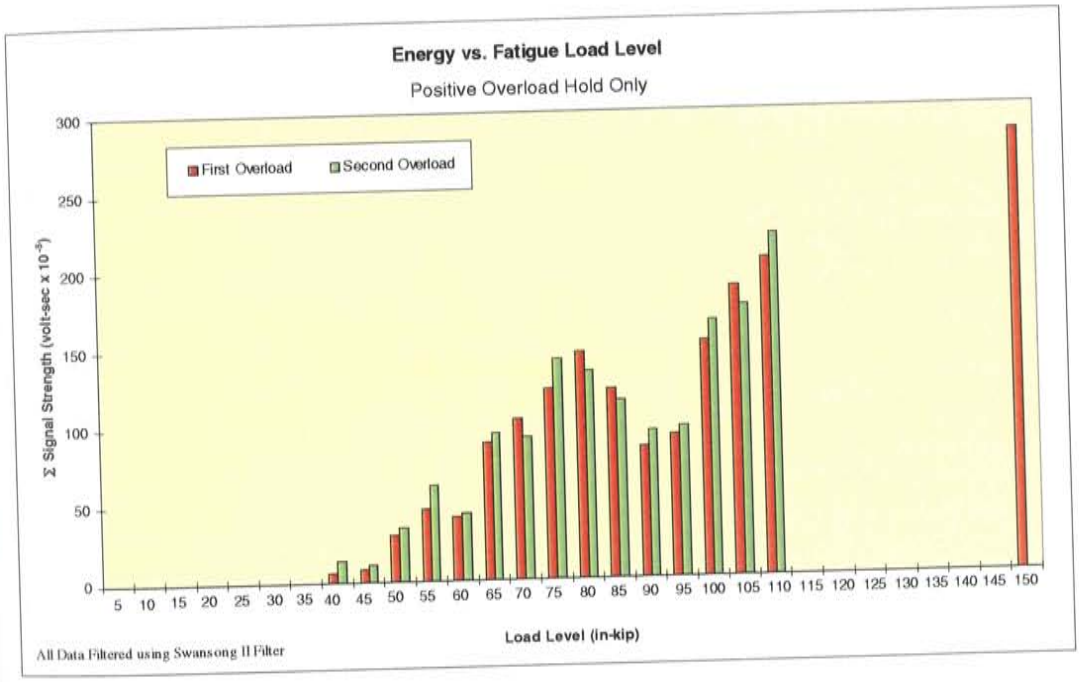

Figure 4.17: Energy vs. Fatigue Load during Positive Overload Load Holds

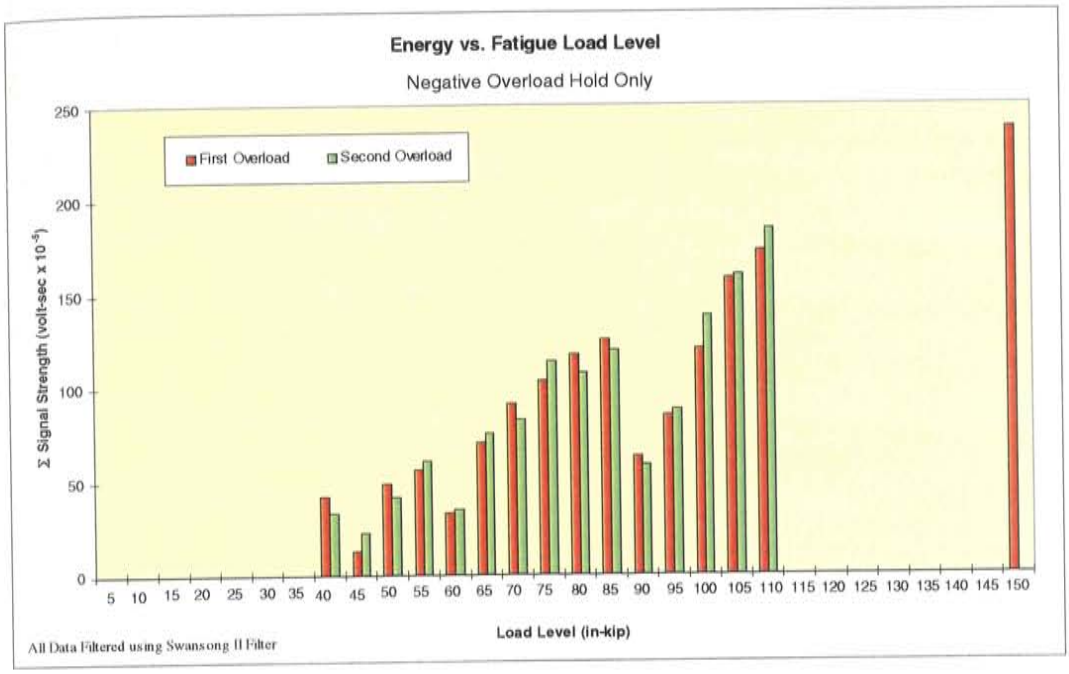

Figure 4.18: Energy vs. Fatigue Load during Negative Overload Load Holds

As with the overload data, a strong linear trend in the load hold data can be seen. The amount of ongoing damage after loading has stopped increases with increasing fatigue load levels. An important feature to realize with the load hold data is that the magnitude of the events are much lower than with the overload data (250 $\text{volt} \cdot \text{seconds} \times 10^{-5}$ compared to 3,000 $\text{volt} \cdot \text{seconds} \times 10^{-5}$), but the magnitude of the positive and negative load holds events are roughly equal. This observation lends credence to the entire notion that the load hold data is truly representative of the amount of damage that has occurred in the shaft, regardless of which direction it is being loaded in.

4.3.4 Fatigue Loading

The post test filtering of the fatigue loading data was carried out somewhat differently than with the foregoing data sets. Positive and negative loads were considered separately, but the load, load hold, and unloading data were all grouped in the same data set. This is shown graphically in Figure 4.19. As with the overload data, the first 30% of the load in either direction was filtered out.

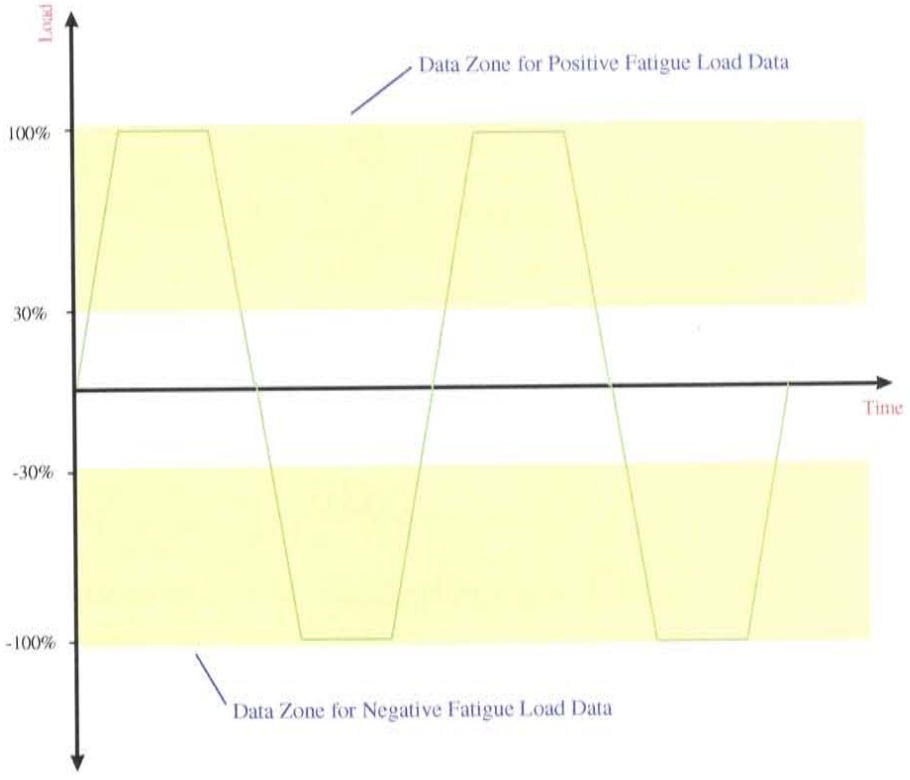

Figure 4.19: Data Zones for Positive and Negative Fatigue Load Data

It would have been much more desirable to filter within the blocks defined in Figure 4.19; for example to differentiate the data sets into data obtained while the load was increasing, data collected during the load hold, and data from when the load was decreasing. This would have allowed for pinpointing the type of emission generated during a fatigue cycle of the crack opening (during positive loading, for example) and the crack closing (during positive unloading) and would perhaps have allowed some signature analysis to be carried out. Due to limitations within the ATPOST software this was not possible, although at the time of writing Physical Acoustics Corporation was working on incorporating second order filters into subsequent releases of their software.

Part of a typical fatigue cycle is shown in Figure 4.20. The figure shows the positive portion of one of the fatigue cycles. The emission observed where the load level is low, at the start and end of the half cycle shown, is likely caused by some type of background noise. The emission observed just prior to the ultimate load and during the load hold is considered genuine data, and is precisely what the filter selectively accepts. The figure is typical insofar as when emission occurred during a cycle, remaining cycles looked similar to what is shown. The majority of all fatigue cycles, however, had much less, if any, emission - both when the load was changing and remaining constant.

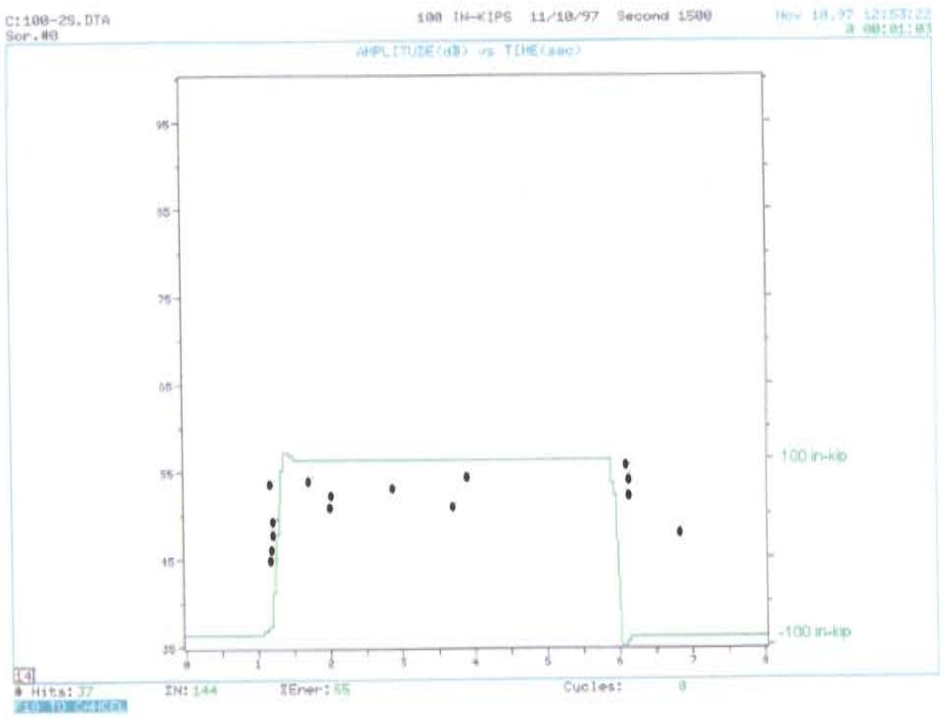

Figure 4.20: Typical Positive Portion of a Fatigue Load Cycle

The cumulative signal strength for each of the three, 1,500 fatigue loadings for each load level were calculated, and are shown in Figures 4.21 and 4.22.

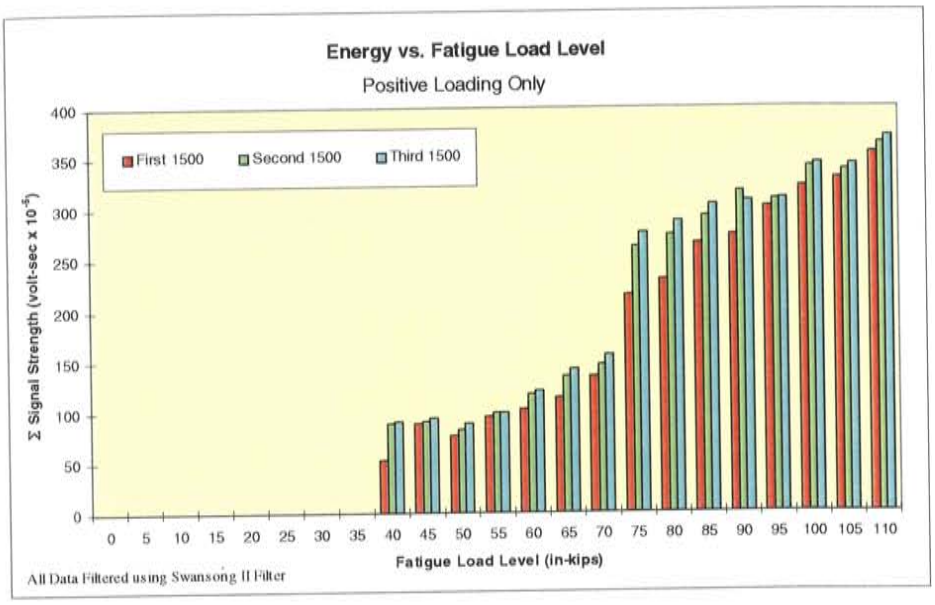

Figure 4.21: Signal Strength vs. Load Level for Positive Fatigue Loading

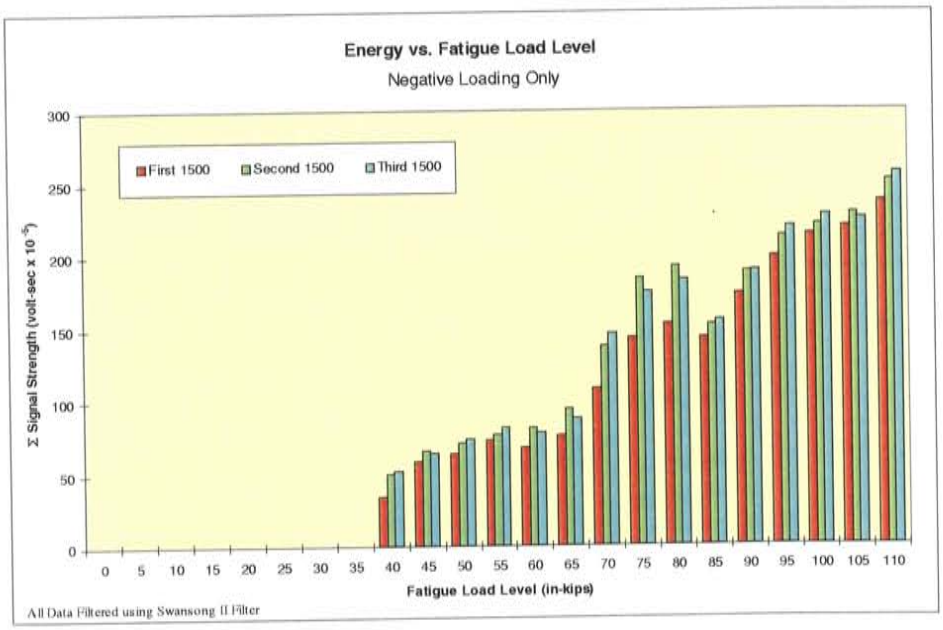

Figure 4.22: Signal Strength vs. Load Level for Negative Fatigue Loading

The positive and negative data may be discussed together, as for the most part they show the same trends. As with all the foregoing cases, the emission during negative loading is notably smaller in magnitude than the emission during positive loading. The emission during the first 1,500 cycles is lower than the emission of any of the succeeding 1,500 cycles at the same load. This result conclusively shows that more damage occurs at any given load level as the number of fatigue cycles grows. The emission occurring after the first and second overloads, for the most part, are very similar in their magnitude, indicating perhaps that damage occurs at a slower rate initially, and then transitions into a linearly increasing rate, with a more gradual slope.

It is worth noting that the cumulative emission during the fatigue cycles is less than the emission during the overload cycle that follows. This suggests that yielding during the overload causes more emission than the minute crack growth steps.

The data in the form presented in Figures 4.21 and 4.22 make an overall trend analysis difficult. To better observe what is occurring with the data on a macroscopic level, the data was examined in a different way. Figures 4.23 and 4.24 show the heretofore presented data, but in a cumulative manner. That is to say, the total signal strength at each load increment (all 4,500 cycles) was added to the total signal strength of the preceding load increment. In essence, the integral with respect to load of the bar charts in Figures 4.21 and 4.22.

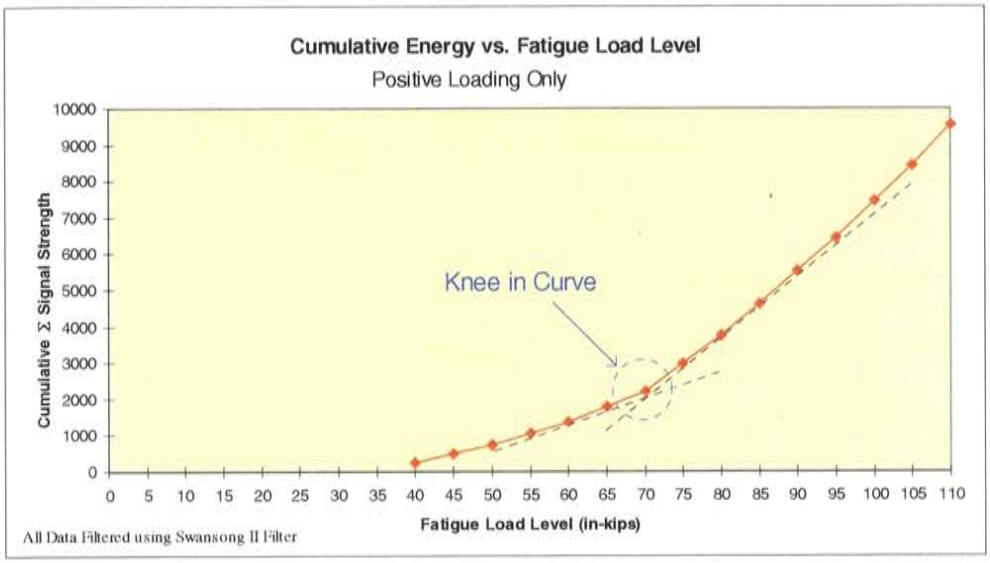

Figure 4.23: **Cumulative Energy vs. Fatigue Load Level for Positive Loading. Overload Data Not Included.**

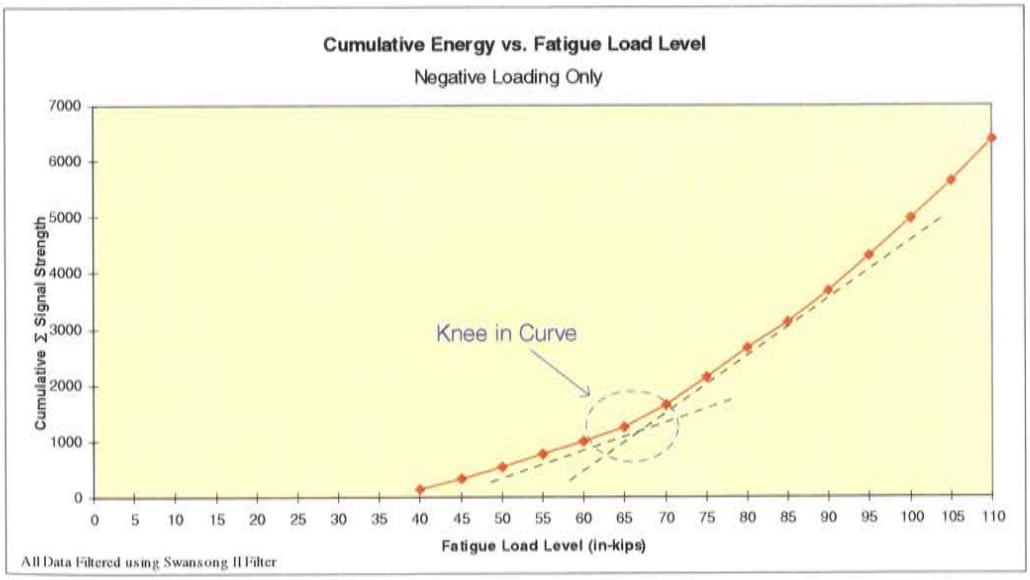

Figure 4.24: **Cumulative Energy vs. Fatigue Load Level for Negative Loading. Overload Data Not Included.**

The curves in both the positive and negative loading cases appear quite bilinear, with a distinct knee separating the two slopes as shown with the indicated tangents. Before the knee in the curve, damage to the shaft was occurring at a slower rate than after the knee. It is very interesting to note that in both cases, the load level at which the knee occurs is the same load level at which the Felicity ratio was seen to consistently fall below unity in the overload data. This observation reinforces all the previous results, and additionally shows that the Felicity ratio is a very powerful tool in assessing the structural significance of a defect.

It was of some interest to look at the distribution of hits with time for the fatigue loading. Two different load levels are shown in Figures 4.25 and 4.26.

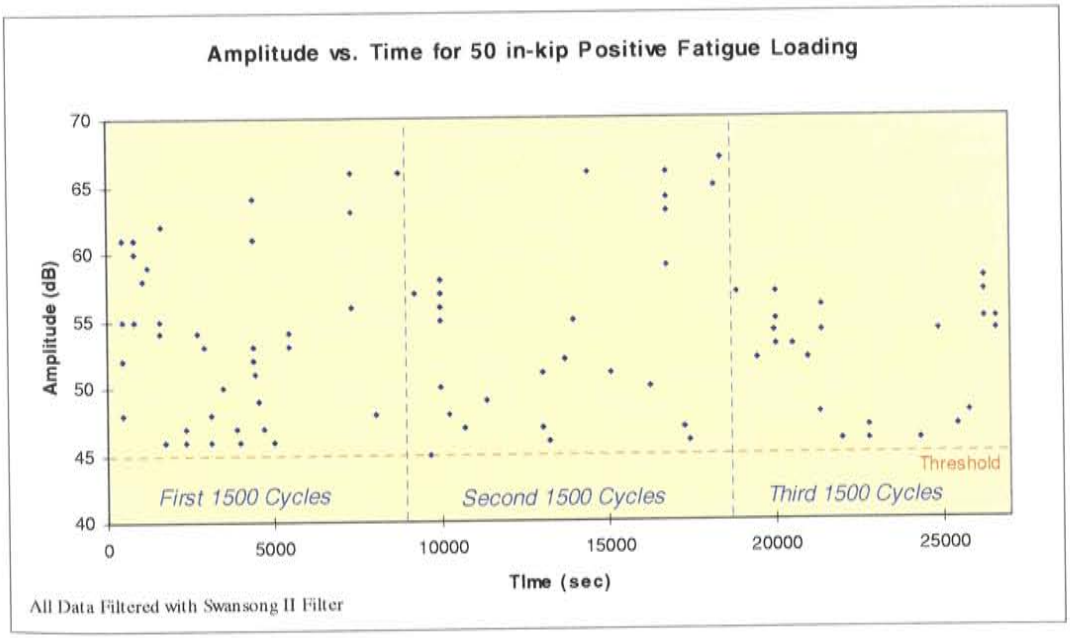

Figure 4.25: Amplitude vs. Time for 50 in-kip Positive Fatigue Loading

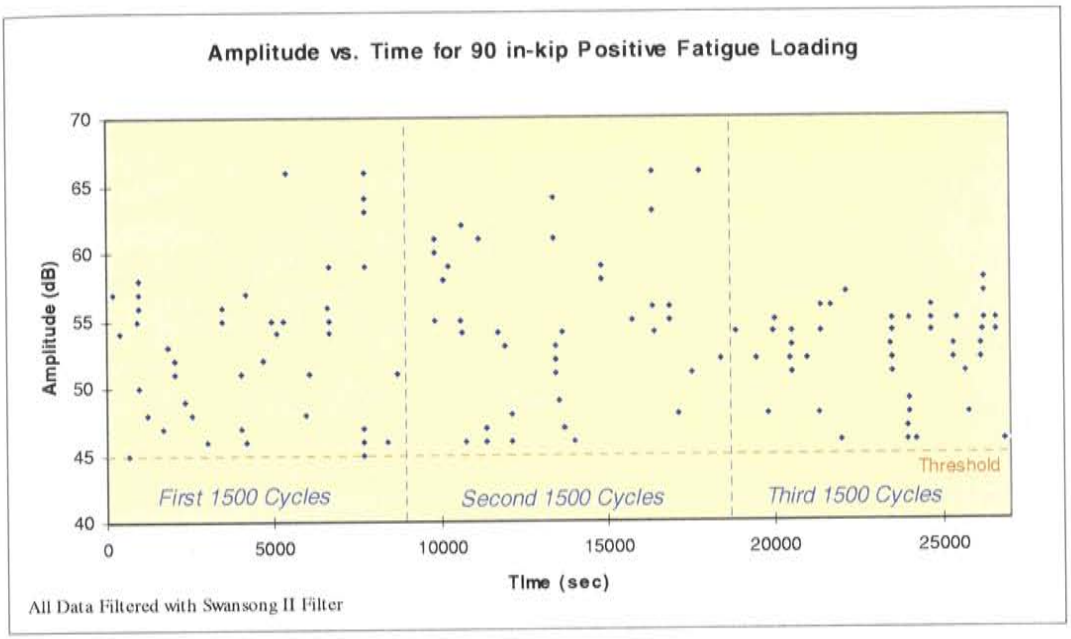

Figure 4.26: Amplitude vs. Time for 90 in-kip Positive Fatigue Loading

The data for the two load levels shows some interesting trends. Although it appears quite random initially, spikes of emission activity (occurring over a time period of less than one tenth of a second) can be seen at certain time increments. It is suspected that these spikes are the result of crack progression or further crack tip yielding. The crack can be seen to be growing, or at the very least worsening, in distinct stages. It is also interesting to note that emission dies down immediately following the overloads. This is consistent with what is being accomplished during the overload – blunting of the crack tip.

A final thing that may be noted about the fatigue data, which was seen indirectly with an examination of the signal strength data from fatigue cycling, is

that at the 90 in-kip load level, both the number of hits and the average amplitude of those hits was higher than with the 50 in-kip data. This is further evidence of the failure model proposed, and reinforces the fact that the crack, or at least the effects of the crack, have worsened with increased fatigue loading.

4.3.5 Results from Pearl Harbor Field Test

The loading schedule for the main and boom hoist shafts is shown in Figure 4.31. Acoustic emission data was collected during the entire load schedule. The load data is given in percent of maximum rated load vs. seconds. Before the load was increased, it was returned to the nominal load value of 10% of the rated capacity. Keeping a nominal load on the cable at all times may have helped limit extraneous noise due to cable stretching; however, it was shown that such noise could be removed via post test filtering if it occurred.

Before testing, the Dunnegan Crackers were used to characterize the attenuation characteristics of the shaft in the field. It was confirmed that the sensors were capable of recording actual emission events (not only simulated ones) from all regions of the shaft. The Dunnegan Crackers provided a more realistic waveform than did the other simulation methods. This is shown in Figures 4.27 through 4.30

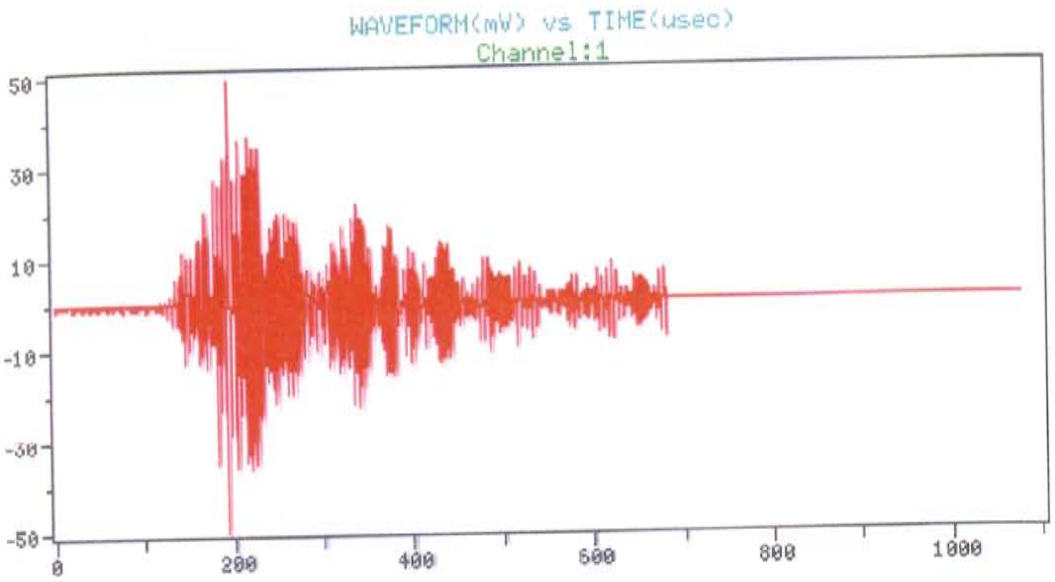

Figure 4.27: Actual AE Event as Recorded by R15I Sensor

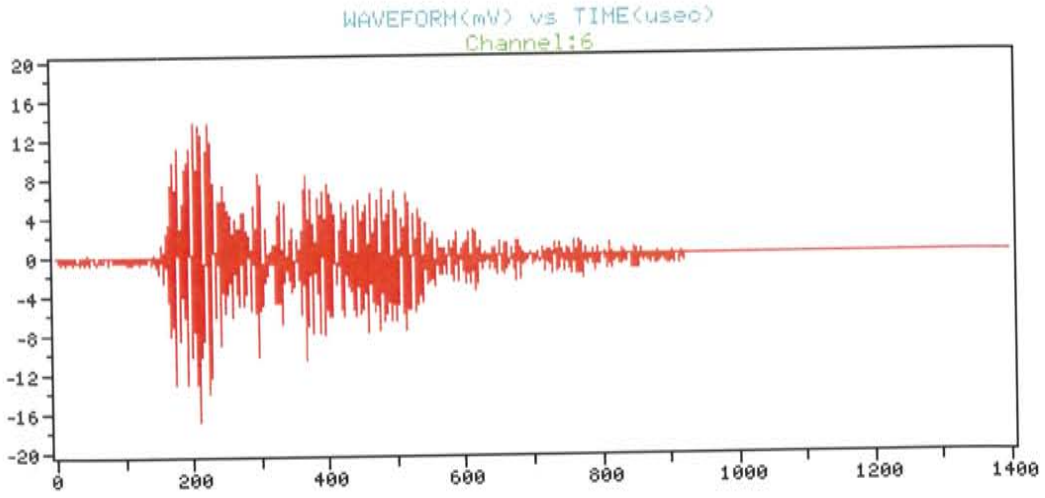

Figure 4.28: Dunnegan Cracker Waveform as Recorded by R15I Sensor

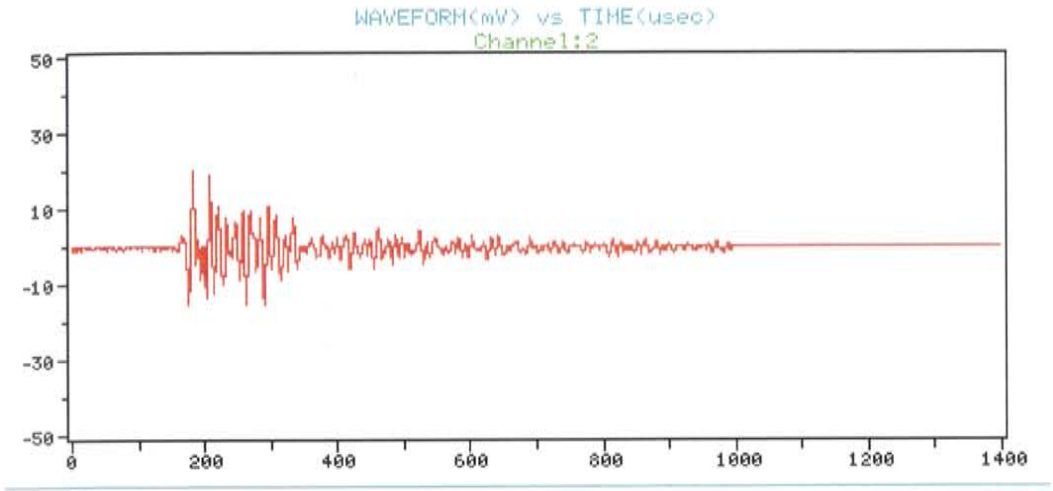

Figure 4.29: Pencil Lead Break Waveform as Recorded by R15I Sensor

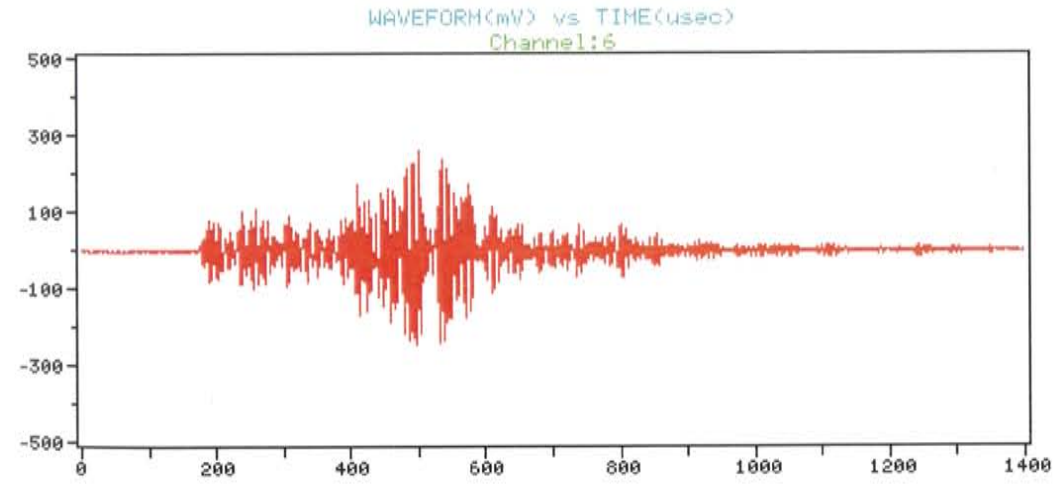

Figure 4.30: PAC AE Pulser Waveform as Recorded by R15I Sensor

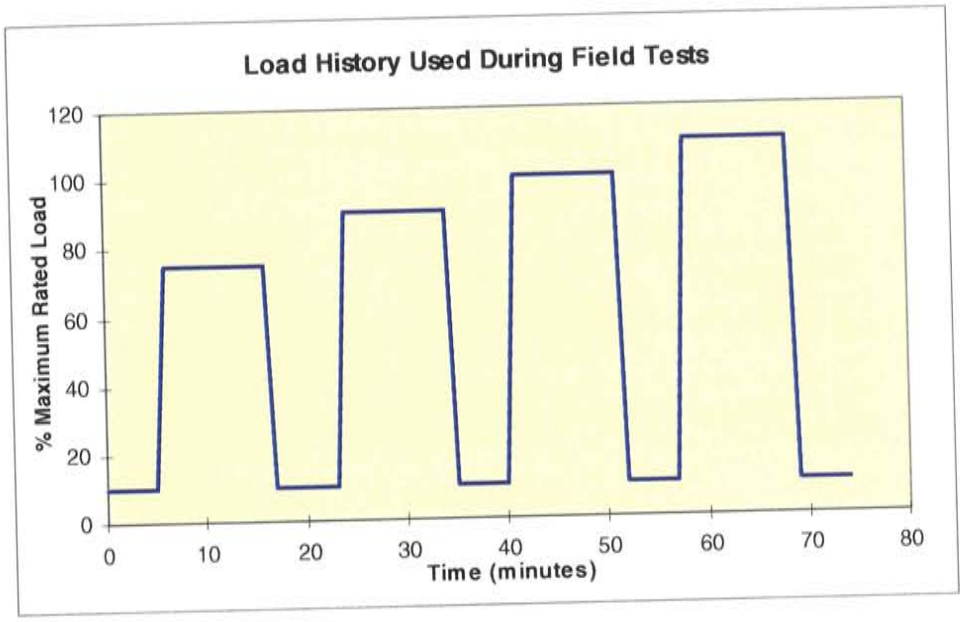

Figure 4.31: Load vs. Time for Main and Boom Hoist Shaft Tests

Main Hoist Shafts

Figure 4.32 shows duration versus amplitude for all the hits collected during the entire load sequence. Hits for both the main hoist drum shaft and the main hoist boom shaft are included here. The data in this figure has not been subjected to any filters, and data due to EMI and mechanical rubbing are present in this plot. This being the case, the total number of AE hits total only 117, quite a small number in AE parlance.

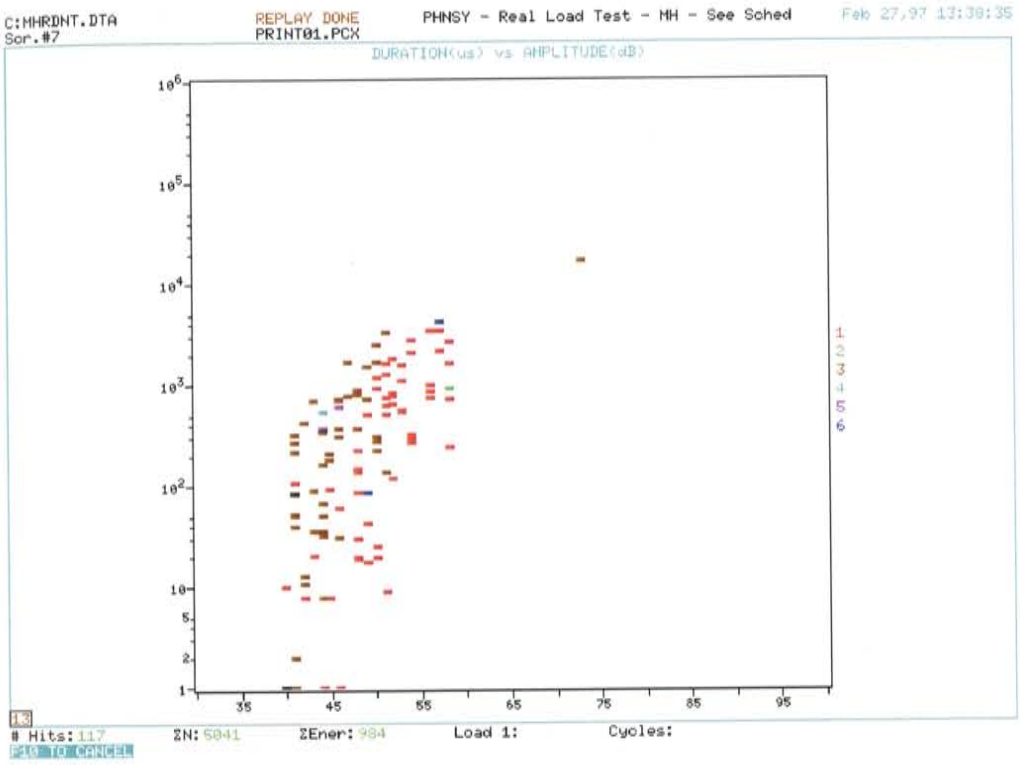

Figure 4.32: Correlation Plot for All Sensors (Included Both Main Hoist Drive and Main Hoist Drum Shaft Sensors). The Data in this Plot is Unfiltered, and Hits from EMI and Mechanical Rubbing are Still Present.

Figure 4.33 shows the number of hits vs. channel of the unfiltered data given in the previous Figure. Note that the majority of the data was detected by the broadband sensors #1 and #3, which were located at each end of the main hoist drum shafts. The broadband sensors were expected to pick up more data than the resonant sensors #2 and #4, which were are only sensitive to hits in a limited frequency range. However, it is interesting to note that the broadband sensor #5 located on the main hoist drive shaft picked up very little data. This

indicates that the majority of the AE data collected during the test originated from the drum shaft.

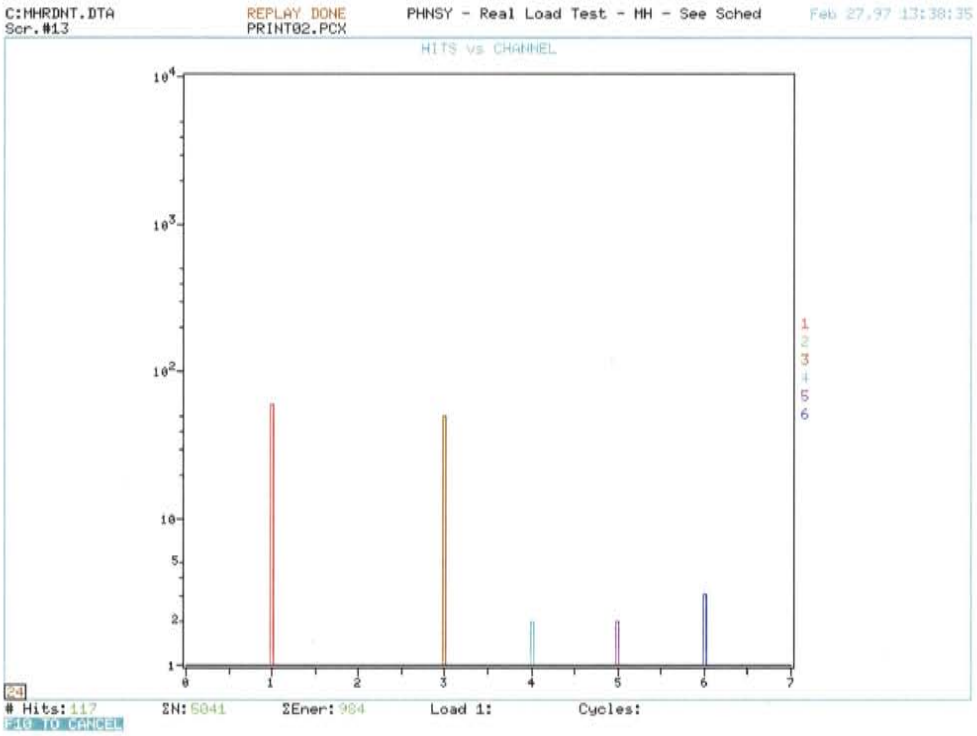

Figure 4.33: Total Number of Hits vs. Channel for the Unfiltered Data given in the Previous Figure

Figure 4.34 shows the remaining hits after removal of EMI only. Note that the number of hits decreased from 117 to 27. The number of hits, qualitatively, is considered to be a very small.

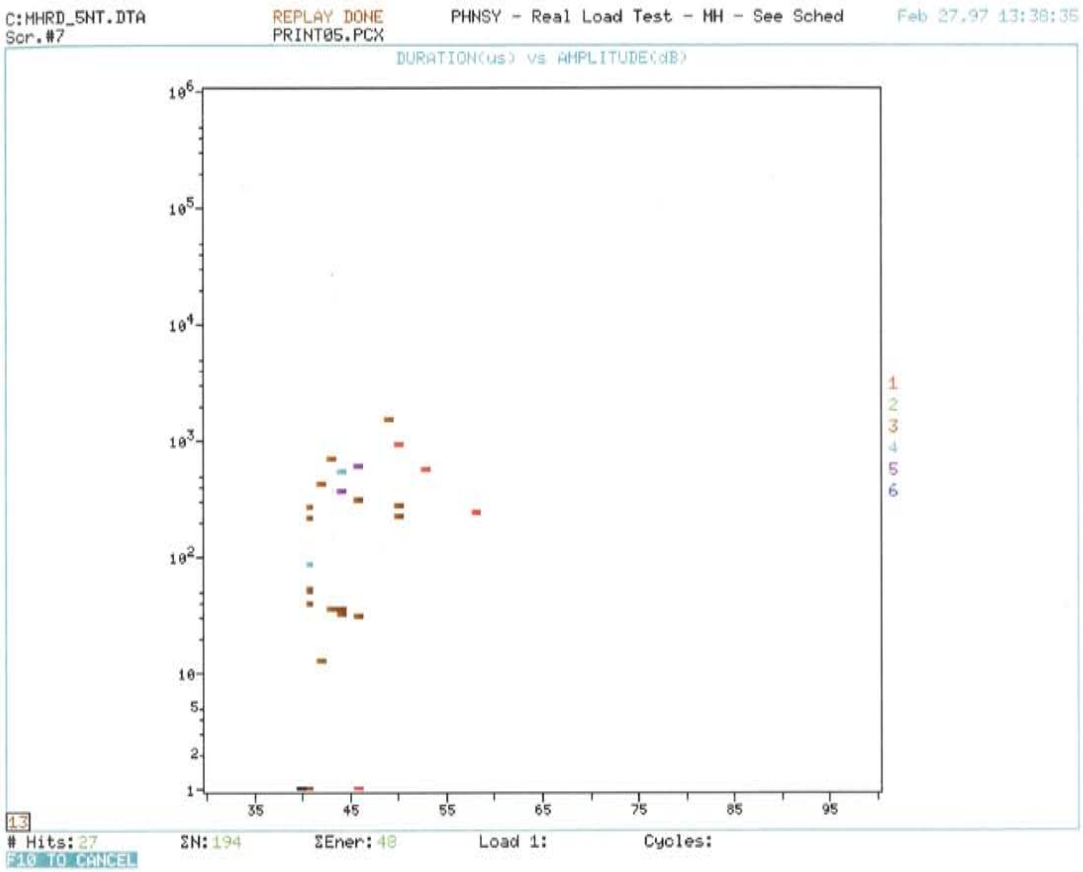

Figure 4.34: Correlation Plot for All Sensors (Including Both Main Hoist Drive and Main Hoist Drum Shaft Sensors). The Data in this Plot has been Filtered to Remove EMI, but Hits from Mechanical Rubbing are Still Present

Before the EMI data was removed, the Swansong II filter was applied. The filter removed no hits from the data set. This indicates that mechanical rubbing was not a problem during main hoist drive and drum shaft testing. Most of the mechanical rubbing problems experienced in the laboratory was likely an artifice of the experimental technique used, and not indicative of what would be

experienced in the field. The use of the Swansong filtering technique with the lab data, however, made the results obtained in the laboratory fully applicable for comparison to results obtained in the field.

EMI was a known problem during the field testing. The cause stemmed from banks of relays on the walls of the crane cab opening and closing causing electrical arcing and sparks. The precise time which a control movement was made that caused the relays to activate was manually noted, electronically, in the data file. Using the ATPOST software, all hits occurring within a time zone of ±1 second of the EMI event were removed. This was done by means of a time filter.

The 27 remaining hits, after EMI had been filtered, can thus be considered to be genuine emission. Note that the vast majority of this data has an amplitude lower than 50 dB, and the cumulative signal strength for all 27 hits is a mere $48 \text{ volt} \cdot \text{sec} \times 10^{-5}$.

From a qualitative standpoint, all the data collected suggests that the main hoist shafts do not have large, rapidly growing, structurally significant cracks. Quantitatively, this is also true. The amount and magnitude of emission for the entire test sequence is much smaller than that collected during a single overload procedure on a single shaft in the laboratory. This indicates that no defects are present which are being stressed by the loading scheme used, and in all likelihood the main hoist drive shaft and main hoist drum shafts are fully serviceable.

Boom Hoist Shafts

The data collected from the boom hoist drive and drum shafts was similar in many ways to that collected from the main hoist shafts. A correlation plot of the data, without any filtering, is shown in Figure 4.35. As with the former case, the EMI emitted from the large banks of relays on the walls of the crane cab was responsible for much of the emission detected. The data with the EMI filtered out is shown in Figure 4.36.

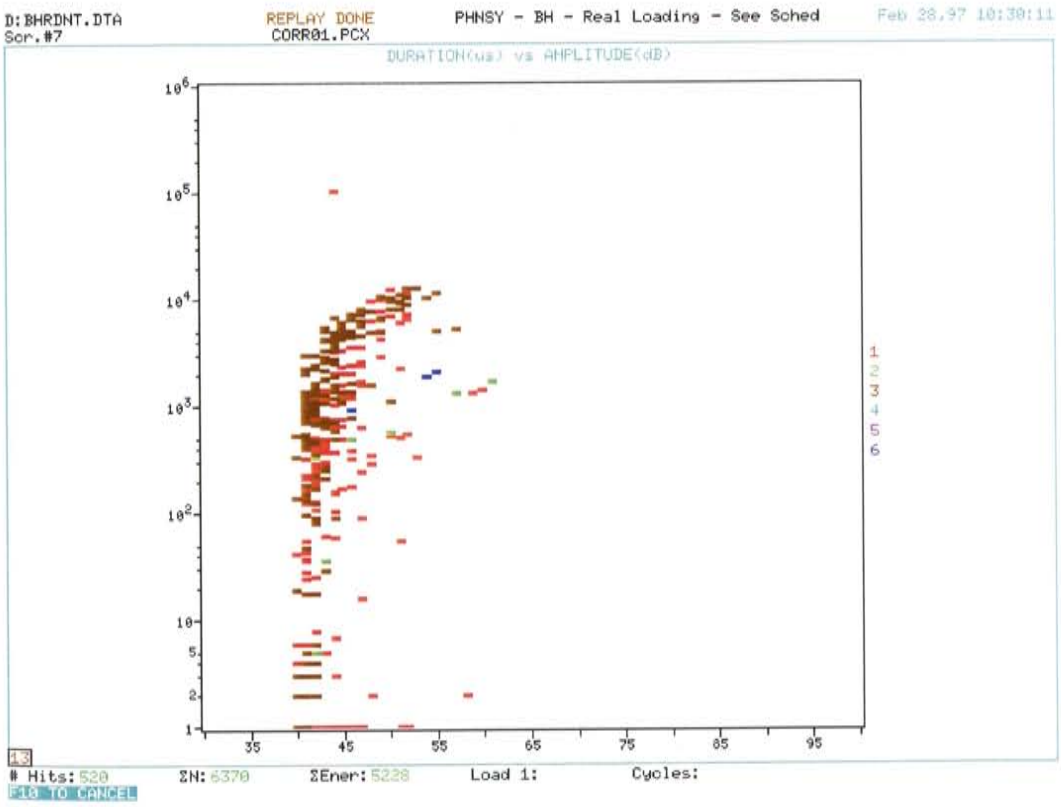

Figure 4.35: Correlation Plot of the Boom Hoist Drive and Drum Shaft Data Before Filtering

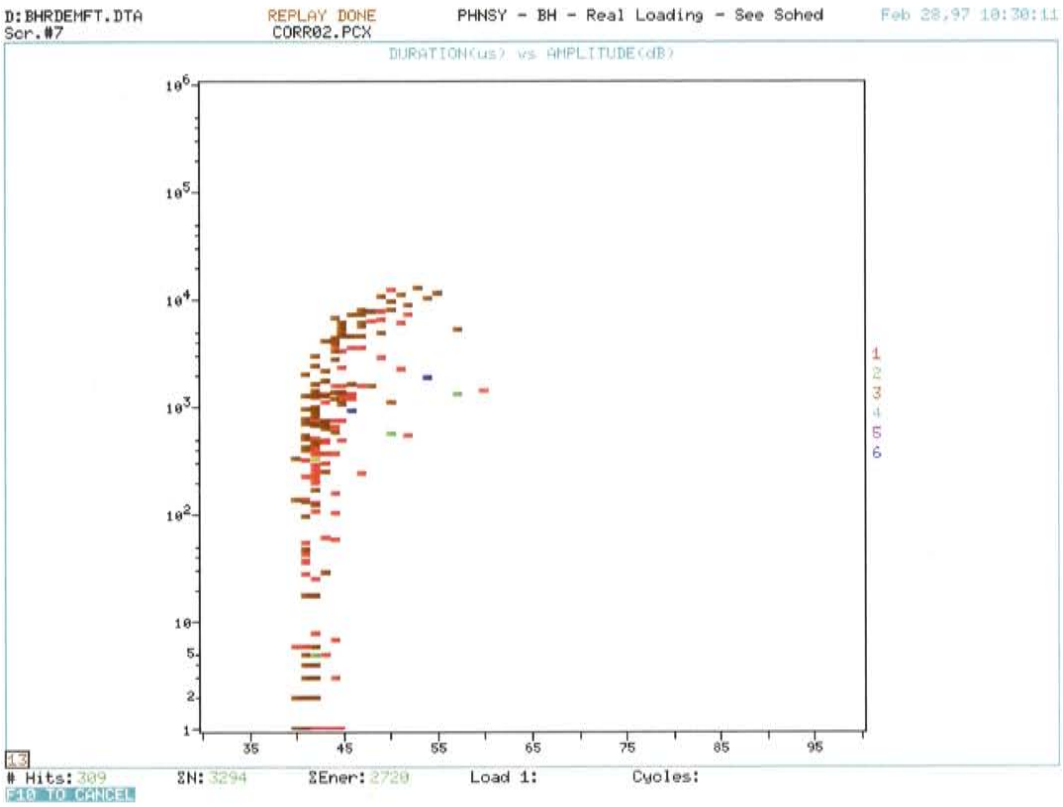

Figure 4.36: Correlation Plot of the Boom Hoist Drive and Drum Shaft Data with EMI Removed

With the EMI removed, the number of recorded hits was reduced from 520 to 309. When the data set was subjected to the Swansong II filter, a further 170 hits were removed, leaving a total of 139 genuine AE hits. This is shown in Figure 4.37. The 170 hits resulting from mechanical rubbing are in stark contrast to the case of the main hoist shafts where no rubbing hits were seen to have been recorded. This observation cannot be explained, but it is speculated that noise borne in the crane is more readily transferred to the boom hoist shafts

as opposed to the main hoist shafts because the boom hoist shafts are loaded more directly (i.e., through a fewer number of gears) than their main hoist counterparts.

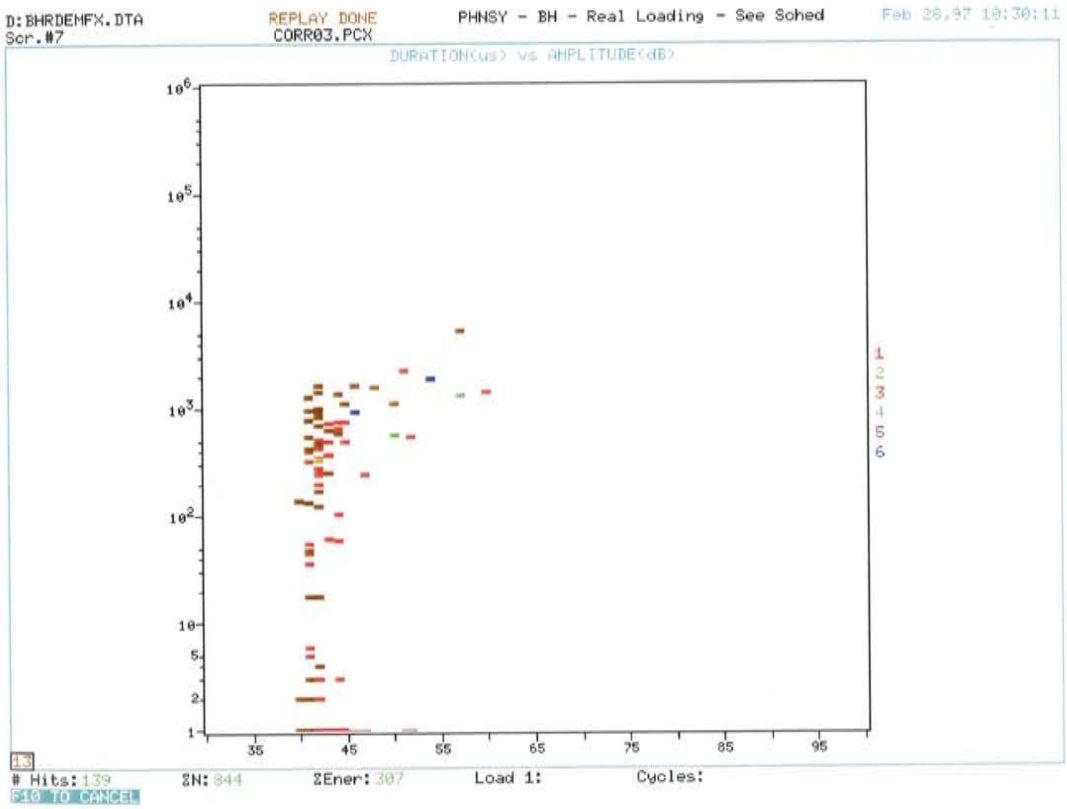

Figure 4.37: Correlation Plot of the Boom Hoist Drive and Drum Shaft Data with EMI and Rubbing Removed

While the 139 AE hits recorded on the boom hoist shaft test is over 5 times the number of genuine AE hits observed on the main hoist test, compared with the laboratory data, it is still a modest number of hits. Also, the amplitude

of the vast majority of the hits is below 55 dB; these hits can thus be qualitatively described as low amplitude. Quantitatively, the cumulative signal strength of the filtered data was calculated to be 307 volt $\cdot$ sec $\times 10^{-5}$, again, quite a small number when compared to a single overload cycle in the laboratory.

From a qualitative standpoint, as with the main hoist shafts, all the data collected suggests that the boom hoist shafts do not have large, rapidly growing, structurally significant cracks. Quantitatively, this is also true. The amount and magnitude of emission for the entire test sequence is much smaller than for a single overload procedure on a single shaft during the laboratory testing. This indicates that no defects are present which are being stressed by the loading scheme used, and the boom hoist drive shaft and boom hoist drum shafts are fully serviceable.

4.3.6 Intensity Analysis

An intensity analysis was carried out on the positive overload data using the traditional MONPAC intensity analysis charts. The results for both the 150 kHz sensors and the 300 kHz sensors are shown in Figures 4.38 and 4.39, respectively.

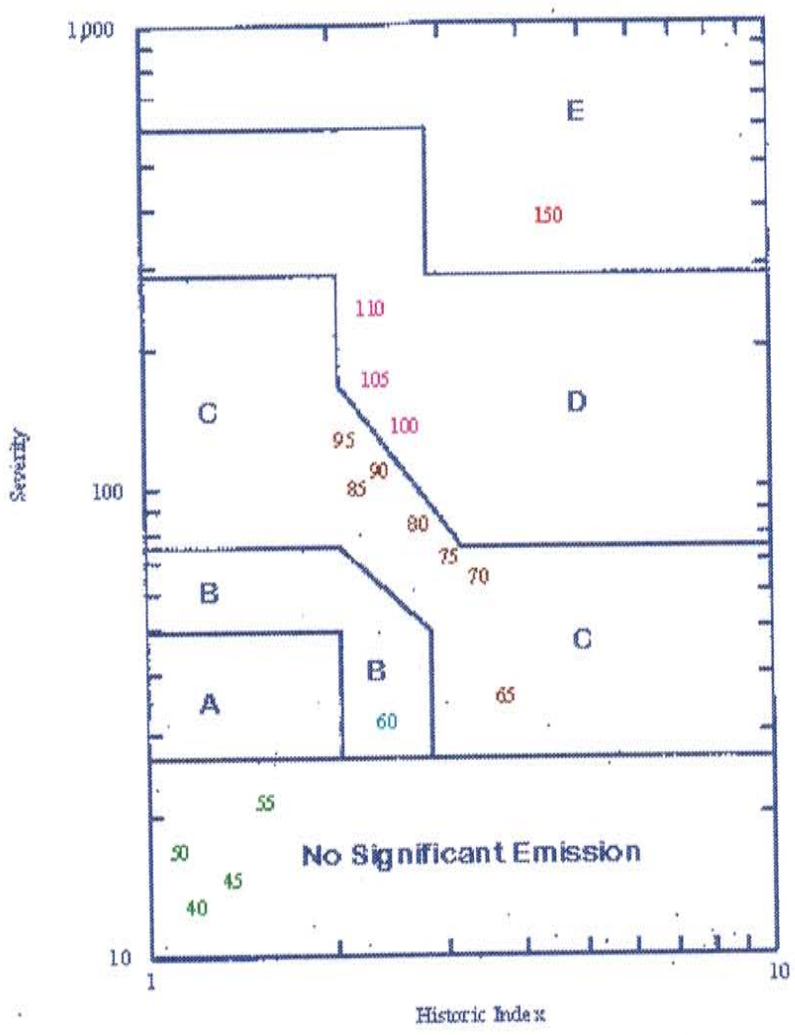

Figure 4.38: **MONPAC Intensity Analysis for Positive Overload Data using R15I Sensors**

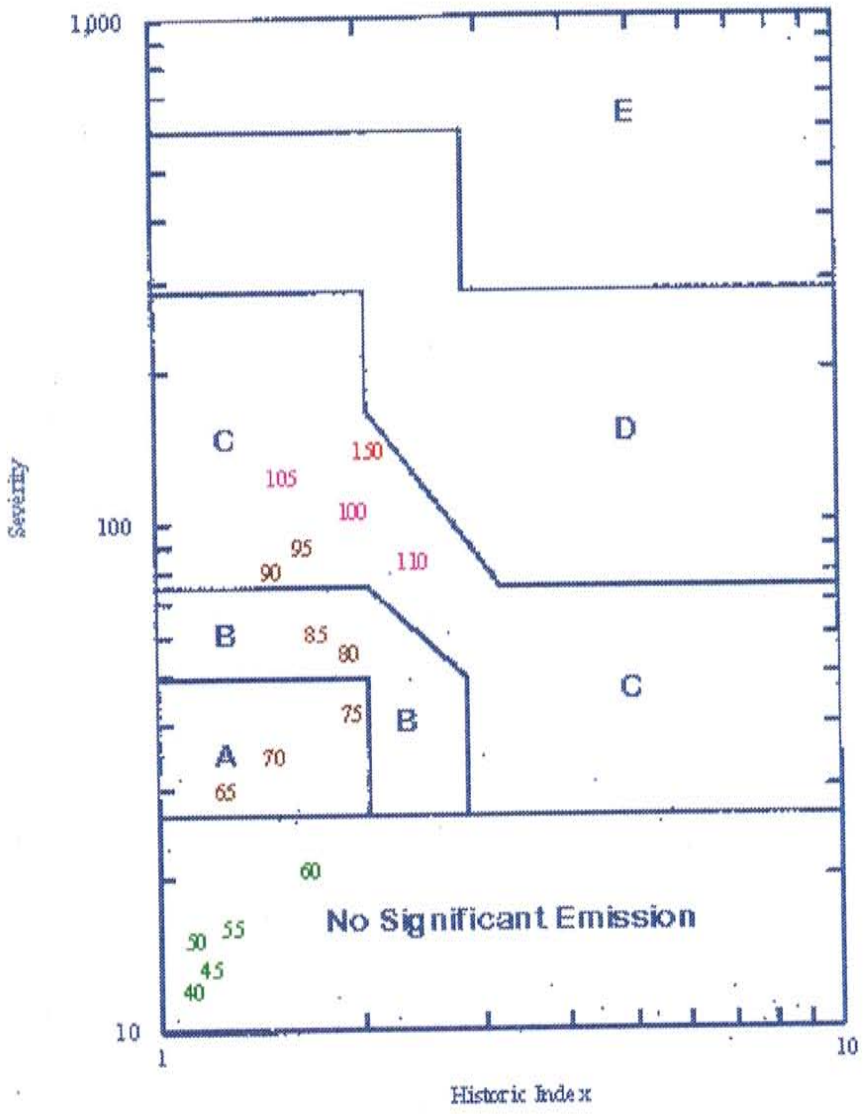

Figure 4.39: MONPAC Intensity Analysis for Positive Overload Data Using R30I Sensors

The intensity analysis confirms much of what was seen in the signal strength based analysis. As fatigue load level increases, so does the intensity of the emission. Note the fact that the intensity of the 300 kHz sensor data is less than for the 150 kHz sensor data. As discussed previously, this stems from the higher attenuation at the 300 kHz central frequency range and the reduced sensitivity of the sensors.

Definite "groups" of numbers can be seen in the charts for both frequencies of sensors. These groupings were used to propose a simpler type of intensity analysis chart to be used in the standardized test procedure, as shown and discussed in Chapter 5.

4.3.7 Source Location

The Jolly-Stuart method of zonal source location was used with the lab data to determine the location of the defect in the shaft. For the purposes of the present analysis, overload data taken at fatigue load levels above 75 in-kips was considered, as the analysis up to the present point indicates that damage was definitely occurring in the shaft at 75 in-kips and above. Although each overload was analyzed, a trend in the data quickly became apparent. For the purposes of the present discussion, a typical overload will be discussed in detail with the realization that virtually all the other data, even that taken at fatigue load levels of less than 75 in-kips, follows the identical pattern.

The Jolly-Stuart source location analysis of the R15I data shows that the source of the majority of the emission comes from the front of the shaft, and that

the defect is most active under clockwise loading. Similar data is found on the R30I sensors, however, because of the attenuation, fewer second hits are present and no reflections are recorded. The emission from the back of the shaft may be caused by other sources. It was suspected, for example, that the welds attaching the end blocks to the transfer beam were a bit noisy. Those welds were of particularly poor quality, and eventually failed. The number of first hits recorded near the back of the shaft increased slightly as the load level went up, as the weld got closer to failure. Even with the noisy weld at the back end of the shaft, on average, the number of first hits recorded at the back were on the order of one eighth the number recorded at the front of the shaft. When the welds were repaired with ones of suitable quality, virtually all genuine emission from the back end ceased.

Table 4.2: Jolly-Stuart Analysis of 150 kHz and 300 kHz Data for a Typical Overload Cycle. Data Presented is for the Second Overload at a Fatigue Load Level of 85 in-kips.

	Front End Sensors	*Back End Sensors*
R15I SENSORS		
Clockwise Loading		
First Hits	63	8
Ancillary Hits Relative to Front End	6	1
Ancillary Hits Relative to Back End	3	16
Counterclockwise Loading		
First Hits	16	2
Ancillary Hits Relative to Front End	3	1
Ancillary Hits Relative to Back End	1	2
R30I SENSORS		
Clockwise Loading		
First Hits	9	5
Ancillary Hits Relative to Front End	1	0
Ancillary Hits Relative to Back End	0	1
Counterclockwise Loading		
First Hits	2	1
Ancillary Hits Relative to Front End	1	0
Ancillary Hits Relative to Back End	0	1

4.3.8 Results From Other Nondestructive Examination Methods

Following the failure of the first crane shaft, the Navy ordered all other crane shafts from the same manufacturer and of the same vintage to be nondestructively examined for cracks. The Navy's in-house NDT personnel used ultrasonic, eddy current, and wet fluorescent magnetic particle testing to try and detect the cracks. The results were less than satisfactory.

The geometry of the shaft, especially mounted in-situ, makes obtaining good results with traditional NDT methods very difficult. The problems experienced by the Navy were typified in one of the methods giving a positive indication of a defect, and then the other methods would not. In one case, all three methods gave no indications of defects and then the shaft failed catastrophically only a few days after the inspection took place. The failure analysis reveled the presence of a major structural crack in the location where it was suspected when the nondestructive examination was ordered. It is impossible to say with any degree of certainty why the defect was missed. As with most traditional applications of the aforementioned NDT techniques, operator skill and acuity plays a key role in the sensitivity of the method.

Ultrasonic and wet fluorescent magnetic particle testing of the shafts also took place in the laboratory. Matrix Engineering and Testing in Houston, Texas performed the inspections. The shafts used during the static loading phase (phase I) and the dynamic loading phase (phase II) of the laboratory testing were both examined.

The magnetic particle examination showed no indication of defects. The ultrasonic examination, performed by Dr. John McMillan, one of the foremost experts in the field, was attempted using almost every conceivable technique and approach known. Pulse-echo and time of flight diffraction were both attempted, using many different frequencies, sensor configurations, and wave types. Special transducer shoes were even manufactured specifically for the radius of the shafts being inspected, all to no avail. The ultrasonic testing from the outside of the shaft did not reveal with any degree of certainty the presence or location of a crack. There were some indications during the testing, but they were sporadic and difficult to narrow down, much less assess.

The ends of the shaft used during phase I of the testing, which was not to be reused during subsequent testing were sectioned off and sent to Matrix for ultrasonic inspection. Once sectioned, cracks at the inside corner of the keyway were identified. The cracks were small, but still well within the resolution of the ultrasonic techniques attempted. It is suspected that the complex geometry of the specimen prevented the detection of the cracks before sectioning.

This result has profound implications for the Navy, although it is likely one already known to them; the proof being in the commissioning of the present work. The acoustic emission techniques proposed and demonstrated in the laboratory and in the field are global in nature and not as susceptible to operator skill especially when clearly defined failure criteria are used for analyzing the results. This is discussed further in Chapter 5.

4.3.9 Verification

In the present research, as with any other innovative work in science that has never before been done, it is important to establish that the emission did indeed result from a crack which grew during the fatigue cycling. One way of doing this would be to section the shaft, find the crack, further section the specimen along the crack face, and then finally use electron microscopy to identify the location of the crack tip at various stages of the loading history. Because of the very small size of the cracks present in the shaft (indeed, even a small crack can be critical in this material) and the difficulty in locating them using complimentary NDT methods, it is doubtful that this method would have been successful.

Recall, one of the bases on which it was determined that the crack was growing as the number of cycles increased was the increasing energy being released at higher load levels. It could be argued that it was the increasing load which caused the higher emission, and the fatigue cycles between overloads had no part to play. This argument is paramount to saying the crack did not grow and the increased emission from the crack tip at higher load levels was simply a function of the increased stress. In order to counter such an argument, another, more elegant, method than sectioning the shaft was needed to prove that the crack did indeed grew as a function of the fatigue loading.

Such a method was devised, and proved that the crack had to have grown during the fatigue cycling. By simply subjecting the specimen to the overloads and not the intermediary fatigue cycles, the data resulting from monitoring such

a process with acoustic emission could be used to prove the point by inference. This is precisely what was done, and the results are shown in Figure 4.40.

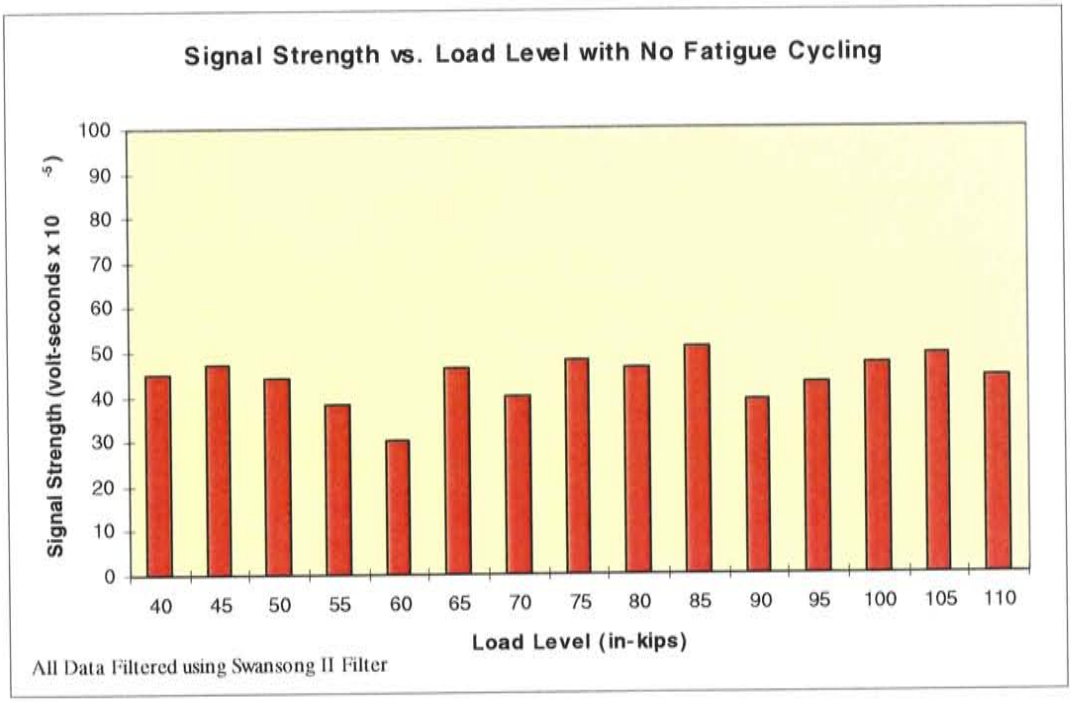

Figure 4.40: Signal Strength vs. Load Level with No Fatigue Loading

The Figure shows that without any fatigue loading, the amount of emission remains quite constant as the load level increases. The fact that no linear increase in emission with load level is seen, as was the case with the overload data, it may be concluded that the increase seen previously was in reality a function of the crack growing under the fatigue cycling, and not an

artifice of the increasing stress level. It is interesting to note that the magnitude of the emission is orders of magnitude less than for the equivalent loads under the overload procedures in the fatigue cycling regime. Signal strengths as low as $60 \text{ volt} \cdot \text{sec} \times 10^{-5}$ are very, very small indeed. Figure 4.41 shows a cumulative plot of the data shown in Figure 4.40. Note the absence of a knee in the curve, indicating that the strong trends seen in the fatigue cycling data were not an artifice of the experimental technique used.

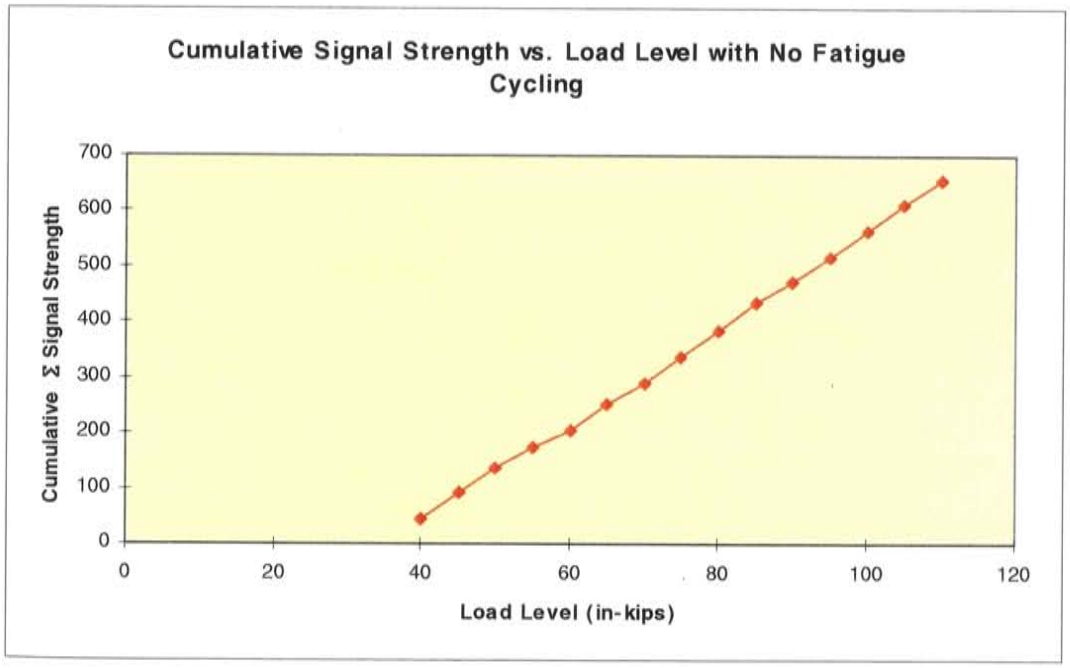

Figure 4.41: Cumulative Signal Strength vs. Fatigue Load Level. Note absence of knee in curve

CHAPTER 5

APPLICATIONS

5.1 STANDARDIZED TEST PROCEDURE

Using the results of the data collected in the laboratory during both the static and dynamic loading phases, a test procedure to be used by the Navy's NDT personnel was proposed. The procedure is built upon the American Association of Railroads procedure for railroad and intermodal tank cars[15]. In order to assure that the crane shaft is exposed to a load level greater than any in the previous six months, it is recommended that the AE monitoring be done during annual crane certification proof loading. This is, in essence, an overloading procedure, and thus the results from the overload data obtained in the lab are used as a basis for comparison.

The procedure encompasses all traditional aspects of a standardized AE procedure, including instrument settings and calibration, sensor types and placement, specimen surface preparation, attenuation characterization, personnel qualification and interpretation of test data.

The procedure allows for two different operating frequency ranges for sensors, preamplifiers, filters and other frequency sensitive instrumentation. The two ranges are centered on a nominal frequency of 150 kHz and 300 kHz. Selection of the appropriate operating frequency depends on the characteristics

of the emission recorded during a preliminary background noise check. The 150 kHz range is preferred. Separate evaluation criteria are proposed for the two operating ranges.

The procedure requires mechanical loading of the shaft. Loading is accomplished by pulling against a large mass while monitoring with a load cell. Normally, the load that is lifted off the ground during certification is used as the large mass. Details of the loading sequence follow. The test procedure specifies loading to a maximum load determined on the basis of the crane's design load. The procedure does not apply to shafts loaded above the maximum rated load during the six month period prior to performing an AE test. Typically, the maximum AE test load is 110 percent of the maximum rated load. The loading test assesses the shaft for defects such as cracks, corrosion, and other defects which are stressed during loading.

Two loading options are proposed in the procedure. The first applies load to the shaft of interest which remains in a fixed position. The second varies the angular position if the shaft under a number of successive loadings. The angular position of the shaft is changed to allow bending moments and shear stresses to be applied in different directions in order to develop the most serious combination of stresses. The fixed position loading was used for the field test at Pearl Harbor. The variable shaft position was suggested as a result of the work carried out during the first field test, (to ensure that the crack tip is activated under one of the loading directions) and is recommended for subsequent tests.

The master load schedule, in terms of percent of maximum rated load, is proposed as follows:

- Begin by applying a load of 10% (-0% +5%) of maximum rated capacity. Use this load to keep tension on the shaft: it becomes the baseline, or minimum load.
- Increase to 75% (-0% +5%); hold for 10 minutes; decrease to 10%; hold for 5 minutes.
- Increase to 90% (-0% +5%); hold for 10 minutes; decrease to 10%; hold for 5 minutes.
- Increase to 100% (-0% +5%); hold for 10 minutes; decrease to 10%; hold for 5 minutes.
- Optional: Increase to 110% (-0% +5%); hold for 10 minutes; decrease to 10%; hold for 5 minutes.

The load schedule for variable shaft position test is essentially similar in terms of load magnitudes, but at each load level a step is included to release the load, lower the boom slightly, and repeat 3 times to obtain other angular rotations.

After the data has been collected, post-test filters are applied. The two filters suggested for use are the Swansong II filter, as it was seen to be very effective both in the lab and in the field in removing background noise.

Evaluation criteria for each individual channel are proposed. Table 5.1 details the acceptable emission levels for which a shaft can be considered safe. The values in the table are a direct product of the static and dynamic loading

phase laboratory testing carried out at the Ferguson Structural Engineering Laboratory.

Table 5.1: Individual Channel Acceptance Criteria

Criterion	*150 kHz Sensors*	*300 kHz Sensors*
Cumulative Signal Strength During Loading and Load Holds, Volts-Seconds^{-5}	< 350	< 100
Felicity Ratio	> 0.95	>0 .95
Cumulative Emission During Load Holds, Hits	20	10

Additionally, an intensity analysis using the traditional parameters of Historic Index and Severity has been incorporated into the evaluation criteria. Again, there are different criteria for different sensor types. The intensity chart for 150 kHz sensors is shown in Figure 5.1. The intensity chart for 300 kHz sensors is shown in Figure 5.2.

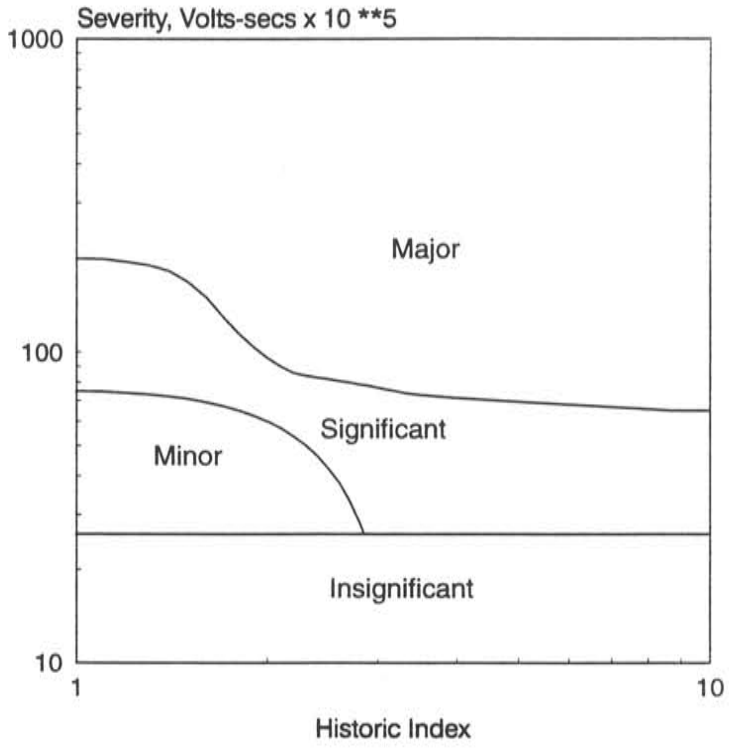

Figure 5.1: Intensity Chart for 150 kHz Sensors

Based on the intensity analysis, minimum recommended follow-up actions were proposed:

- **Insignificant**: Emission source is structurally insignificant.
- **Minor**: Minor emission Note for future reference. Visually inspect accessible areas.

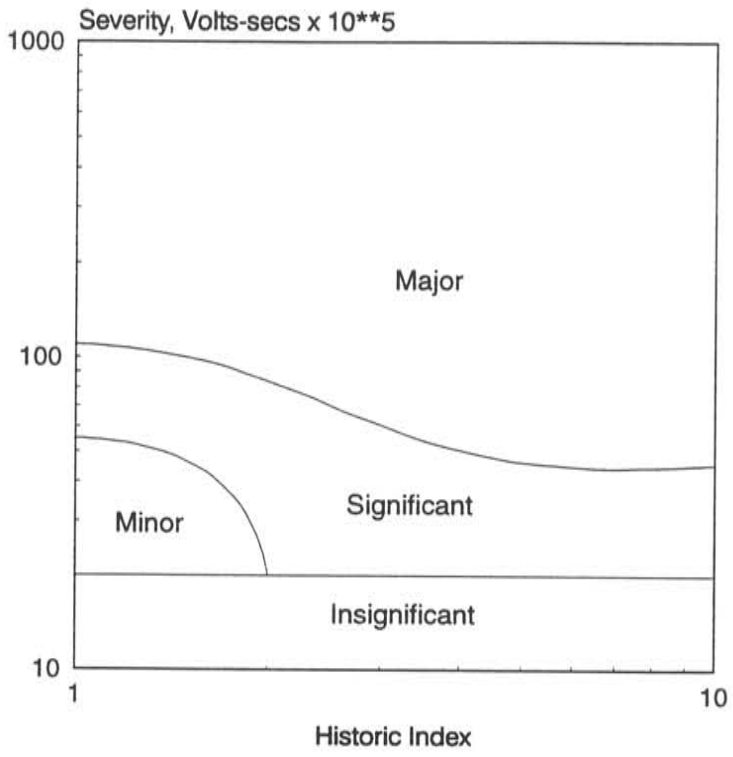

Figure 5.2: Intensity Chart for 300 kHz Sensors

- **Significant**: Significant structural defect requiring follow-up evaluation. As a minimum, evaluation should include further data analysis and visual inspection of accessible areas. Consideration should be given to comprehensive nondestructive examination, retest, and increased frequency of inspection.
- **Major**: Major structural defect. Immediate shutdown and nondestructive examination.

The proposed test procedure is included in the Appendix.

Using the above evaluation criteria in conjunction with the data obtained during the field test at Pearl Harbor, as detailed in Chapter 4 and summarized in Table 5.1, crane P-64 which had been taken out of service because of a shaft failure in its sister crane, was judged to be structurally sound and its return to service was recommended.

Table 7.1: Evaluation of Field Test Data using Criteria Defined in Test Procedure

CRITERIA	*MAIN HOIST SHAFTS*	*BOOM HOIST SHAFTS*
Cumulative Signal Strength During Loading and Load Holds	**182** (<350) ✓	**20** (<100) ✓
Felicity Ratio	**0.98** (>0.95) ✓	**0.98** (>0.95) ✓
Cumulative Emission During Load Holds	**7** (<20) ✓	0 (<10) ✓
Significance	Insignificant ✓	Insignificant ✓
RESULT	**PASS**	**PASS**

5.2 COMMERCIAL AND GOVERNMENT APPLICATIONS

The present work is widely applicable to both government and commercial/industrial applications. The Navy, Department of Defense, and other government clients can use the results of the experimentation as well as the proposed standardized test procedure directly to diagnose the health of cranes in their world theater of operation. The inspections need not be carried out by government personnel, the test procedure may be included in contract bids for consultants or civilian contractors.

Some potential commercial/industrial clients include crane owners at commercial ports, and others in the shipbuilding, steel, railroad, and oil industries. Additional applications include the paper and textile industries, where large diameter shafts are used in spools during manufacturing.

CHAPTER 6

CONCLUSIONS

Acoustic emission is a powerful nondestructive testing technique that has wide ranging applications in traditional civil engineering environments. The experimental program carried out during the research reported here showed that by using acoustic emission, the condition and state of serviceability of Naval portal crane shafts can be definitively and conclusively identified.

The laboratory data showed that acoustic emission can be used to detect the presence of fatigue cracks. Indeed, the larger and more significant the crack is, the more emission it will cause. Traditional parameters such as signal strength, number of hits during load hold, intensity analysis, and the Felicity ratio can be used together to determine the state to which a crane shaft is damaged, and suggest a course of action for further inspection or usage.

The technology was seen to be effective in the relatively noisy environment of dynamic fatigue testing. By acoustically insulating the shaft from the test stand, and being judicious in the selection of sensors, thresholds, and a post-test filtering regime, the background noise problems did not in any way prevent the acquisition of genuine and usable data. The data correlated well to that obtained during static load testing where, as expected, background noise problems were almost non-existent.

The use of 150 kHz and 300 kHz integral resonant sensors, with a 45 dB threshold was effective both in the laboratory and in the field. The Swansong II filter was all that was needed to remove any remaining background noise that was encountered. The effectiveness of the filtering techniques was specifically verified by examining the digital waveforms in the data before and after filtering. Characteristically bad data was completely removed from the data sets in all cases by using the filters.

The work carried out in the laboratory transferred over to field testing quite well. In part this was due to the extreme care that was taken when devising the laboratory test setup to closely replicate field conditions. The shafts tested in the lab were generally shorter than those found in the field. This was not a problem, however, because of the shaft's excellent acoustic transmission properties, as well as the fact that the most critical areas to monitor are the shaft ends, which behave independently of length.

The field test carried out at the Pearl Harbor Naval Shipyard helped identify potential problems that might be encountered during field testing which were not seen in the highly ideal environment of a laboratory. This test, in conjunction with the lab research, led to a proposed standardized test procedure which effectively documents the techniques necessary to test and interpret data from a load test where the critical shafts are monitored with acoustic emission instrumentation. The laboratory data taken during overload cycles were mainly used for this purpose.

The Jolly-Stuart method of zonal source location is effective in determining from which end of the shaft the emission was generated. This result

allows for a detailed follow up inspection with a complementary nondestructive testing technique to more clearly identify the geometry of the defect, and to further dictate follow-up action. Some of the traditional nondestructive testing techniques such as magnetic particle, eddy current, and ultrasonic inspection, however, have been shown by the Navy and by this research to not be as sensitive as acoustic emission in locating structural defects. The Navy's nondestructive testing branch has struggled for years with the lack of consistency in finding defects using an entire host of methods. This, in part, may be attributed to the complex geometry of the key and keyway interface in the shaft, and furthers the need for a global nondestructive technique to be adopted. Acoustic emission is one such technique, one which can be applied to a wide range of materials and geometries, and one whose data analysis results are readily identifiable and relatively independent of the acuity of the operator.

Fundamentally, this research has valuable technical information concerning fatigue crack development and detection. This work has broad implications beyond the present research. The laboratory program shows how a well conceived program and complementary field test program can be used to apply acoustic emission technology to new applications. Future research in acoustic emission stemming from this research includes basic lab work in data analysis and signature analysis. Indeed, there is a wealth of data that was collected during the course of this research that can be analyzed.

During a time in history where cost cutbacks and financial restraint rule the day, material infrastructure is being called upon to perform its function well past its intended design life. Enabling this to occur safely is clearly in the

interest of most. The decisions which are made must be based on clearly defined criteria on the existing condition of the subject of study. A global nondestructive testing technique that can be used to quickly, inexpensively and decisively evaluate that condition empowers those who make the decisions to do so using as much information as possible. This enables the greatest common good for the greatest public safety, which after all is the primary duty and responsibility of a structual engineer.

APPENDIX

Standardized Testing Procedure

PROCEDURE FOR ACOUSTIC EMISSION EVALUATION OF NAVAL CRANE SHAFTS

BACKGROUND INFORMATION

During DoD Phase I and Phase II SBIR efforts (Topic N95-225), **Texas Research Institute Austin, Inc.** (TRI/Austin) worked with the **Ferguson Structural Engineering Laboratory** (FSEL) at the University of Texas in Austin to investigate methods for the nondestructive analysis of fatigue cracks in cranes. This work was sponsored by the **Naval Facility Construction Command (NAVFAC)**, under the technical guidance of the **Naval Facilities Engineering Service Center (NFESC)** at Port Hueneme, CA. Navy portal cranes have experienced sudden catastrophic failures in spool and rotate pinion (sluing) drive shafts; these failures have resulted in uncontrolled dropping of the load. These cranes are routinely used to lift nuclear materials and other sensitive payloads. *The continued safe operation of these cranes depends on the development of nondestructive evaluation (NDE) techniques that can detect fatigue cracks in-situ.*

During Phase I, TRI/Austin established the feasibility of using **Acoustic Emission (AE)** techniques to detect the presence of structurally significant fatigue cracks in sample crane shafts. TRI/Austin visited Naval cranes at Long Beach naval shipyard. An **in-field testing format** was defined, and drawings, reports, and photographs were obtained illustrating the cranes, their components, and their fatigue, failure, and metallurgical history. A **literature search** identified all relevant NDE methods that related to this difficult problem.

Acoustic emission tests were performed at the **University of Texas Ferguson Structural Engineering Laboratory (FSEL)** on sluing shaft P-68, in which fatigue cracks had previously been identified. *Analog and digital AE data were collected under light duty*

service loads. This data provided evidence of crack yielding and crack growth. Ultrasonic methods were used to verify the presence and location of cracks in a shaft segment from crane P-70, and successfully diagnosed the presence and size of introduced flaws. TRI /Austin also demonstrated that both AE and UT data can be successfully obtained by placing the transducers on the shaft sides and faces, which can be accessed without crane disassembly. Four crane drive shafts were obtained and tested in Phase I; all were pulled from service for safety reasons.

A **crane acoustic emission (CAE)** test stand was built in Phase I to apply both service and certification loads to crane drive shafts. The CAE test stand can apply a 200,000 in-lb. torque to a crane drive shaft - nearly twice shaft design strength. This capability allowed development of AE methods under realistic service conditions without tying up a Navy crane. The state-of-the-art AE systems used during Phase I detected AE signals from real cracks and distinguished actual crack growth in P-68 sluing shaft tests. These assets will be available to continue the test program and to develop CAE inspection methods and standards for Navy cranes in Phase II.

CAE data collected in Phase I included AE time series, frequency spectra, and event histories during "load and hold" cycles. Sensors were placed at the ends of the shafts - the primary available location in an active crane. Data were collected with both analog and digital AE systems, and both detected drive shaft crack signatures indicating that the P-68 sluing shaft may have been on the verge of catastrophic failure at the time it was removed from service.

During Phase II, **on-site** Acoustic Emission (AE) testing carried out on Navy portal crane # P66, located at **Pearl Harbor Naval Shipyard** (PHNSY), Hawaii during the period 24 - 28 February, 1997. Crane P-66 has been removed from service due to vibration problems reported by an operator, and has undergone other methods of nondestructive testing

carried out by PHNSY personnel. There was an urgent need to assess the condition of P-66 so that appropriate steps could be taken to return it to service.

Using the laboratory test stand, **torsional fatigue cycle tests** were conducted on samples of Navy Portal Crane rotate pinion shafts. The shaft segment test results resemble classic examples of fatigue cycle crack growth.

Commercial applications for the crane AE (CAE) inspection methods developed in this project include diagnosis of crane health for the **Navy, DoD** and other **government clients**. Potential **industrial customers** include crane owners at commercial ports and in the shipbuilding, steel, railroad, and oil industries. Additional applications exist in the paper and textile industries, where large diameter shafts are used in spools during manufacturing.

1. SCOPE

1.1 **General** - This procedure defines instrumentation requirements, test procedures, and evaluation criteria for acoustic emission (AE) testing of crane shafts. The test is used to detect the presence of cracks in a shafts and to asses their structural significance. The procedure requires loading of the shaft while monitoring with acoustic emission. It applies to in-service crane shafts constructed of carbon steel. The procedure has been demonstrated on drum, hoist, spool, and drive shafts in the field, and is also applicable to whip, auxiliary, and rotate pinion shafts.

1.2 **Limitations** - Test methods described in this procedure are subject to the following specific limitations.

1.2.1 Acoustic emission will only detect defects that are stressed during the course of the test.

1.2.2 The procedure is limited to temperatures in the range of -35 °F to 400°F.

1.2.3 The procedure does not apply to shafts that have been lift certified, or AE tested to the provisions of this document, during the six month period prior to performing the AE test.

1.2.4 This procedure applies only to crane shafts, and does not provide an evaluation of the condition of bearings, gears, and other components associated with the shaft.

1.3 **Table of Contents** - This procedure includes the following sections, paragraphs and appendixes:

2. APPLICABLE DOCUMENTS

2.1 **American Society for Testing and Materials** (ASTM).

E569, Standard Practice for Acoustic Emission Monitoring of Structures During Controlled Stimulation.

E650, Standard Guide for Mounting Piezoelectric Acoustic Contact Sensors.

E750, Standard Practice for Measuring Operating characteristic of Acoustic Emission Instrumentation.

E1316 Standard Terminology for Nondestructive Examinations

2.2 **The American Society of Mechanical Engineers** (ASME) Boiler and Pressure Vessel Code.

Section V, Article 12, Acoustic Emission Examination of Metallic Vessels During Pressure Testing.

2.3 **The American Society for Nondestructive Testing**.

Recommended Practice No. SNT-TC-1A, Personnel Qualification and Certification in Nondestructive Testing.

3. DEFINITIONS

3.1 **Definitions** - The following definitions shall apply to this Procedure.

3.1.1 **Channel, Acoustic Emission** - An assembly of sensor(s), preamplifier or impedance matching transformer, filters, secondary amplifier or other instrumentation as needed, connecting cables, and detector or processor (ASTM E1316). Each channel shall be analyzed independently.

3.1.2 **Electronic Calibrator** - A device which can repeatably induce a transient signal into an acoustic emission processor for the purpose of checking, verifying, and calibrating the test instrument.

3.1.3 **Event, Acoustic Emission (Emission Event)** - A local material change giving rise to acoustic emission (ASTM E1316).

3.1.4 **Felicity Effect** - The presence of detectable acoustic emission at a fixed predetermined sensitivity level at stress levels below those previously applied (ASTM E 1316). The fixed sensitivity level will be the same as was used for the previous loading or test.

3.1.4.1 **Felicity Ratio** - The ratio of the stress at which the Felicity effect occurs to the previously applied maximum stress (ASTM E 1316). As used in this procedure, the Felicity ratio is determined from the ratio of the load at the onset of significant emission to the previously applied maximum load.

3.1.5 **Historic Index** - A measure of the change in signal strength throughout a test.

3.1.6 **Hit** - Detection and measurement of an AE signal on a channel.

3.1.7 **Hit Definition Time** - A specified time interval defining the end of a hit during which no additional threshold crossings occur. The hit definition time is measured from the last threshold crossing of the hit. The first threshold crossing following the hit definition time is part of the next hit. The hit definition time to be used under this procedure is given in paragraph A7.6.

3.1.8 **Hit Duration (Duration)** - The time from the first threshold crossing to the last threshold crossing of the signal or envelope of the linear voltage time signal. Hit duration does not include the hit definition time at the end of a hit.

3.1.9 **Intensity** - A measure of the structural significance of an acoustic emission source. An intensity analysis compares the change in signal strength throughout the test (historic index) with events having large signal strength values (severity). For purposes of this procedure, intensity is measured on a per channel basis and is referred to as channel intensity.

3.1.10 **MARSE** - Measured area of the rectified signal envelope (ASME S.V, A.12). A measurement of the area under the envelope of the rectified linear voltage time signal from the sensor.

3.1.11 **Processor** - A circuit that analyzes the AE waveform as required in Paragraph 7.3.

3.1.12 **Rearm Time** - An interval following acquisition of a hit during which a channel is unable to accept additional data. The rearm time to be used under this procedure is given in paragraph A7.7.

3.1.13 **Severity** - A measure of events having large signal strength values. Severity is the average signal strength for a predefined number of hits having the largest numerical value of signal strength.

3.1.14 **Signal Amplitude, Acoustic Emission** - The peak voltage of the largest excursion attained by the signal waveform from an emission event (ASTM E1316). For purposes of this procedure signal amplitude shall be measured in decibels.

3.1.15 **Signal Strength** - Area under the envelope of the linear voltage time signal from the sensor. The signal strength will normally include the absolute area of both the positive and negative envelopes. For purposes of this procedure, MARSE (3.1.7) can be used as an approximation of signal strength.

3.1.16 **Simulated Acoustic Emission Source** - A device which can repeatably induce a transient elastic stress wave into the structure.

3.1.17 **Source, Acoustic Emission** - The position of one or more AE events.

3.1.18 **Voltage Threshold (Threshold)** - A voltage level on an electronic comparator such that signals with amplitudes larger than this level will be recognized (ASTM E1316).

3.1.18.1 **Test Threshold** - The threshold setting for a particular test. For this procedure, the test threshold shall be set at the data analysis threshold.

3.1.18.2 **Data Analysis Threshold** - A threshold number used in analysis of the test data. The data analysis threshold for tests carried out under this procedure is given in paragraph B2.1.

3.1.19 **Zone** - The area surrounding a sensor from which AE can be detected and from which AE will strike the sensor before striking any other sensors.

3.1.20 **Zone Location** - A source location method which uses sensor activity as an indication of the position of the source of emission.

4. SUMMARY OF METHOD

4.1 **General** - The method consists of subjecting crane shafts to predetermined loads and monitoring the shafts with sensors capable of detecting acoustic emission (transient stress waves) caused by stressed defects. Instrumentation, test methods, evaluation criteria, and report preparation are described in this procedure.

4.2 **Frequency Range** - Two different operating frequency ranges are permitted for sensors, preamplifiers, filters and other frequency sensitive instrumentation. The two ranges are centered on a nominal frequency of 150 kHz and 300 kHz. Selection of the appropriate operating frequency will depend on the characteristics of the emission recorded during a preliminary background noise check. The 150 kHz range is preferred. Separate evaluation criteria are given in Section 12 for the two operating ranges.

4.3 **Loading** - The procedure requires mechanical loading of the shaft. Loading is accomplished by pulling against a large mass while monitoring with a load cell. Normally, the load that is lifted off the ground during certification is used as the large mass. Section 11 gives details of the loading sequence. The test procedure specifies loading to a maximum load determined on the basis of the crane's design load. The procedure does not apply to shafts loaded above the maximum rated load during the six month period prior to performing an AE test. Typically, the maximum AE test load is 110 percent of the maximum rated load. The loading test assesses the shaft for defects such as cracks, corrosion, and other defects which are stressed during loading.

4.3.1 **Loading Options** - Two loading options are given in this procedure. The first applies load to the shaft which remains in a fixed position. The second varies the angular position of the shaft under a number of successive loadings. The angular position of

the shaft is changed to allow bending moments to be applied in different directions in order to develop the most serious combination of stresses. The fixed position loading was used for the demonstration test at Pearl Harbor. The variable shaft position loading was suggested by Navy personnel at Pearl Harbor but has not been demonstrated in the field.

4.4 **Data Evaluation** - Data evaluation is based on cumulative signal strength, number of hits during load holds, Felicity ratio, and intensity analysis of individual AE channels. Data are recorded during loading and load hold periods at loads defined in Section 11. Specific evaluation criteria and intensity analysis methods are given in Section 12.

4.5 **Test Report** - Following data evaluation a test report is issued for each shaft tested. This report presents the results of the AE test as specified in Section 13 of this procedure.

5. PERSONNEL QUALIFICATION

5.1 **General** - It is required that personnel performing acoustic emission testing of crane shafts be fully conversant with the construction of cranes and shafts of the type to be tested, and have passed the training course specified in Paragraph 5.2.

5.2 **Training Course** - Personnel performing acoustic emission testing of crane shafts are required to attend a dedicated training course on acoustic emission testing of metal equipment and pass a written examination. Such personnel shall also be familiar with the provisions of this procedure. The training course shall be appropriate for specific NDT Level II qualification according to Recommended Practice No SNT-TC-1A of the American Society for Nondestructive Testing, and should include as a minimum the following general topics:

1. Basic technology of acoustic emission.
2. Failure mechanism of metals, including fatigue.
3. Acoustic emission instrumentation.
4. Instrumentation calibration and check out.
5. Data collection and interpretation.

5.3 **Trainees** - Personnel who have not attended training as prescribed above and passed an examination are considered trainees. Such persons may participate in crane testing for the purposes of familiarization prior to attending the training and examination course. Trainees may participate only under the direct instruction of a person who has passed the Level II examination. They may not take any direct responsibility for performance of the procedure.

6. SIGNIFICANCE

6.1 **General** - The AE test method is designed to detect defects and damage in metal equipment. Among the mechanisms that generate emissions are:

a. cracks, including fatigue cracks
b. the effect of corrosion, including cracking of corrosion products or local yielding
c. stress corrosion cracking
d. certain metallurgical changes, including yielding and crystal dislocations
e. embrittlement
f. pits and gouges
g. voids and porosity
h. inclusions
i. contamination
j. laminations

6.2 **Application of Procedure** - This procedure is used for determining the structural integrity of crane shafts. The AE test method will detect major structural defects and structural defects that have grown or developed since the previous test, which are stressed during the course of the test.

6.3 **Minimum Stress** - The stress concentration due to a defect magnifies the local nominal stress in the metal. In order to generate significant emission, the maximum local stress at a defect must reach a minimum of 90% of the material yield stress. For a structurally significant defect, this requires that the nominal stress caused by the test load in the region of a defect be at least 10% of the material yield. Defects in unstressed areas and defects which are structurally insignificant under the applied load will not generate

AE. Theoretical and experimental studies have shown that the loadings specified in this procedure are sufficient to generate emission from recently formed fatigue cracks.

6.4 **Follow-up** - Defects detected by AE should be examined on the basis of the significance of emission. Other nondestructive examination techniques, repair, and retesting may be required as appropriate. Repair procedure recommendations are outside the scope of this procedure.

7. INSTRUMENTATION

7.1 **General** - The AE instrumentation consists of sensors and electronic signal processing and recording equipment, and digital hardware and software for analyzing and displaying data in accordance with the provisions of this procedure.

7.2 **Sensors** - The sensors shall have a nominal resonant response of either 150 kHz or 300 kHz. Each sensor shall incorporate integral preamplifier circuitry including a band pass filter centered on the resonant peak and shielding against electromagnetic and radio frequency interference. Sensors may not be commoned (teed) into a single channel.

7.3 **Data Measurement and Recording** - The instrumentation shall be capable of measuring and recording by channel number and within a specific frequency range the following parameters for each AE hit; hit arrival time, hit duration, peak amplitude, signal strength, and a parametric representing the applied load. The instrumentation shall be capable of measuring and recording data at a minimum rate of 100 hits per second. This rate shall apply to the entire instrument, regardless of the number of channels and the distribution of hits between channels. The data acquisition system shall have sufficient channels to provide sensor coverage as defined in Paragraph 9.2.1. The instrument shall store the year, month, day, hour and minute of the start of each data file as part of the test record. Data from all hits having an amplitude greater than the test threshold shall be recorded.

7.3.1 **Test Threshold** - The test threshold for tests performed under this procedure is typically set at 45 dB, subject to the provisions of paragraph B2.1.

7.3.1 **Rearm Time** - Individual channel rearm times are permitted under this procedure. If used, the rearm time shall commence immediately following the end of the hit definition time. The rearm time shall apply only to the channel which detected the hit, and shall not effect other channels. The rearm time shall not exceed the limit specified in A7.7.

7.4 **Test Load** - As specified in 7.3, the test load on the crane must be continuously recorded as part of the AE data file. The load parametric shall be recorded at a time interval no greater than 5 seconds.

7.5 **Front End Filters** - Band pass filters of the type defined in Appendix A shall be used. No other front end filters shall be used. It is an axiom of this procedure that all hits from all sources will be measured and recorded. Spurious, nonrelevant, and false data is removed by post test analysis. Nevertheless, and as described in paragraph 8.5, extraneous sources of emission should be eliminated from the system prior to testing.

7.5.1 **Lockouts and Guard Sensors** - These techniques use designated sensors to monitor ares where spurious or nonrelevant emission may arise. If emission is detected from these areas, data acquisition by other sensos is suspended for a period of time. Lockouts and guard sensors shall not be used.

7.6 **Instrument Displays** - The instrumentation shall be capable of providing the following real time displays.

1. Bar chart of cumulative signal strength versus channel
2. Hit amplitude versus time.
3. Hit duration versus time.
4. Log of hit duration versus hit amplitude.
5. Log of Hit Signal Strength vs Hit Amplitude
6. Cumulative signal strength per channel versus time.
7. Cumulative or differential amplitude distribution.
8. Tabulated listing by channel number of total hits equal to and greater than defined amplitude values. Amplitude values shall be in increments of not greater than 5dB and shall be for a range of at least 40dB starting at the data analysis threshold.
9. Data listing of the most recent sensor hits. Data shall include the hit parameters required in 7.3.
10. Load parametric versus time.

The ability to overlay a plot of load parametric versus time on any of the time based displays should be included.

7.7 **Data Analysis** - Provision shall be included for playback, post-test filtering, and hard copy listing of the test data.

7.8 **Performance Requirements and Calibration** - The AE instrumentation shall meet the performance requirements of Mandatory Appendix A and shall be calibrated at intervals not exceeding one year. Calibration shall be in accordance with Appendix A requirements and the calibration values

defined in Mandatory Appendix B. Certification of the date of the most recent calibration shall be carried with the instrumentation.

8. TEST PREPARATION

8.1 **Preliminary Information** - Prior to setting up the test instruments, the inspector shall be furnished with the following information.

8.1.1 Construction details of the shaft, including the type and position of the keyway. In most instances this information can be obtained from previous test reports, by visually examining the crane, or will be shown on drawings.

8.1.2 Type of steel used for construction of the shaft. Specific grade is not required.

8.1.3 Maximum rated load.

8.1.4 History of service, if available.

8.1.7 Previous acoustic emission test and evaluation results.

8.1.8 Inspection reports of previous nondestructive inspections.

8.1.9 Availability and weight of certification concrete test blocks (8.2).

8.1.10 Certification of load cells to be used for monitoring the test load.

8.2 **Test Loads** - Calibrated concrete test blocks of the type used for crane lift certification shall be available for use in the test. The blocks shall have a combined weight greater than the maximum test load specified in Paragraph 11.4.

8.3 Safety - All safety requirements unique to the test location shall be met.

8.3.1 Protective clothing and equipment (e.g. ear protection) that is normally required in the area in which the test is being conducted shall be worn.

8.3.2 A fire permit may be needed to allow use of the electronic instrumentation.

8.3.3 Precautions shall be taken to protect against the consequences of catastrophic failure when loading, i.e., flying debris and breaking cables.

8.4 **Environmental** - For ambient temperatures below 32 °F (0C) care should be taken to eliminate ice buildup which can cause emissions during loading.

8.5 **Background Noise** - Prior to testing a background noise check shall be carried out. The check shall be performed under conditions which simulate the test loading procedure as closely as possible. Loads applied during the background noise check shall be up to 10% of the maximum rated capacity. Care should be taken to ensure that this load is not exceeded. The purpose of the background noise check is twofold. First, the decision to use 150 kHz or 350 kHz instrumentation will depend on this check. Second, the check will be used to review and eliminate or reduce sources of false emission.

8.5.1 **Operating Frequency Range** - The inspector shall chose the operating frequency of the sensors, filters, etc., based on the characteristics of the emission recorded during background noise check. The 150 kHz range is preferred. However, if excessive emission is detected by sensors operating in this range, and the

excessive noise cannot be eliminated, 300 kHz sensors shall be used.

8.5.2 **Spurious Emission** - The inspector shall review the loading techniques to identify all potential sources of extraneous noise. It is important to capture real emissions during monitoring periods. To accomplish this, background noise must be at a minimum. Guidelines for an unacceptable level of background noise are given in paragraph 11.3.

8.5.2 **Electromagnetic and Radio Frequency Interference** - Field experience has shown that care should be exercised in dealing with electrical background noise sources; for example, electromagnetic interference (EMI) is usually due to motors, switch gear, solenoids, and the like. A severe EMI problem caused by nearby relays was encountered during the demonstration test at Pearl Harbor. In this case, metal foil was placed around the relays to shield the AE instrumentation from the EMI. EMI can also be caused by a bad power supply, particularly an inadequate ground. Radio frequency interference (RFI) can be distinguished from EMI with an oscilloscope and correlation plot. Both RFI and EMI shall be controlled by using suitably shielded or designed sensors and narrow band filters. Power source EMI can be controlled with a constant voltage supply unit.

8.6 **Power Supply** - A stable grounded uninterruptable power supply meeting the specifications of the instrument manufacturer is required at the test site. It is likely that the power supply available from the crane will be inadequate. To reduce the probability of data loss from unanticipated instrument shutdown, the instrumentation shall be protected with a surge protector and an uninterruptable power supply.

8.7 **Load Cell** - A load cell shall be used to measure the loads specified in paragraph 11.5. The load cell shall have been calibrated within the past twelve months, and have the capability to measure the test load to an accuracy of at least 1% of the maximum applied load.

9. SENSOR MOUNTING

9.1 **General** - ASTM E650 gives guidance on sensor mounting. The location and spacing of sensors are discussed in Paragraph 9.2 of this procedure. The sensors shall be placed in the designated location with a couplant between the sensor face and surface of the crane shaft. Care must be exercised to assure that adequate couplant is applied. All signal cables must be constrained to prevent stressing the sensor or loss of coupling, and to avoid extraneous noise from movement of the cables.

9.1.1 **Attachment** - Sensors shall be attached to the crane shaft with a suitable couplant applied between the sensor face and the metal surface. In order to test a shaft that has been painted, it is necessary to remove the paint from the areas where the sensors will be attached and clean with sandpaper. The preferred methods of securing sensors in place are high temperature hot melt glue, and duct tape. The hot melt glue serves as an acoustic couplant, making it important that the glue layer be as thin as possible to minimize signal losses. Couplant losses shall be checked per the procedures described in paragraph 9.2.2.3. Where considered necessary, the area of the shaft where the paint was removed to allow for sensor placement may need to be repainted after the test..

9.1.2 **Surface Contact** - The sensor shall be mounted with the center of the sensor face directly coupled to the surface of the shaft. Reliable coupling between the sensor and metal surface must be assured and the surface in contact with the sensor face must be clean and free of particulate matter.

9.2 **Sensor Locations** - A primary consideration in choosing sensor locations is the need to detect structural defects at critical sections, e.g., high stress areas and geometric discontinuities. It is important that the sensor placement requirements specified in Paragraph 9.2.1 be used. These locations are the minimum sensor location requirements for load tests. Additional sensors can be used at the option of the inspector to provide supplemental data from regions of interest.

9.2.1 **Sensor Spacing** - The sensors shall be placed near the shoulders of each end of the crane shaft (see Figure 9.2.1). It is not possible to place sensors at both ends of the shaft for some drive shafts. In these situations it is permissible to place the sensors at one end only. Under no circumstance should the free space distance between the sensor and shoulder be smaller than ½ inch and, if possible, the distance should be no greater than 3 inches. The sensors shall be mounted perpendicular on the circumference of the shaft. One of the sensors shall be positioned directly above the keyway and the other sensor shall be located 120° counter-clockwise from it on the circumference (12 and 8 o'clock).

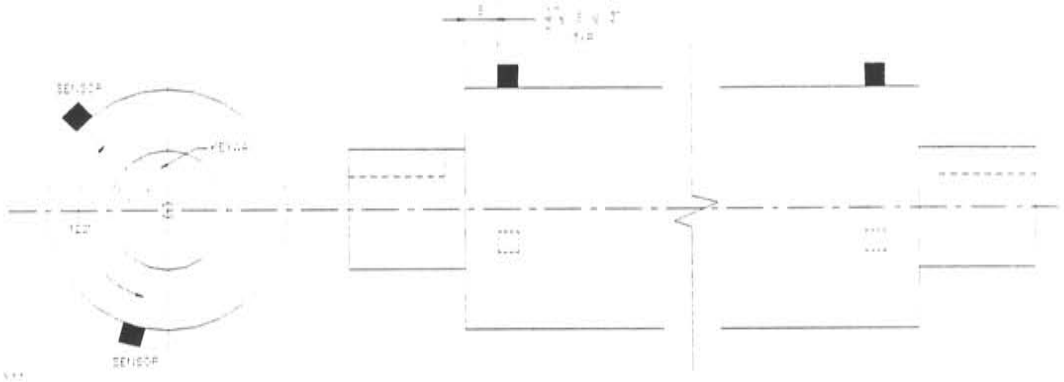

FIGURE 9.2.1 - SENSOR LOCATIONS ON CRANE SHAFT

9.3 **Coupling Loss** - In order to determine that the sensor mounting technique is adequate, pencil lead break tests shall be performed to determine the signal loss between the sensor and metal surface. Break 0.3 mm (2H) pencil leads next to the sensor then at a distance of 6 inches and 12 inches along a straight line from the sensor. The breaks shall be done with the lead at an angle of approximately 30 degrees to the test surface and with a 0.1 inch (2.5 mm) lead extension. The test data shall be judged according to the criteria set forth in Table 9.3. If a sensor does not meet the criteria after three attempts, the sensor shall be removed from the shaft and reattached or replaced.

Distance of Break from Sensor (inches)	Minimum Amplitude (dB)
Next to sensor	75
6	67
12	60

TABLE 9.3 - MINIMUM AMPLITUDE OF PENCIL LEAD BREAKS

9.4 **Source Location** - Real time source location shall be based on the zone location method. This method uses sensor activity from each area of interest as an indication of the approximate location of the source of emission. A zone is defined in Section 3. In a homogeneous material such as the steel used in the crane shafts, a zone is the region around each sensor which is closer to the sensor than it is to any other sensor. Zone location using the method described in paragraph 9.4.1.1 has been used in field tests of crane shafts to determine which end of the shaft contains the source of the emission. The method described in paragraphs 9.4.1.4 has been of value in laboratory testing. The other techniques described in paragraph 9.4.1 have been used in the petrochemical industry for testing metal pressure vessels.

9.4.1 **Location Refinement** - An improved approximation of the location of a source can be obtained by five different methods.

9.4.1.1 **Comparative Signal Strength** - This method is based on a comparison of the relative signal strength at adjacent sensors responding to the same source. Large emission bursts on multiple channels are recognized as being from a common source when responding channels show a sharp increase in signal strength at the same time. Such occurrences can be seen on the cumulative signal strength per channel vs time plots. When this is observed, the relative distance of the source from each sensor can be estimated from the relative magnitude of the signal strengths at the time of the emission burst.

9.4.1.2 **Reduced Zone Sizes** - If an AE test indicates a source in a particular zone, the zone can be subdivided into smaller zones by adding additional channels to the original zone. The emission source is then stimulated to emit by a small additional increase in load.

9.4.1.3 **Post Test Lockouts** - During post test data analysis, lockouts may be used to more closely identify the location of emission sources.

9.4.1.4 **Jolly-Stuart Method (also known as Hit Sequence Method)** - The Jolly-Stuart method is a refinement of zone location and is based on the order that a given event strikes a group of sensors. Rather than providing an "exact" location, the method defines a subzone from which the event originated. The greater the number of sensor hits, the smaller the resulting subzone and the greater the

accuracy of the location. Field experience has shown that hit sequence source location normally provides a reliable indication of where the growing defect(s) is positioned. However, only a small percentage of events strike more than one sensor. Accordingly, the technique provides improved zone location for a portion of the data. This data may not be representative of all data originating from a given zone. With Jolly-Stuart source location, signals that hit a single sensor are considered important, as are those that hit two or three sensors.

9.4.1.5 **Time Difference Source Location** - This method uses triangulation techniques based on the exact difference in time between the arrival time of a given event at different sensors. Field experience has shown that this method often gives very poor results for practical applications. It is not recommended as the primary method of source location. However, useful information can sometimes be obtained from post test analysis. The accuracy of the method can be very sensitive to errors in sensor positioning and differences in wave speed, and the results should be treated with caution. It should also be noted that in many practical applications, a large number of events do not strike sufficient sensors to permit time difference location.

10. INSTRUMENTATION SETTING AND SYSTEM PERFORMANCE CHECK

10.1 **Threshold** - The test threshold shall be set at or below the data analysis threshold. Normally, the test threshold will be set at the data analysis threshold.

10.2 **Sensor Coupling and Circuit Continuity Verification** - Verification shall be performed before testing begins and immediately upon completion of testing using the following methods:

10.2.1 **Before Testing** - Three 0.3mm (2H) pencil leads shall be broken at a specific distance from each sensor. The average peak amplitude shall meet the provisions of paragraph 9.3 and shall not vary more than 4dB from the average of all sensors. Any channel failing this check shall be investigated and replaced or repaired as necessary. These data shall be recorded and retained with the examination record.

10.2.2 **After Testing** - 0.3mm (2H) pencil leads shall be broken at each end of the shaft in order to check that all instrument channels are still active. Channels which do not respond or have low sensitivity after the test shall be noted in the test report.

11. TEST PROCEDURE

11.1 **General** - Each shaft is subjected to programmed increases in load up to a predetermined maximum and monitored with sensors detecting acoustic emission (stress waves) caused by stressed structural defects.

11.2 **Data Quality** - Acquisition of genuine, valid, acoustic emission is essential to the success of the test. To achieve this, the following actions shall be carried out.

- Thoroughly check the instrumentation performance as described in Section 10 immediately prior to the start of testing and after testing is completed.

- Identify and characterize extraneous noise and judge its impact on data quality. Refer to Paragraph 11.3 for additional information on background noise sources or to Paragraph 12.2 for techniques which can be used to evaluate data quality during the course of the test.

- Carefully monitor the performance of the instrumentation during the test.

- Carefully monitor the data during the test to note possible extraneous noise and to ensure that spurious emission, such as that generated by a mechanical movement does not contaminate the data.

11.3 **Test Log** - The inspector shall maintain a test log recording data file names, test times, and other significant test occurrences.

11.4 **Background Noise** - Extraneous noise must be identified and minimized. If the inspector judges background noise to be excessive, either before or during the test, the test may be terminated. "Excessive" background noise either before or during the test is a matter of judgement based on experience. The following guidelines for excessive background noise during a 10 minute initial hold period immediately prior to loading are for a typical instrument with the amplitude and signal strength scales given in Appendix B. For other instruments the values given below should be adjusted as outlined in the Appendix.

- A cumulative signal strength value of greater than 50 on any channel.
- A cumulative signal strength value greater than 100 for all channels combined.
- A hit amplitude greater than 49dB.

Paragraph 12.2 provides information on the use of correlation plots to help in the identification of real time extraneous noise. The following paragraphs identify possible sources of background noise.

11.4.1 **Mechanical Movement** - False emissions can be caused by movement between adjacent components. Such emissions are generally sporadic and can be identified and filtered out in post-test analysis using techniques described in Paragraph 12.3.

11.4.2 **Wind and Vibration** - Visually examine the sensors and other hardware to verify the equipment is securely mounted and will not be subject to wind or vibration induced movement. Isolate the shaft and AE hardware from uncontrollable sources of noise.

11.4.3 **External Noise** - Uncontrolled noise caused by conditions such as rain, sleet, hail, snow, wind blown particles, air hoses, leaks, blasting, etc., shall be evaluated as they occur. The effects of such sources shall be minimized by acoustic isolation where practical. In extreme cases it may be necessary to delay testing until uncontrolled sources can be eliminated.

11.5 **Loading/Stressing** - If an acoustic emission test is being performed in conjunction with a crane lift certification test, the acoustic emission test shall be carried out first. In this regard, particular attention is drawn to paragraph 1.2.3. To avoid problems associated with movement of the sensor cables during shaft rotation, a single large load is used. This load remains static during the loading and consists of concrete calibrated test blocks of the type used for crane lift certification (typically, two 20,000 lb. blocks and two 43,000 lb. blocks). This load is heavier than the maximum load that will be applied during the test and is not lifted off the ground. The load is applied to the crane by "booming up" or raising the boom against the fixed load. Two load sequences are allowed under this Procedure.

- Option 1 was used for a demonstration test at Pearl Harbor and gave satisfactory results.
- Option 2 involves lowering the boom by slight increments to allow testing of the drum shaft at different angular positions. This modified procedure was suggested by Pearl Harbor personnel, but has not yet been tested in the field.

Under the second option, the shaft will experience bending moments in different orientations, reducing the possibility that cracks will not be adequately stressed and that the analysis will underestimate their structural significance. Theoretical calculations indicate that the stresses due to the torsion loading of the shaft are the critical stresses for development of fatigue cracks. Either loading option results in adequate torsion stress and, accordingly, will result in a satisfactory test.

11.5.1 **Option I: Fixed Drum Shaft Angular Position During Loading -** *Master Load Schedule:* (% of maximum rated load) - Use this schedule for both main and boom shafts.

- Begin by applying a load of 10% (-0% +5%) of maximum rated capacity. Use this load to keep tension on the shaft: it becomes the baseline, or minimum load.
- Increase to 75% (-0% +5%); hold for 10 minutes; decrease to 10%; hold for 5 minutes.
- Increase to 90% (-0% +5%); hold for 10 minutes; decrease to 10%; hold for 5 minutes.
- Increase to 100% (-0% +5%); hold for 10 minutes; decrease to 10%; hold for 5 minutes.
- Optional: Increase to 110%; hold for 10 minutes; decrease to 10%; hold for 5 minutes.

11.5.1.1 **Main Hoist Drive and Drum Shaft** - As previously explained, a static (non-lifting) load scheme will be used. The crane will be boomed up against a large load to apply tension to the shafts.

- Set the boom to near minimum radius (to minimize the load on the boom shafts while testing the main hoist shafts)
- Boom up to apply loads; follow the master load schedule.

11.5.1.2 **Boom Hoist Drive and Drum Shaft**

- Set the boom to near maximum radius (to maximize the load on the boom shafts)
- Boom up to apply loads; follow master load schedule.

11.5.2 **Option II: Variable Drum Shaft Angular Position During Loading**

- *Master Load Schedule:* (% of maximum rated load) - Use this schedule for both main and boom shafts.

- Begin by applying a load of 10% (-0% +5%) of maximum rated capacity. Use this load to keep tension on the shaft: it becomes the baseline, or minimum load.
- Increase to 75% (-0% +5%); hold for 10 minutes; decrease to 10%; hold for 5 minutes. Release load, lower boom slightly, and repeat 3 times to obtain other angular orientations.
- Increase to 90% (-0% +5%); hold for 10 minutes; decrease to 10%; hold for 5 minutes. Release load, lower boom slightly, and repeat 3 times to obtain other angular orientations.
- Increase to 100% (-0% +5%); hold for 10 minutes; decrease to 10%; hold for 5 minutes. Release load, lower boom slightly, and repeat 3 times to obtain other angular orientations.
- Optional: Increase to 110%; hold for 10 minutes; decrease to 10%; hold for 5 minutes. Release load, lower boom slightly, and repeat 3 times to obtain other angular orientations.

11.5.2.1 **Main Hoist Drive and Drum Shaft** - As previously explained, a static (non-lifting) load scheme will be used. The crane will be boomed up against a large load to apply tension to the shafts. The drum shaft will be exposed to different bending loads under different angular orientations when the boom is slightly lowered. The following load procedure will accomplish this goal.

- Set the boom to near minimum radius (to minimize the load on the boom shafts)
- Boom up to apply first load (note load, and angular position of main drive and main drum shafts)
- Go back to minimum load
- Lower the boom slightly
- Boom up to apply the second load (note load, and new angular position of main drive and main drum shafts)
- Go back to minimum
- Lower the boom slightly
- Boom up to apply the third load (note load, and new angular position of main drive and main drum shafts)
- Repeat the previous three steps until the master load schedule is completed.

Remember: the drum shaft has a bending moment under load. This procedure will result in application of this bending moment in several drum shaft angular positions. By doing this, we should be able to detect cracks dependent on drum shaft angular orientation

11.5.2.2 **Boom Hoist Drive and Drum Shaft**

- Set the boom to near maximum radius (to maximize the load on the boom shafts)
- Boom up to apply first load (note load, and angular position of boom drive and boom drum shafts)
- Go back to minimum load
- Lower the boom slightly
- Boom up to apply the second load (note load, and new angular position of boom drive and boom drum shafts)
- Go back to minimum
- Lower the boom slightly
- Boom up to apply the third load (note load, and new angular position of boom drive and boom drum shafts)
- Repeat the previous three steps until the master load schedule is completed.

12. INTERPRETATION OF TEST DATA

12.1 **General** - The test data is analyzed by first performing a data quality analysis which, on the basis of emission characteristics, assures that genuine events caused by changes within the material have been recorded. After the data quality is completed, emissions are examined relative to the evaluation criteria given in Table 12.4. An acceptable crane shaft shall meet all the criteria set forth in the table. If the shaft has produced emissions exceeding one or more of the criteria, an intensity analysis shall be performed to determine the structural significance of any defects. Based on the results of this additional analysis, follow-up nondestructive examination and/or repair may be necessary.

12.2 **Data Quality Analysis** - ASTM E1316 states that an indication is subject to interpretation as false, nonrelevant, or relevant. In order to make this interpretation, the emission characteristics shall be examined to determine if data from nonstructural sources are included in the data set. This examination should include a review of data correlation plots, graphs, and data listing. In addition, the test log should be reviewed to determine if any unusual occurrences or background noise were observed at the time of test. The following paragraphs describe plots which are useful in performing the data quality analysis.

12.2.1 **Log of Hit Duration vs Hit Amplitude** - Genuine AE is characterized by hits concentrated in the 30 microsecond to 2 millisecond range of hit duration. As amplitudes increase, duration also increases, giving the data a banded appearance on the correlation plot. Low amplitude, long duration hits which plot

outside of the band, may indicate sliding or rubbing at metal surfaces. Hits above 55dB with duration less than 60 microseconds are often caused by electromagnetic interference (EMI).

12.2.2 **Log of Hit Signal Strength vs Hit Amplitude** - This plot is used to identify false emission from sources other than structural damage. Low amplitude, high signal strength hits may indicate an instrument problem. Genuine AE has a banded distribution similar to that described in Paragraph 12.2.1. Intensity analysis is based on signal strength. Accordingly, it is important to identify any hits with unusually high signal strength and to examine the validity of these hits and the associated data.

12.2.3 **Hit Amplitude vs Time and Hit Duration vs Time** - These two correlation plots are helpful in identifying hits due to sliding or rubbing which will typically occur over a short time window of approximately 0.1 sec. Genuine data, such as that due to a delamination, will occur over a longer time window.

12.2.4 **Cumulative Amplitude Distribution** - A plot of genuine AE will consist of two or more straight lines. If the plot has a continuously changing slope, it may indicate an instrument problem.

12.3 **Post-test Filters** - Post-test filters are used to remove data which gives a false or nonrelevant indication (ASTM E1316), or extraneous noise (Paragraph 11.4).

12.3.1 **Swansong Filters** - The set of filters known as Swansong filters are an important tool for removing emission generated by nonstructural sources. The filters key on telltale hits having a long duration and low amplitude. This type of hit is characteristic of sliding and mechanical rubbing. Such emission sources often generate a large burst of emission which reverberates throughout the shaft and is picked up by many of the sensors. For this reason the Swansong filters remove all data from all channels for a defined period of time. Data files should be run through one of the Swansong filters whenever the correlation of log duration vs amplitude reveals hits in the low amplitude, long duration range. It is important that the inspector be alert to a continuous accumulation of Swansong telltale hits during a test. Such data may indicate a leak or other foreign noise source which invalidates the entire test result. In contrast, a small number of Swansong hits during testing usually signals mechanical noise such as mechanical sliding. This type of noise can be filtered from the data set using one of the Swansong filters. The Swansong II is the preferred filter for use with crane shafts.

12.3.1.1 **Swansong II Filter** - The Swansong II filter keys on telltale hits and removes all data within plus and minus half a second of such a hit. This filter has been found to be particularly effective in removing false emissions caused by sliding and mechanical movement. The Swansong II filter uses three amplitude/time range relationships to identify telltale hits.

The Swansong II filter is defined by:

If $(A_i - A_{th}) < 5$ and $D_i > 2$

or $(A_i - A_{th}) < 10$ $D_i > 3.5$

or $(A_i - A_{th}) < 15$ and $D_i > 4.5$

eliminate all hits during the period (seconds)

$(T_i - 0.5)$ to $(T_i + 0.5)$

where for a given hit i:

A_i = Amplitude (dB)

A_{th} = Data Acquisition Threshold (dB)

D_i = Hit Duration (ms)

T_i Arrival Time (secs)

12.3.2 **Time Filters** - Time filters are used to eliminate bursts of extraneous noise such as wind induced noise, impact, or other types of mechanical noise. These sources of interference should be noted in the test log along with their time of occurrence. A time filter can then be used to reject the interference noise from the data set, leaving only genuine AE.

12.3.3 **Channel Filter** - Some noise sources are local and may effect only one or two channels. Faulty instrumentation may also have also manifest itself in this manner. With this type of source, all hits on channel(s) showing a response to the noise source must be removed from the data set for the period of the noise. If a large percentage of data for a particular channel is removed an AE evaluation of nearby areas of the shaft is not possible. An inclusive channel filter may be used to allow a user to closely examine data on a particular channel.

12.3.4 **Amplitude Filter and Signal Strength Filter** - Amplitude and signal strength filters are used to allow the inspector to closely examine data characteristics within a given range of amplitudes or signal strengths. For example, the inspector may wish to examine high signal strength or large amplitude hits to determine the source and seriousness of the emission.

12.4 **Structural Evaluation** - Following the data quality analysis (12.2) and completion of post test filtering (12.3), the genuine AE is compared with the evaluation criteria.

12.4.1 **Acceptance Criteria** - The acoustic emission evaluation criteria given in Table 12.4.1 shall form the basis for accepting or rejecting crane shafts. Evaluation shall be on a per channel basis. An acceptable shaft must meet all of the criteria listed in the table for the appropriate frequency sensors. The cumulative signal strength values given in the table are for instruments with a MARSE signal strength circuit giving the calibration values listed in Table B3. The criteria for other instruments must be adjusted as described in paragraph B3.

Criterion	150 kHz Sensors	300 kHz Sensors
Cumulative Signal Strength During Loading and Load Holds, Volts-Seconds $^{-5}$	<350	<100
Felicity Ratio	>0.95	>0.95
Cumulative Emission During Load Holds, Hits	20	10

TABLE 12.4.1 - INDIVIDUAL CHANNEL EVALUATION CRITERIA

12.5 **Significance of Criteria**

12.5.1 **Cumulative Signal Strength** - Cumulative signal strength is a measure of the relative stress wave energy detected by the sensor. Accordingly, it provides an indication of how much damage occurs at the emission source during loading. This criterion is a measure of the structural significance of the source. Increasing cumulative signal strength with increasing stress indicates that an emission source is sensitive to the magnitude of the load.

12.5.2 **Felicity Ratio** - The Felicity Ratio provides a measure of the structural significance of previously induced damage and is measured from the unload/reload cycles. The onset of "significant" emission for determining the Felicity ratio is a matter of operator experience. The following are offered as guidelines for determining onset of significant emission on an individual channel.

- More than 5 bursts of emission during a 10% increase in load. One or more hits constitute a burst, and all hits for the five seconds following the initial hit are considered part of the same burst.
- Emission continues at a load hold. Continuing emission is defined as a rate of 3 hits per minute. For purposes of this guideline, a short (one minute or less) unprogrammed load hold can be inserted in the procedure.

12.5.3 **Emission During Load Hold** - Emission during load hold is particularly significant. Continuing emission indicates continuing damage. For example, creep, additional yielding, or a defect which is continuing to grow under constant stress. Background noise will generally be at a minimum during a load hold. Accordingly, this criterion is relatively easy to apply and interpret.

12.6 **Intensity Analysis** - The evaluation criteria specified in Paragraph 12.4.1 are pass/fail and indicate the presence of defects. If a shaft fails one or more of the evaluation criteria an intensity analysis should be performed. Intensity analysis is a method of measuring the structural significance of a defect and is carried out on a per channel basis. The method uses two factors based on signal strength. The first factor is known as historic index, and compares the signal strength of the most recent hits to the signal strength of all hits. The second factor, referred to as severity, is the average of the hits having the largest magnitude signal strength. Intensity analysis has been used extensively in the petrochemical industry for analysis of defects in metal equipment. The technique is based on destructive vessel tests, controlled tests with detailed follow-up nondestructive evaluation, and a substantial number of field tests. The

empirical factors and intensity gradings have been developed by comparing the acoustic emission data from known defects with the type of defect, theoretical analyses, and defects rejectable by other nondestructive test methods. The data sets include a wide range of field detected defects, controlled laboratory samples, and destructive tests. Research at the University of Texas Ferguson Structural Engineering Laboratory has confirmed that intensity analysis is a sensitive method for detecting growing fatigue cracks in crane shafts.

12.6.1 **Historic Index** - Historic index is defined by:

$$H(t) = \frac{N}{N-K} \quad \frac{\sum_{i=K+1}^{i=N} S_{Oi}}{\sum_{i=1}^{i=N} S_{Oi}}$$

where:

H(t) is the historic index at time *t*.

N is the number of hits (ordered by time) up to and including time *t*.

S_{oi} is the signal strength of the i*th* hit.

K is an empirically derived factor that varies with the number of hits. Values for *K* are given in Table 12.6.1

Number of Hits, N	K
<10	Not applicable
10 to 15	0
16 to 75	N - 15
76 to 1000	0.8N
>1000	N - 200

TABLE 12.6.1 - K FACTOR FOR HISTORIC INDEX

Historic index has been found to be a sensitive method of detecting a change in slope in the cumulative signal strength versus time curve. This change in slope is often referred to as the "knee in the curve". At the knee, the historic index will increase sharply. This will be followed by a decline in value until another knee is encountered. Historic index is particularly valuable for determining onset of new damage mechanisms and is essentially independent of specimen size. Historic index is a form of trend analysis, and is performed continuously for each hit. The greater the number of hits on a channel the more accurate will be the results. An analysis requires a minimum number of data points, and is not valid when only a small number of hits are recorded. The historic index is set to unity if a channel has 15 or fewer hits.

12.6.2 **Severity** - Severity S_r is defined as the average signal strength for the J hits having the largest numerical value of signal strength:

$$S_r = \frac{1}{J} \sum_{m=1}^{m=J} S_{Om}$$

where:

S_{om} is the signal strength of the *m*th hit. *m* is ordered on the magnitude of the signal strength with m=1 being the hit having the largest signal strength.

J is an empirically derived constant that depends on the material of construction. Values for *J* for steel crane shafts are given in Table 12.6.2

Total Number of Hits	J
<10	Not applicable
≥10	10

TABLE 12.6.2 - J FACTOR FOR SEVERITY

Severity is a measure of structural damage. An increase in severity will often correspond to new structural damage of the type detected by a Felicity ratio measurement. Severity is based on the hits with the largest magnitude of signal strength and is only valid if 10 or more hits are recorded. Severity cannot decrease during a test.

12.6.3 **Evaluation** - The results of the intensity analysis for each channel are plotted on a chart of log historic index versus log severity. As

shown on Figures 12.6.3.1 and 12.6.3.2 each channel is assigned an intensity based on its historic index and severity values. The results are plotted on an intensity chart divided into zones labeled "Insignificant", "Minor", "Significant", and "Major". The boundaries between the intensity zones are defined in Table 12.6.3. If less than 10 hits are recorded on a channel, the intensity cannot be calculated because the channel only detected a small number of hits. If this occurs, it should not be interpreted as an indication that defects are minor or insignificant. Decisions for these channels should be on the basis of the acceptance criteria in Table 12.4.1. Figure 12.6.3.1 applies to 150kHz sensors and Figure 12.6.3.2 applies to 300 kHz sensors.

12.6.4 **Intensity Analysis Follow-up Action** - Recommended follow-up actions for the different intensities are set out in Table 12.6.4. These recommended actions are considered minimum requirements. In some cases more extensive inspection may be justified. The crane owner and the inspector should make decisions regarding follow-up inspections on the basis of the zone intensities and the consequences of an failure. In some instances where failure cannot be tolerated, it may be necessary to shutdown and perform detailed inspection for Minor intensity indications.

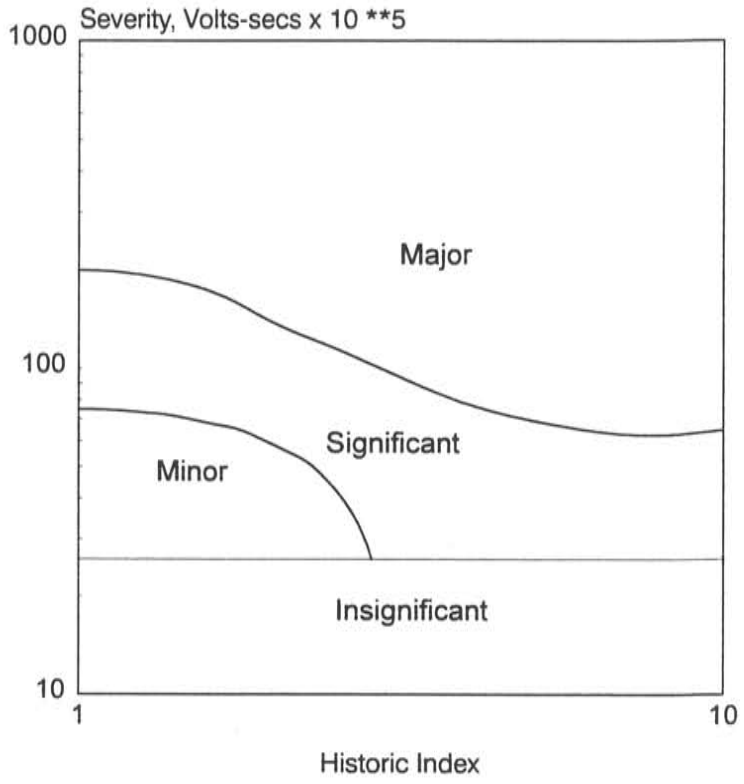

FIGURE 12.6.3.1 - INTENSITY CHART FOR 150 kHz SENSORS.

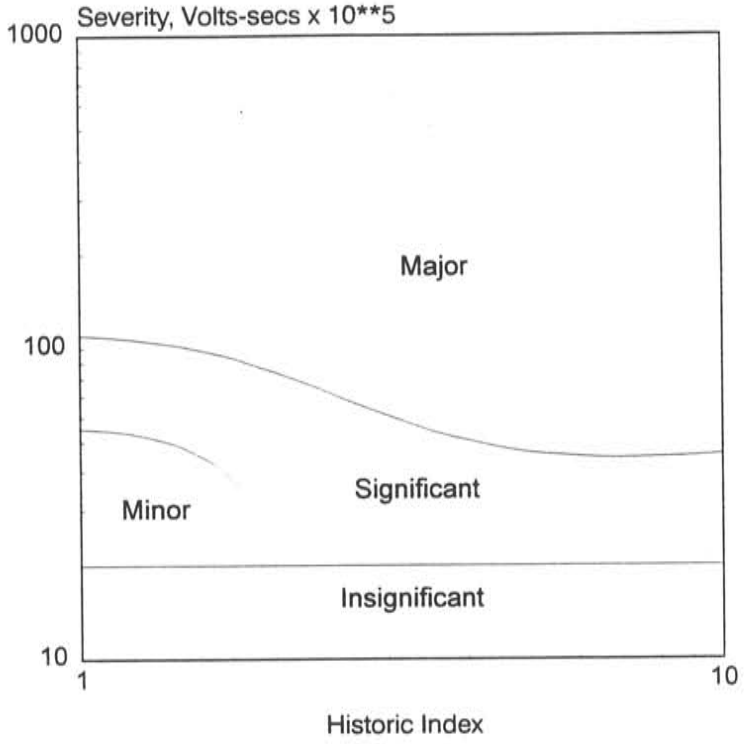

FIGURE 12.6.3.2 - INTENSITY CHART FOR 300 kHz SENSORS.

Zone	150 kHz Intensity Chart	300 kHz Intensity Chart
Insignificant	$S_r = 26$	$S_r = 20$
Minor	$S_r = \{G-K(\ln[H(t)])^2\}^{1/4}$ Where: G = 5625 K = 4512	$S_r = \{G-K(\ln[H(t)])^2\}^{1/4}$ Where: G = 3003 K = 5364
Significant	$S_r=A+B/H(t)+C/H(t)^2+D/H(t)^3$ $+E/H(t)^4$ Where: A = 85.29 B = -346.25 C = 1638.70 D = -1722.45 E = 544.71	$S_r=A+B/H(t)+C/H(t)^2+D/H(t)^3$ $+E/H(t)^4+F/H(t)^5$ Where: A = 60.16 B = -247.34 C = 1135.00 D = -1295.24 E = 356.28 F = 101.10

TABLE 12.6.4 - UPPER BOUNDARY BETWEEN THE INTENSITY ZONES FOR FIGURES 12.6.3.1 and 12.6.3.2

Intensity	Recommended Action
Insignificant	Emission source is structurally insignificant.
Minor	Minor emission. Note for future reference. Visually inspect accessible areas.
Significant	Significant structural defect requiring follow-up evaluation. As a minimum, evaluation should include further data analysis and visual inspection of accessible areas. Consideration should be given to comprehensive nondestructive examination, retest, and increased frequency of inspection.
Major	Major structural defect. Immediate shutdown and nondestructive examination.

TABLE 12.6.4 - MINIMUM RECOMMENDED FOLLOW-UP ACTION FOR CHANNEL INTENSITIES

13. TEST REPORT

A test report shall be issued for each shaft tested. A typical report should include the following.

1. Complete identification and description of the shaft tested.
2. The maximum rated crane load.
3. The loading/stressing sequence used for the test.
4. Date of the last crane lift certification.
5. Sketch showing sensor locations for the test.
6. Identification of emission areas based on the appropriate criteria as given in Paragraph 12.4. Defect areas can be marked on the sensor layout sketch.
7. Any unusual effects or observations during or prior to testing.
8. Date of test.
9. Date and results of previous AE evaluation if a prior test has been performed.
10. AE instrumentation, including manufacturers name, model number, and sensor type.
11. Date of most recent calibration of instrumentation.
12. Test company and name(s) of inspector(s).
13. Test location.
14. Permanent record of AE data, including data diskette and plots of interest as described in Section 12.

14. RECORDS RETENTION

Examination and calibration records shall be maintained by the owner for at least five years.

APPENDIXES

MANDATORY APPENDIX A - INSTRUMENTATION PERFORMANCE REQUIREMENTS

A1 Sensors

A1.1 **General** - AE sensors shall be temperature-stable over the range of intended use, and shall not exhibit sensitivity changes greater than guaranteed by the manufacturer over this range. Sensors shall incorporate integral preamplifier circuitry and shall be shielded against radio frequency interference (RFI) and electromagnetic noise interference (EMI) through proper shielding practice and/or differential (anticoincident) element design. Band pass filters shall be used to reduce EMI and RFI. Sensors shall have omnidirection response, with variations not exceeding 2dB from the peak response.

A1.2 **Sensor Characteristics** - Sensors operating in two different frequency ranges are permitted under this procedure. Sensors shall have a nominal resonant response at 150 kHz or at 300 kHz and shall not vary more than ±10 kHz from this value. Minimum sensitivity shall be -80dB referred to 1 volt/microbar, determined by face-to-face ultrasonic calibration. This method measures relative sensitivity of the sensor. AE sensors used in the same test shall operate in the same resonant frequency range and should not vary in peak sensitivity more than 3dB from the average.

A2 **Couplant** - Commercially available couplants for ultrasonic flaw detection may be used. Silicone based stopcock grease has been found to be particularly suitable. Hot melt glue or quick-setting adhesives may be used, provided

couplant sensitivity is no lower than with fluid couplants. Couplant selection should be made to minimize changes in coupling sensitivity during a test. Consideration should be given to testing time and to the surface temperature of the shaft.

A3 **Preamplifier** - The preamplifier shall be mounted in the sensor housing and shall be shielded against RFI and EMI through proper shielding practice. If the preamplifier is of differential design, a minimum of 40dB of common-mode noise rejection shall be provided. The unfiltered frequency response shall not vary more than 3dB over the operating frequency and temperature range of the sensors, filters and preamplifiers.

A4 **Filters** - Filters shall be located in the preamplifier, or may be integrated into the component design of the sensor and preamplifier. Additional filters shall be incorporated into the processor to limit frequency range and thereby EMI and RFI. The combination of sensor/preamplifier and processor filters shall be of the band pass type, and shall provide a minimum of 24dB/octave signal attenuation. Filters and/or integral design characteristics shall ensure that the principal processing frequency from sensors is in the range specified in A1.2.

A5 **Power-Signal Cable** - The cable providing power to the preamplifier and conducting the amplified signal to the main processor shall be shielded against electromagnetic noise. Signal loss shall be less than 1dB per 100 ft (30 m) of cable length. Five hundred feet is the recommended maximum cable length to avoid excessive signal attenuation.

A6 **Main Amplifier** - The main amplifier, if used, shall have signal response with variations not exceeding 3dB over the frequency range of 100 kHz to 200 kHz for 150 kHz sensors, or 250 to 350 kHz for 300 kHz sensors and temperature range of 40° to 125°F (4° to 52°C).

A7 **Main Processor**

A7.1 **General** - The main processor(s) shall have processing circuits through which sensor data will be processed. It shall be capable of processing hits, hit arrival time, hit duration, peak amplitude, and signal strength on each channel. Sensors may be commoned (teed) into a single channel.

A7.2 **Signal Strength** - Signal strength shall be measured on a per channel basis and shall have a resolution of 1% of the value obtained from a one millisecond duration, 150 kHz pulse having an amplitude 25dB above the data analysis threshold. Useable dynamic range shall be a minimum of 35dB. Relative values of signal strength given in Table B4 shall be accurate to ± 5%.

A7.3 **Peak Amplitude Detection** - Amplitude shall be measured in decibels referenced to 0dB as 1μV at the preamplifier input. Comparative calibration must be established per the requirements of Appendix B. Usable dynamic range shall be a minimum of 60dB with 1dB resolution over the frequency band of 100 kHz to 200 kHz, and the temperature range of 40 ° to 125° F (4° to 52° C). Not more than 2dB variation in peak detection accuracy shall be allowed over the stated temperature range. Amplitude values shall be stated in dB, and must be referenced to a fixed gain output of the system (sensor or preamplifier).

A7.4 **Hit Duration** - Hit duration shall be accurate to ± 5 microseconds.

A7.5 **Arrival Time** - Hit arrival time shall be recorded globally by channel accurate to within 250 nanoseconds.

A7.6 **Hit Definition Time** - The hit definition time shall be 400 microseconds.

A7.7 **Rearm Time** - The rearm time shall be not greater than 200 microseconds.

MANDATORY APPENDIX B - INSTRUMENT CALIBRATION

B1 **General** - The performance and threshold definitions vary for different types of acoustic emission instrumentation. Parameters such as signal strength and amplitude vary from manufacturer to manufacturer and from model to model by the same manufacturer. This appendix describes techniques for generating common baseline levels for the different types of instrumentation. The amplitude decibel values are for a typical piezoelectric crystal using the measurement scale specified in paragraph A7.3. Signal strength values are typical MARSE values measured in volt-seconds multiplied by 10^{5}. The procedures defined in this appendix are intended for baseline instrument calibration by the instrument manufacturer and should be performed at 60° to 80° F (15° to 27° C). It is recommended that instrument users develop approximate calibration techniques, along the lines outlined in this appendix. For field use, a portable acrylic rod can be carried with the equipment and used for periodic checking of sensor, preamplifier, and channel sensitivity.

B2 **Thresholds**

B2.1 **Data Analysis Threshold** - The data analysis threshold shall be determined using a 1 ft x 10 ft x ½ in (31 m x 310 cm x 1.3 cm), 99% pure lead sheet suspended clear of the floor with the long side parallel to the floor. The data analysis threshold is defined as the average measured amplitude of 10 hits generated by a 0.3 mm pencil lead (2H) break at a distance of 63 in (160 cm) from the sensor. Each break shall be done at an angle of approximately 30 degrees to the test surface with a 0.1 in (2.5 mm) lead extension. The sensor shall be mounted 12 in (31 cm) from the end of the sheet and mid-distance between the 10 ft (310 cm) sides of the sheet. The sensor may be mounted using duct tape tightly

wrapped around the back side of the sheet to firmly hold the sensor against the lead sheet. Silicone based stopcock grease shall be applied between the face of the sensor and the lead sheet. The test threshold shall be the same as the data analysis threshold. Typically, the data analysis threshold for this procedure is 45 dB.

B2.2 **Decibel Calibration** - Instruments shall be calibrated using the 1 ft x 10 ft x ½ in (30 cm x 300 cm x 1.3 cm), 99% pure lead sheet. Decibel values shall be determined as the average measured amplitude of ten hits generated by a 0.3 mm (2h) pencil lead break at the distances shown in the table below. Each pencil lead break shall be done at an angle of approximately 30 degrees to the lead sheet surface with a 0.1 in (2.5 mm) lead extension from the pencil. Typical decibel values are given in Table B2.

Distance of Pencil Break From Sensor	Typical Decibel Value
6 ft - 0 in (183 cm)	40
5 ft - 0 in (152 cm)	44
4 ft - 0 in (122 cm)	48
3 ft - 0 in (91 cm)	52
2 ft - 0 in (61 cm)	56
1 ft - 0 in (30 cm)	61
6 in (15 cm)	66
4 in (10 cm)	70

TABLE B2 - DECIBEL CALIBRATION VALUES

B3 **Signal Strength Calibration** - The signal strength calibration shall be confirmed electronically with a constant amplitude 150 kHz pulse of 1 millisecond duration input to each channel. The evaluation criteria given in Section 12 are based on these values. Signal strength calibration values may vary between instruments, but should maintain the same relative values as listed in Table B3. When the numerical signal strength calibration values from an instrument differs from those given in Table B3, the evaluation criteria in Table 12.1.2. must be adjusted by the ratio of the signal strength value at a given decibel level (B2.2) to the signal strength value at the same decibel level.

Amplitude (dB) of Input Signal (1) (2)	Typical Signal Strength calibration Value
55	79
65	251
75	791

(1) See Appendix B2.2 for explanation of decibel values.
(2) Input signal is a constant amplitude 150 kHz pulse of 1 millisecond duration.

TABLE B3 - TYPICAL SIGNAL STRENGTH CALIBRATION VALUES

B4 **Hit Duration** - The accuracy of the hit duration measurement shall be confirmed electronically with a constant amplitude 150 kHz pulse, varied from 50 to 500 microsecond duration, input to each channel. A calibrated transient waveform recorder shall be used to confirm the time duration of the input pulse.

REFERENCES

1. Dingus, M., "Methods for Nondestructive Analysis of Fatigue in Cranes," Report 95-225, Texas Research Institute Austin, Austin, TX.

2. Akhtar, A., J.Y. Wong, G.S. Bhuyan, C.T. Webster, and D. Kung, "Acoustic Emission Testing of Steel Cylinders for the Storage of Natural Gas on Vehicles," NDT&E International, Vol. 25, No. 3, Butterworth-Heinemann Ltd., UK, 1992.

3. Courtesy of the Physical Acoustic Corporation, Princeton, NJ. Calibration Curve for R15I Sensor; Serial Number EF90. Reprinted with permission.

4. Bassim, M.N., and F. Hamel, "Acoustic Emission Associated with Crack Propagation in Fatigue," 1981 Paper Summaries, ASNT Spring and Fall National Conferences, ASTN, Columbus, OH, 1981.

5. Berkovitz, A. and D. Fang, "Fatigue Design Model Based on Damage Mechanisms Revealed by Acoustic Emission Measurements," Durability and Reliability of Airframes, Transactions of the ASME, 1995.

6. Heiple, C.R., S.H. Carpenter, and D.L. Armentrout, "Comments on the Origin of Acoustic Emission in Fatigue Testing of Aluminum Alloys," Journal of Acoustic Emission, Vol. 10, No. 3, January 1992.

7. Heiple, C.R., and S.H. Carpenter, "Acoustic Emission Produced by Deformation of Metals and Alloys - A Review," Parts I & II, Journal of Acoustic Emission, Vol. 10, No. 3, January 1992.

8. "Acoustic Emssion Examination of Metallic Vessels During Pressure Testing", Section V, Article 12, Boiler and Pressure Vessel Code, American Society of Mechanical Engineers, New York, NY.

9. Williams, R.V., Acoustic Emission, Adan Hilger Ltd., Briston, U.K., 1990

10. Whittaker, J.W., "A Note on the Prediction of Fatigue Life of Metal Structures by Use of the Felicity Effect," Journal of Acoustic Emission, Vol. 5, No. 4, Oct. 1986.

11. Siedlaczek, J., S. Pilecki, and F. Dusek, "Acoustic Emssion of the 45HNMFA Structural Steel during Low-Cycle Fatigue," Journal of Acoustic Emission, Vol. 10, No. 3, Jan. 1992.

12. Almeida, A. and E. Hill, "Neural Network Detection of Fatigue Crack Growth in Riveted Joints Using an Acoustic Emission Approach," Materials Evaluation, Vol. 53, No. 1, ASNT, Columbus, OH, 1995.

13. Scala, C.M., S.J. Bowles, and I.G. Scott, "The Development of Acoustic Emission for Structural Integrity Monitoring of Aircraft," ARL/MAT-R-120, Department of Defense, Aeronautical Research Laboratory, Australia, 1988.

14. Broek, D., Elementary Fracture Mechanics, Kluwer Academic Publishers, Norwell, MA, USA. 1991.

15. "Procedure for Acoustic Emission Evaluation of Tank Cars and IM-101 Tanks," Association of American Railroads, Operations and Maintenance Department, Mechanical Division, Washington, D.C.

16. Fowler, T.J., J.A. Blessing, P.J. Conlisk, and T.L. Swanson, "The MONPAC System," Journal of Acoustic Emission, Vol. 8, No. 3, 1989.

17. Fowler, T.J., "Acoustic Emission Testing of Chemical Industry Vessels", *Progress in Acoustic Emission II,* Proceedings for the 7th International Acoustic Emission Symposium, Zao, Japan, The Japanese Society for Nondestructive Inspection, 1984.

18. ASTM. "Standard Terminology for Nondestructive Examinations," Standard E1316. Annual Book of ASTM Standards, Nondestructive Testing, Vol. 03.03. American Society for Testing and Materials, Philadelphia, P.A. 1994.